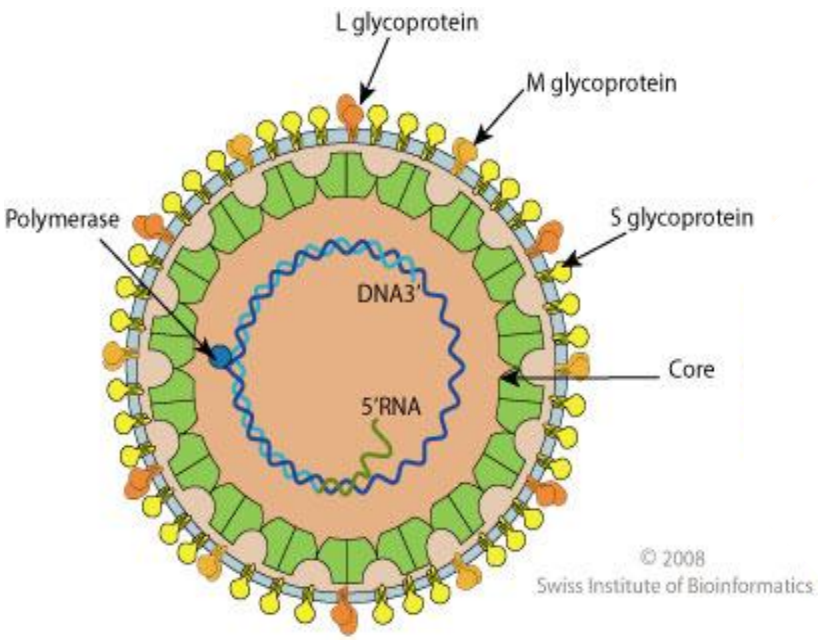

Figure 1.1 Schematic diagram of HBV structure: The HBV virion consists of 3 envelope proteins (S, M and L glycoprotein), a nucleocapsid protein Core, a partially double-stranded DNA genome and a polymerase enzyme that transcribes viral RNA from a DNA template. Figure taken from the Swiss Institute of Bioinformatics website; http://www.isb-sib.ch

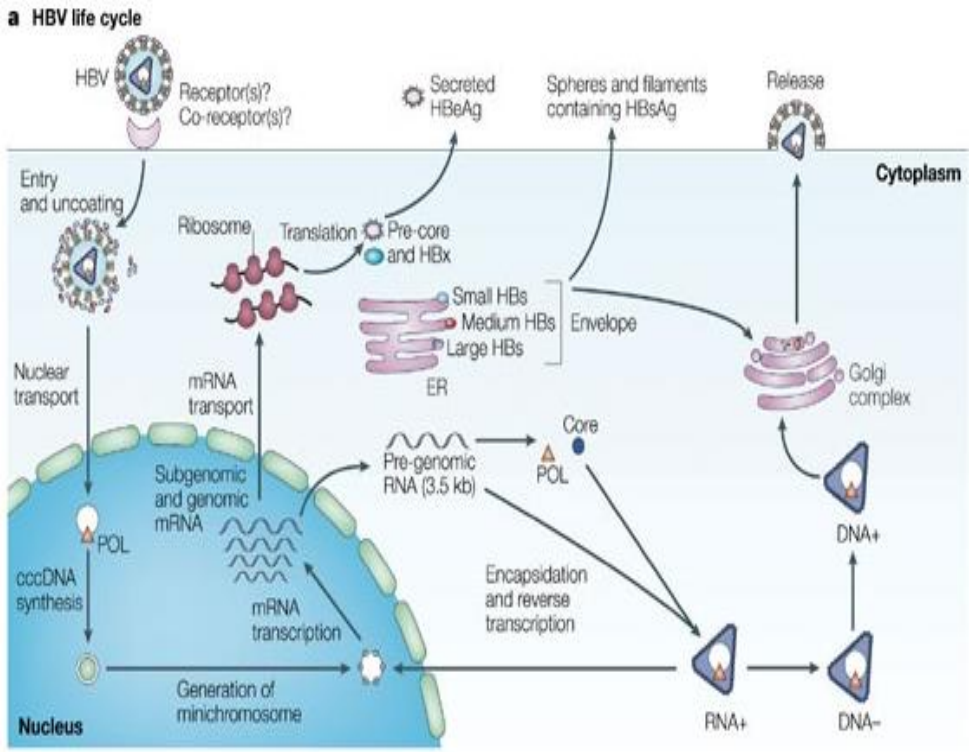

Figure 1.2 Schematic diagram of HBV life cycle: The figure was adopted from Rehermann and Nascimbeni 2006.
HBV binds to an unidentified receptor on the hepatocyte surface and fuses with the cell membrane. After cell entry, HBV nucleocapsids are uncoated and released into the cytoplasm. They are transported to the nucleus, where the covalently closed circular DNA (cccDNA) is formed. Transcription yields four viral RNAs which are subsequently transported to the ribosome and translated to form viral proteins as part of virion formation. Pre-genomic RNA is translated to core and reverse transcriptase proteins. Nucleocapsids are enveloped with Small, Medium and Large envelope proteins (HBs) as they pass through the endoplasmic reticulum (ER) and/or Golgi complex and are then secreted. Alternatively, nucleocapsids can be recycled back to the nucleus where their pre-genomic RNA is reverse transcribed to DNA as part of the viral replication process.

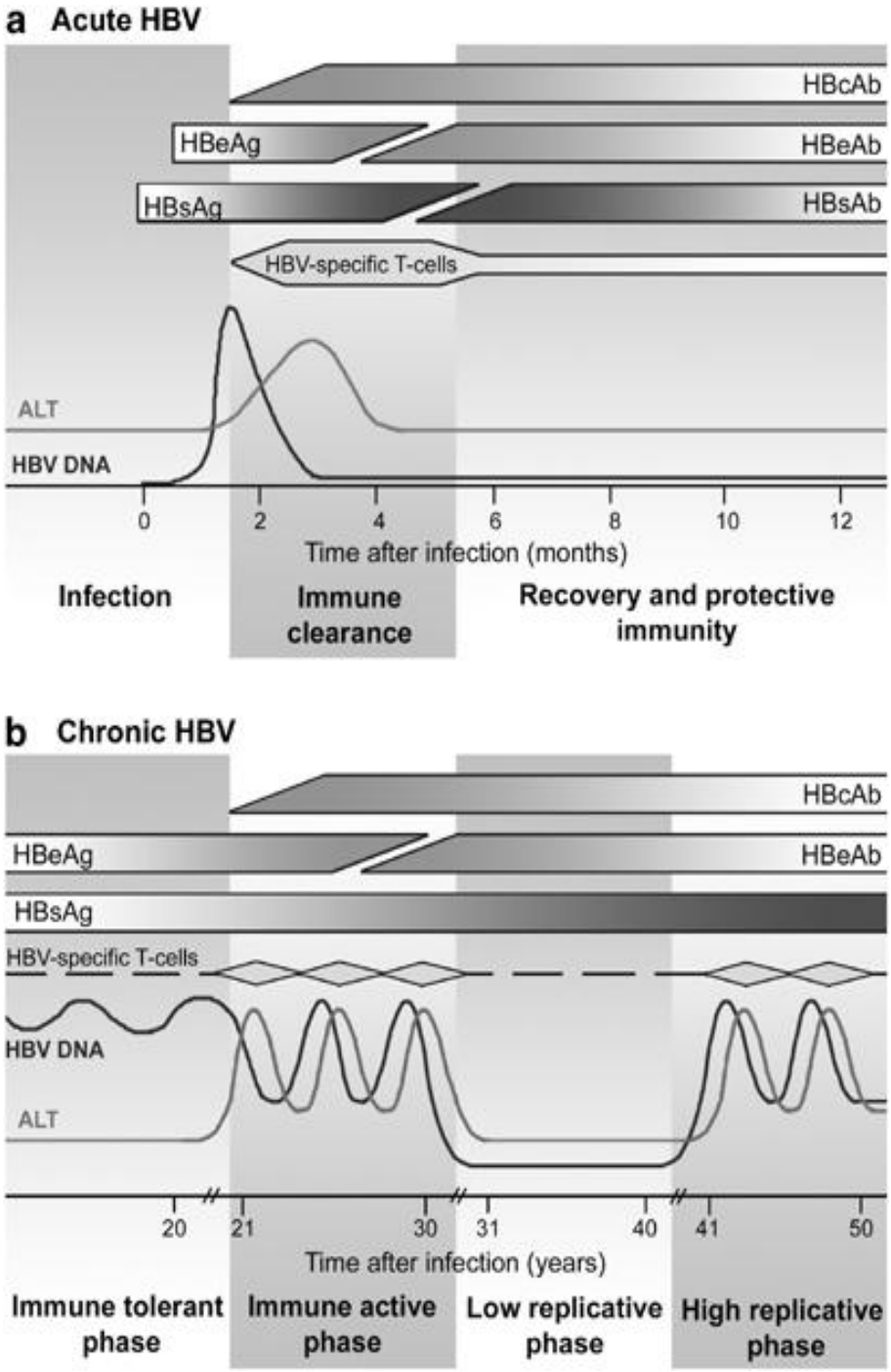

Figure 1.3 The course of acute and chronic HBV infection: shows serology and virology of acute **(a)** and chronic **(b)** HBV infection. Figure adopted from Chang & Lewin 2006.

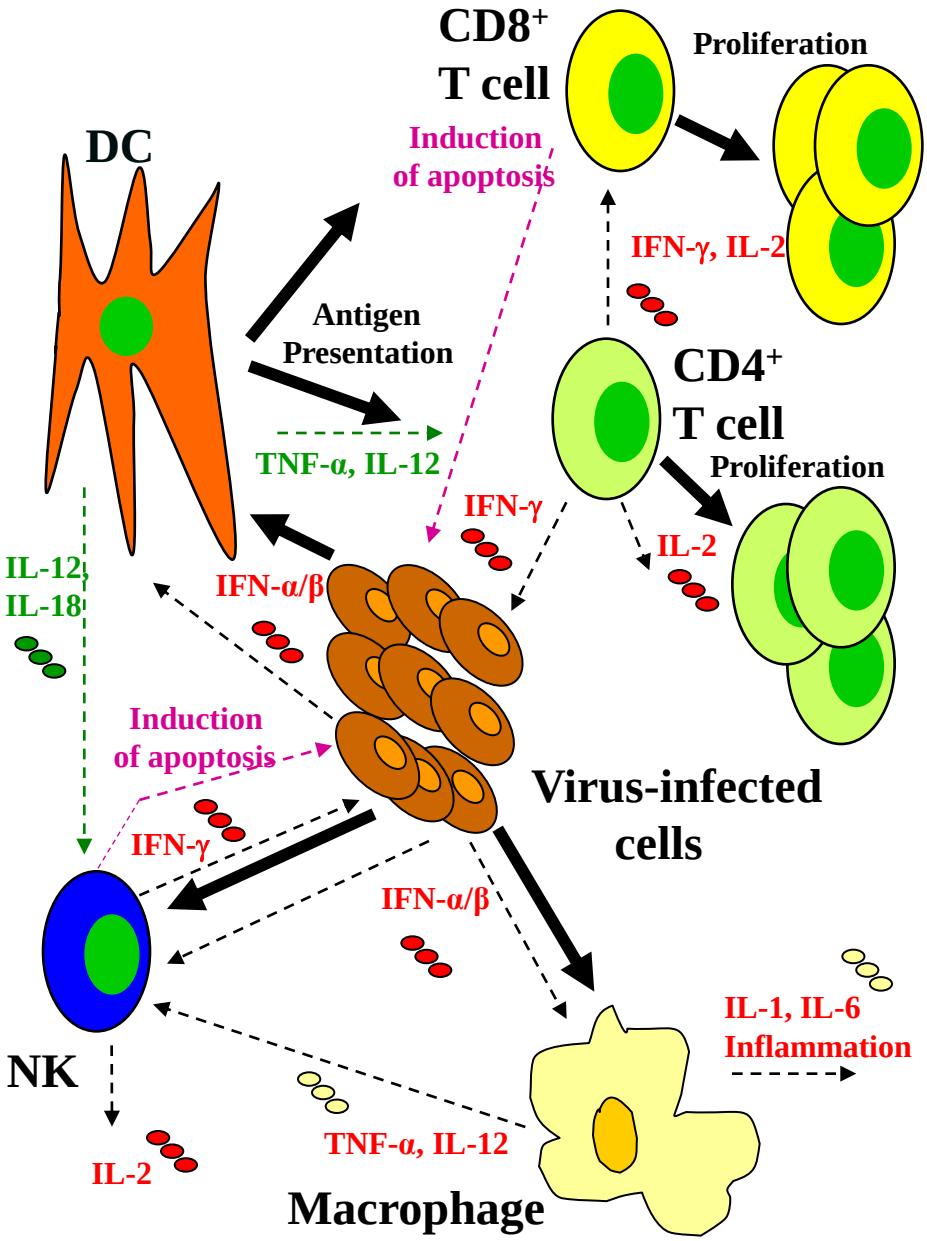

Figure 1.4 Anti-viral immune response: Virus-infected cells release IFN-α/β which activate DC, macrophages and NK cells. The expression of viral antigens or danger molecules on the surface of infected cells also activate these cells. NK cell can also be indirectly activated by DC- or macrophage-derived cytokines. Activated, NK cells can kill infected cells and secrete IFN-γ and TNF-α which can exert direct anti-viral effects, or IL-2 which can promote T cell proliferation. The activated DC can present antigens to $CD4^+$ and $CD8^+$ T cells and also produces IFN-γ, TNF-α and IL-2 which provide signals that stimulate clonal expansion and subsequent cytotoxic T cell responses. The production of IFN-γ and IL-2 by $CD4^+$ T cells can sustain and amplify the anti-viral immune responses. Macrophages can also produce IL-1 and IL-6 to initiate inflammation.

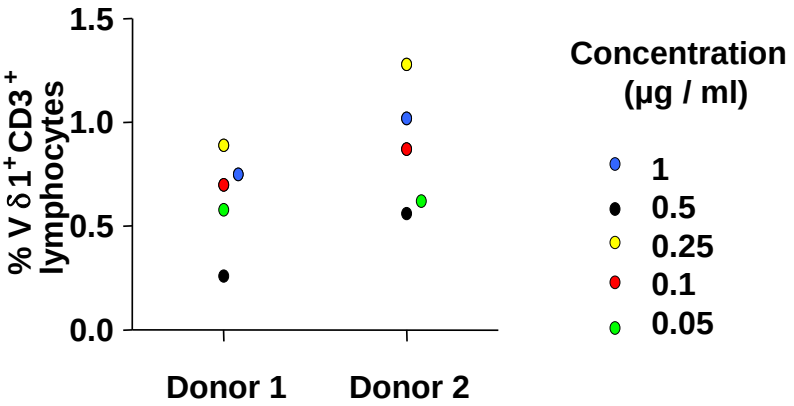

Figure 2.2: The optimal concentration of anti-Vδ1 mAb is 0.25µg/ml. Scatterplot showing the different frequencies of Vδ1$^+$ T cells from 2 healthy donors, quantified for each anti-Vδ1 mAb concentrations used.

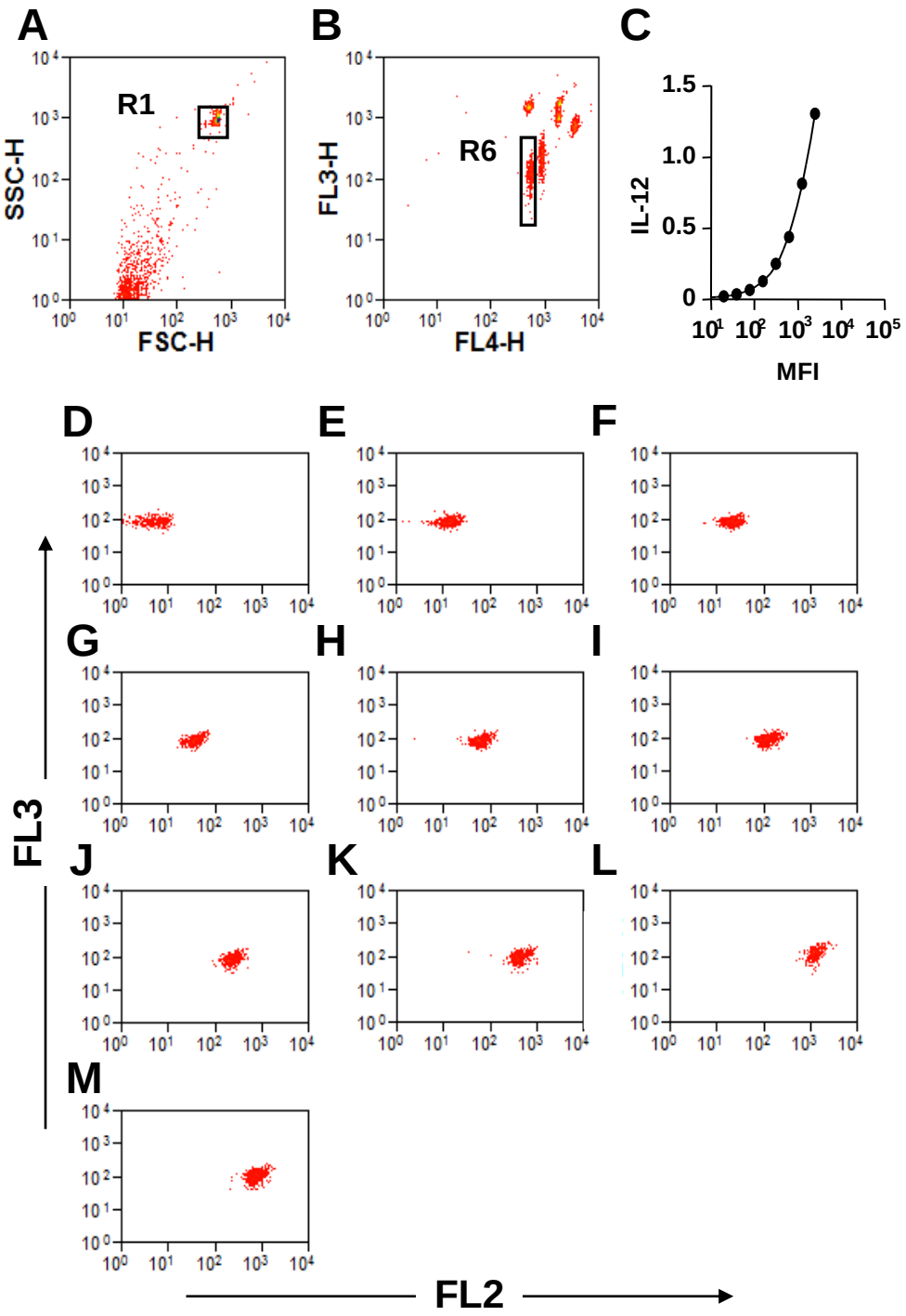

Figure 2.8: Analysis of cytometric bead array standards. A, dot plot of antibody coated beads with electronic gate R1 surrounding the antibody coated beads and excluding the debris. **B,** dot plot of all populations of cytokine beads, previously gated in R1 and now, divided by their fluorescence intensity in the FL3 and FL4 channels. IL-12 conjugated beads are gated in R6. **C,** IL-12 standard curve with MFI of anti-IL-12 coated bead population on X-axis and IL-12 concentration on Y-axis in ng/ml. **D-M,** dot plots showing IL-12 conjugated beads in ten standard tubes, from bottom tube with no IL-12 content **(D)** to the top tube with the highest IL-12 content **(M).**

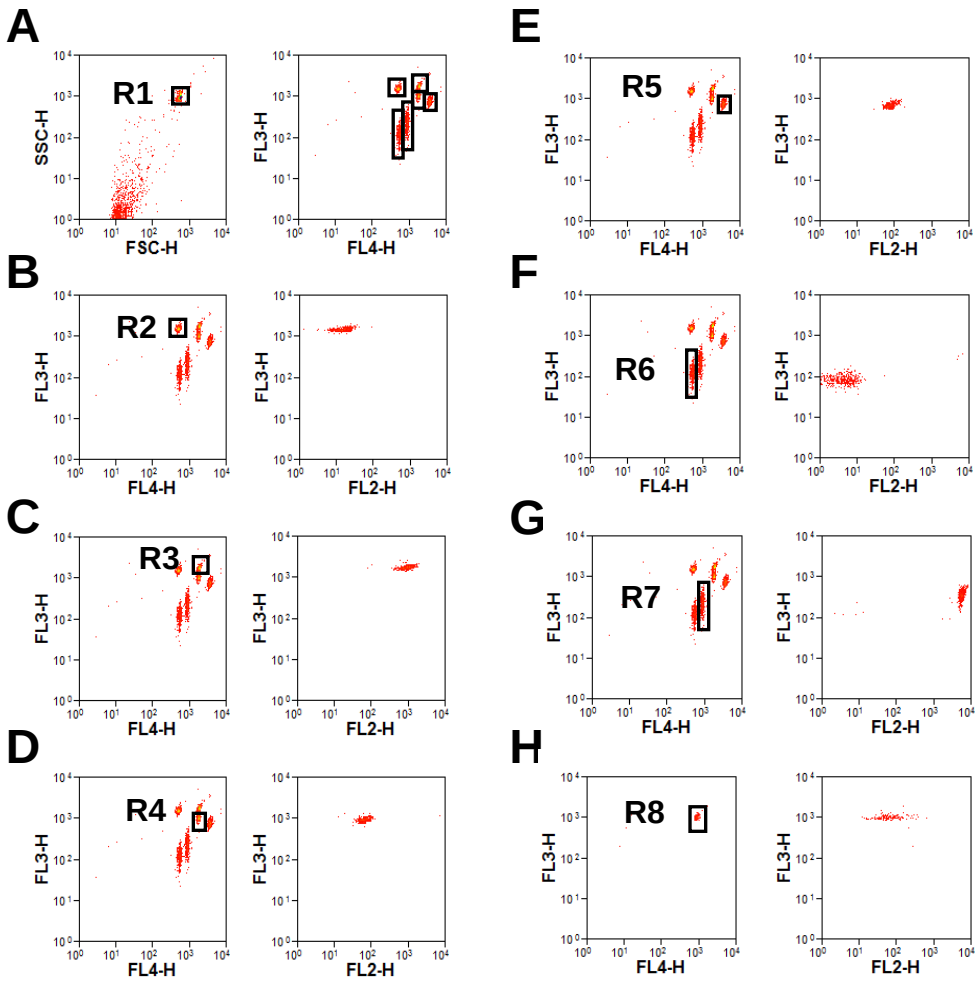

Figure 2.9: Analysis of cytometric bead array. A, representative dot plots of antibody coated beads with electronic gate R1 surrounding the antibody coated beads and excluding the debris **(left)** and representative dot plot of all populations of cytokine beads, previously gated in R1 to exclude debris and now, divided by their fluorescence intensity in the FL3 and FL4 channels **(right). B, C, D, E, F, G, (left),** representative dot plots of all populations of cytokine beads showing gating of conjugated beads for identification of IL-4 in R2 **(B),** IL-6 in R3 **(C),** IL-10 in R4 **(D),** IFN-γ in R5 **(E),** IL-12 in R6 **(F)** and IL-13 in R7 **(G). B, C, D, E, F, G, (right),** representative dot plot showing only IL-4, IL-6, IL-10, IFN-γ, IL-12 or IL-13 conjugated beads, respectively, because the plot has been gated on R2, R3, R4, R5, R6 or R7. The MFI of each single bead population in FL2 indicates the level of cytokine expression in the sample. **H,** representative dot plots showing TGF-β1 conjugated beads only. The TGF-β1 conjugated beads are the only beads present in this sample and are gated in R8 **(left).** The MFI values of the populations in FL2 represents the TGF-β1 concentration of the sample **(right).**

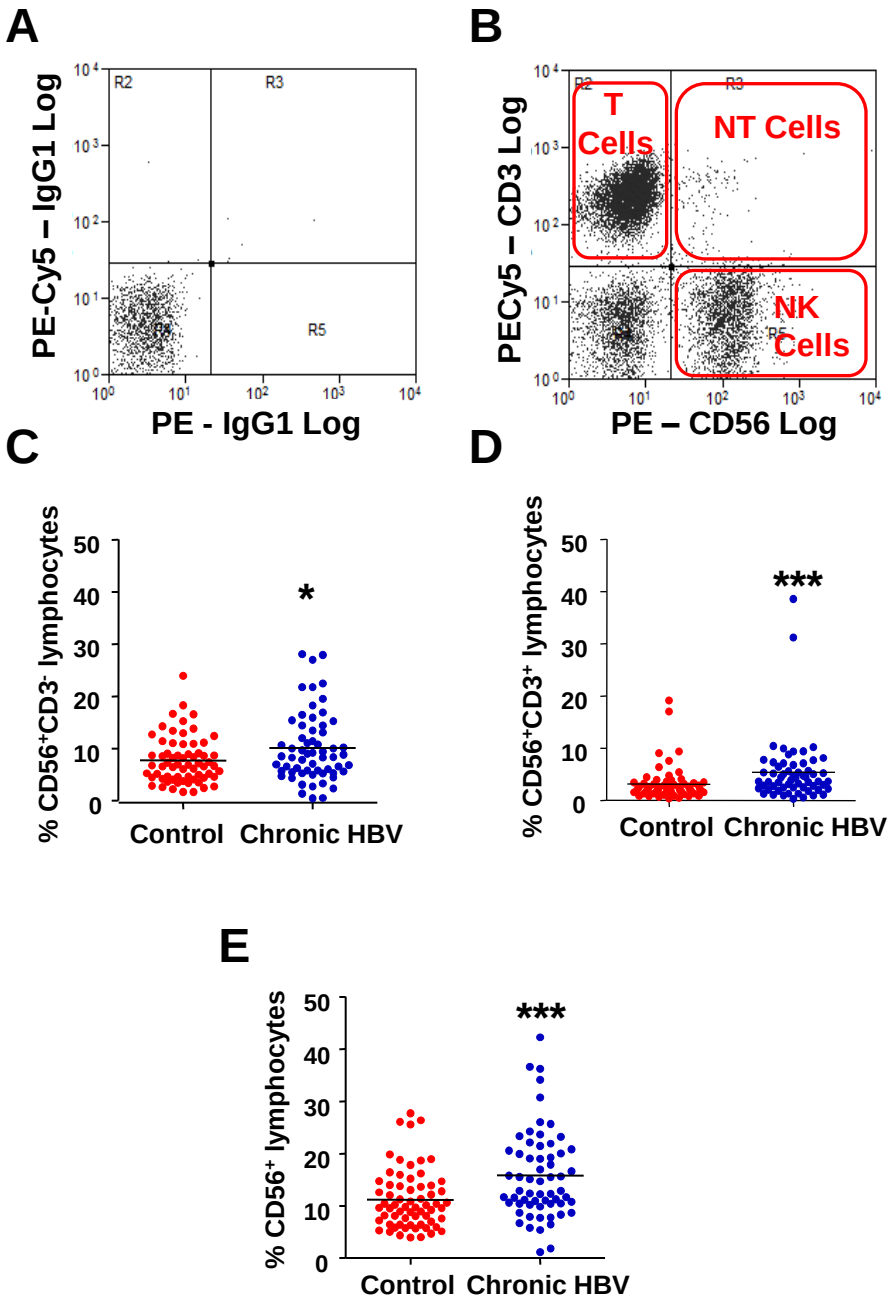

Figure 3.1: Frequencies of circulating NK, NT and total CD56$^+$ cells are significantly higher in HBV patients than in control subjects. A and B, representative dot plots of whole PBMC, gated on lymphocytes and **A,** stained with matched isotype controls PE- and PE-Cy5-labelled anti-IgG1 mAb or **B,** stained with PE-labelled anti-CD56 mAb and PE-Cy5-labelled anti-CD3 mAb for identification of NK, NT and total CD56+ cell populations. **C, D and E,** scatterplots showing the frequencies of circulating CD56$^+$CD3$^-$, CD56$^+$CD3$^+$ and total CD56$^+$ cells from each of the 66 control subjects (red) and each of the 62 HBV patients (blue). * $p<0.05$,*** $p<0.0005$.

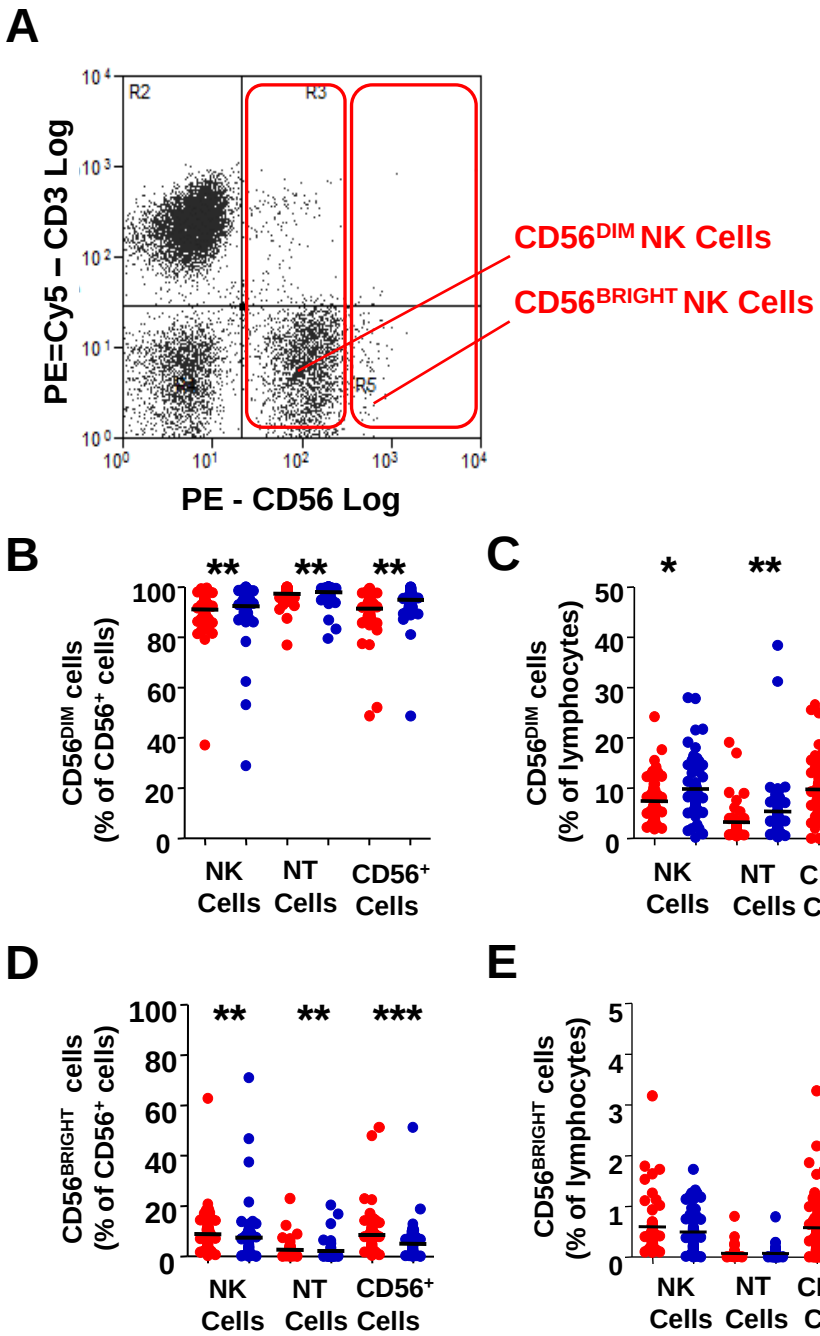

Figure 3.2: The frequencies of the CD56^{DIM}, but not the CD56^{BRIGHT}, NK, NT and total CD56^{+} cells, are significantly higher in HBV infection. A, B, C and D, scatterplots showing the frequencies of CD56^{DIM} cells **(B, C)** and CD56^{BRIGHT} cells **(D, E)** within the CD56^{+}CD3^{-}, CD56^{+}CD3^{+} and total CD56^{+} cell populations as a percentage of each CD56^{+} population **(B, D)** and as a percentage of lymphocytes **(C, E)** from each of the 66 control subjects (red) and each of the 62 HBV patients (blue). * $p<0.05$, ** $p<0.009$, ***$p<0.0007$.

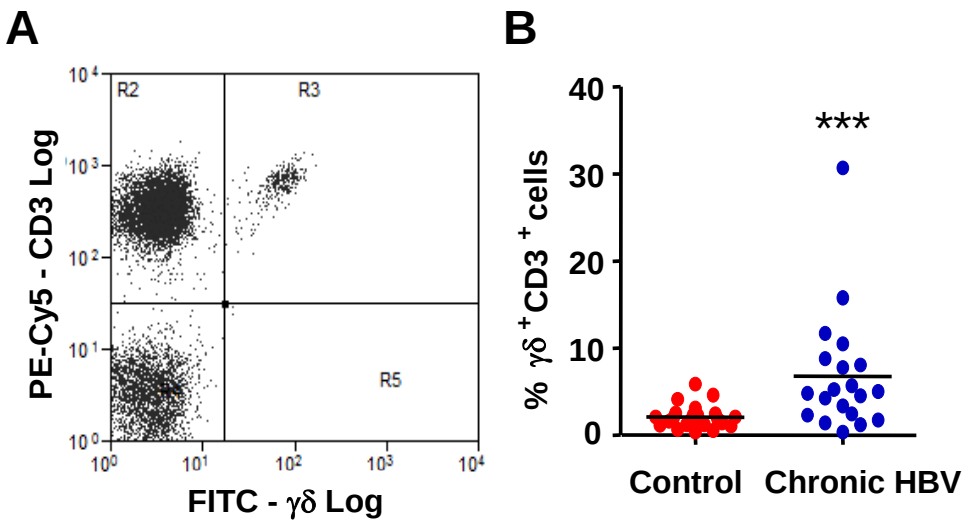

Figure 3.3: The frequencies of $\gamma\delta^+$ T cells are significantly higher in HBV infection. A, representative dot plot of PBMC, gated on lymphocytes and stained with FITC-labelled anti-γδ-TCR mAb and PE-Cy5-labelled anti-CD3 mAb for the identification of $\gamma\delta^+$ T cells. **B,** scatterplot showing the frequency of $\gamma\delta^+CD3^+$ lymphocytes in 23 control subjects (red) and 20 HBV patients (blue). *** p=0.0009.

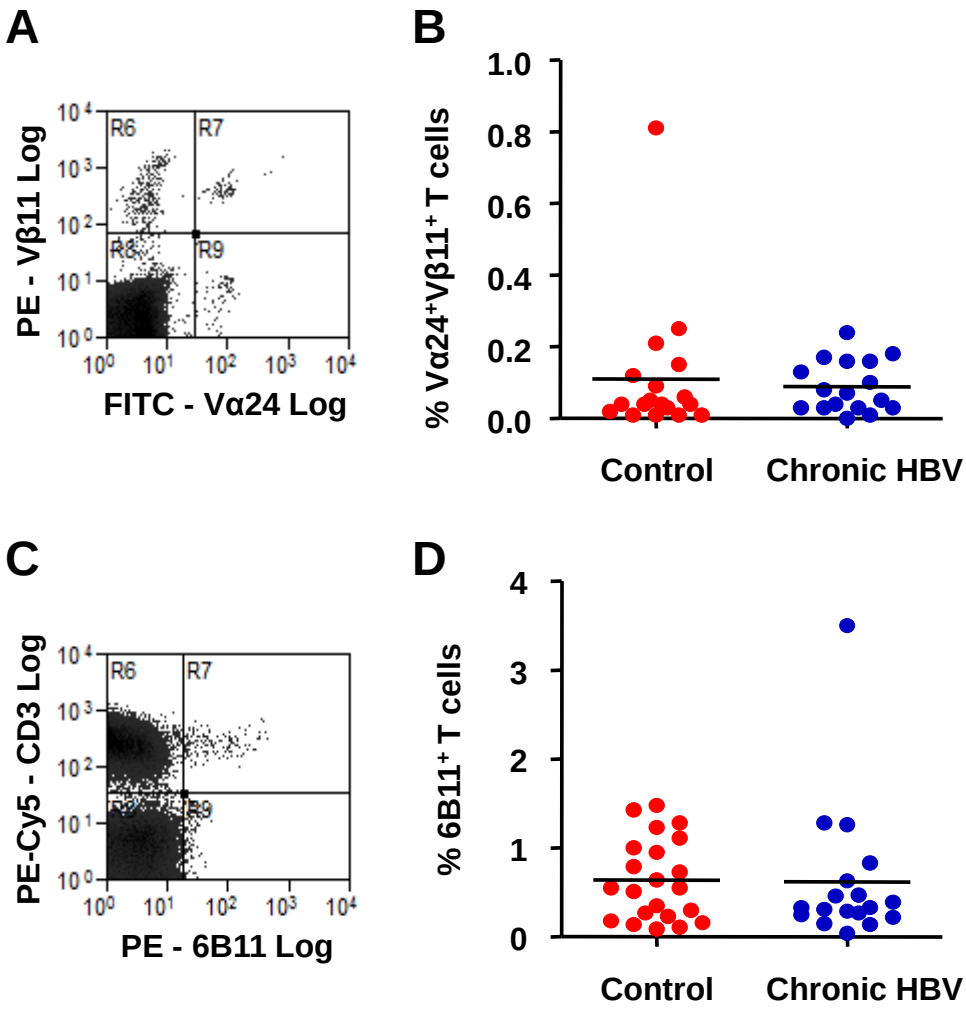

Figure 3.4: There are no significant differences in the frequencies of invariant NKT (iNKT) cells between controls subjects or HBV patients. A, C, representative dot plots of PBMC, gated on lymphocytes and, stained with FITC-labelled anti-Vα24 mAb and PE-labelled anti-Vβ11 mAb **(A)** or PE-labelled anti-6B11 mAb and PE-Cy5-labelled anti-CD3 mAb **(C)**. **B, D,** scatterplots showing frequencies of iNKTs in 23 controls (red) and 20 HBV patients (blue).

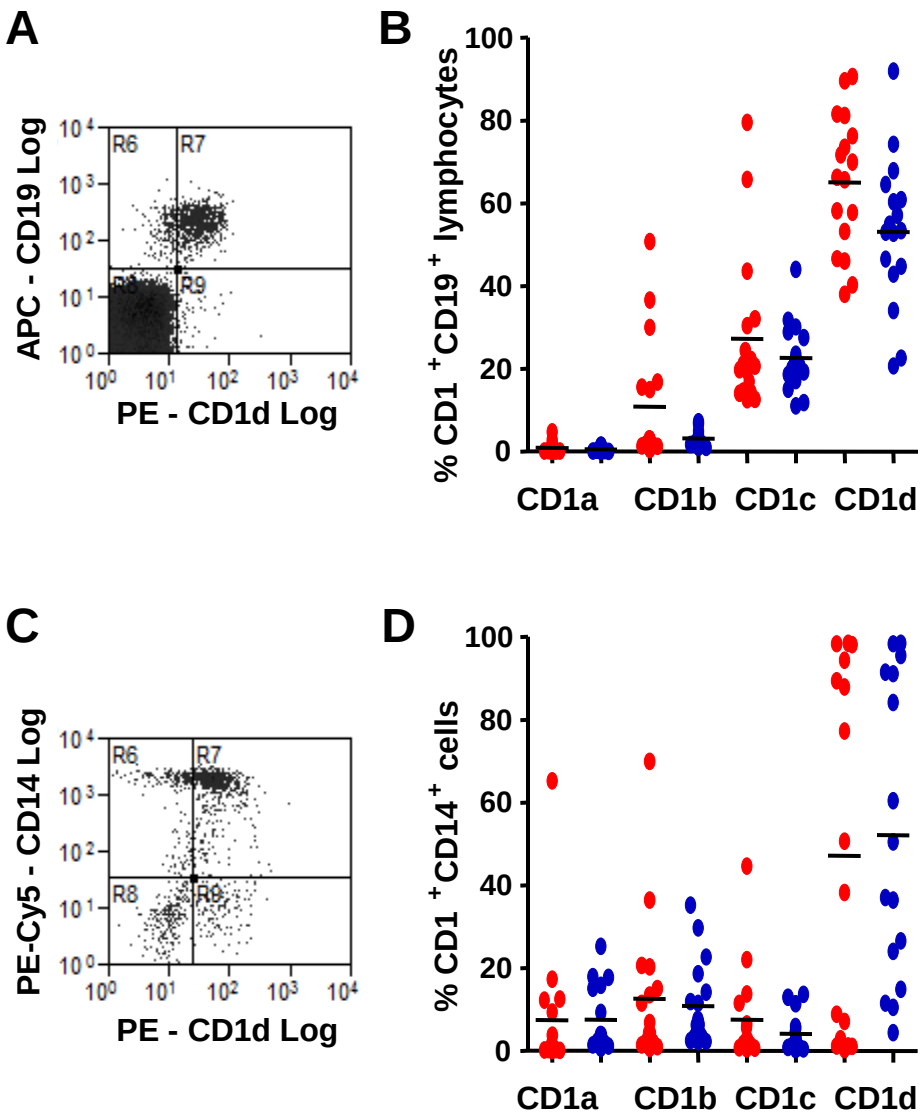

Figure 3.5: There are no significant differences in the frequencies of CD1$^+$ cells between controls subjects or HBV patients. A and C, representative dot plots of PBMC, gated on lymphocytes **(A)** or monocytes **(C)** and, stained with PE-labelled anti-CD1d mAb and APC-labelled anti-CD19 mAb **(A)** or PE-labelled anti-CD1d mAb and PE-Cy5-labelled anti-CD14 mAb **(C)**. **B, D,** scatterplots showing frequencies of CD1a$^+$, CD1b$^+$, CD1c$^+$ and CD1d$^+$ B cells **(B)** or monocytes **(D)** in 18 controls (red) and 18 HBV patients (blue).

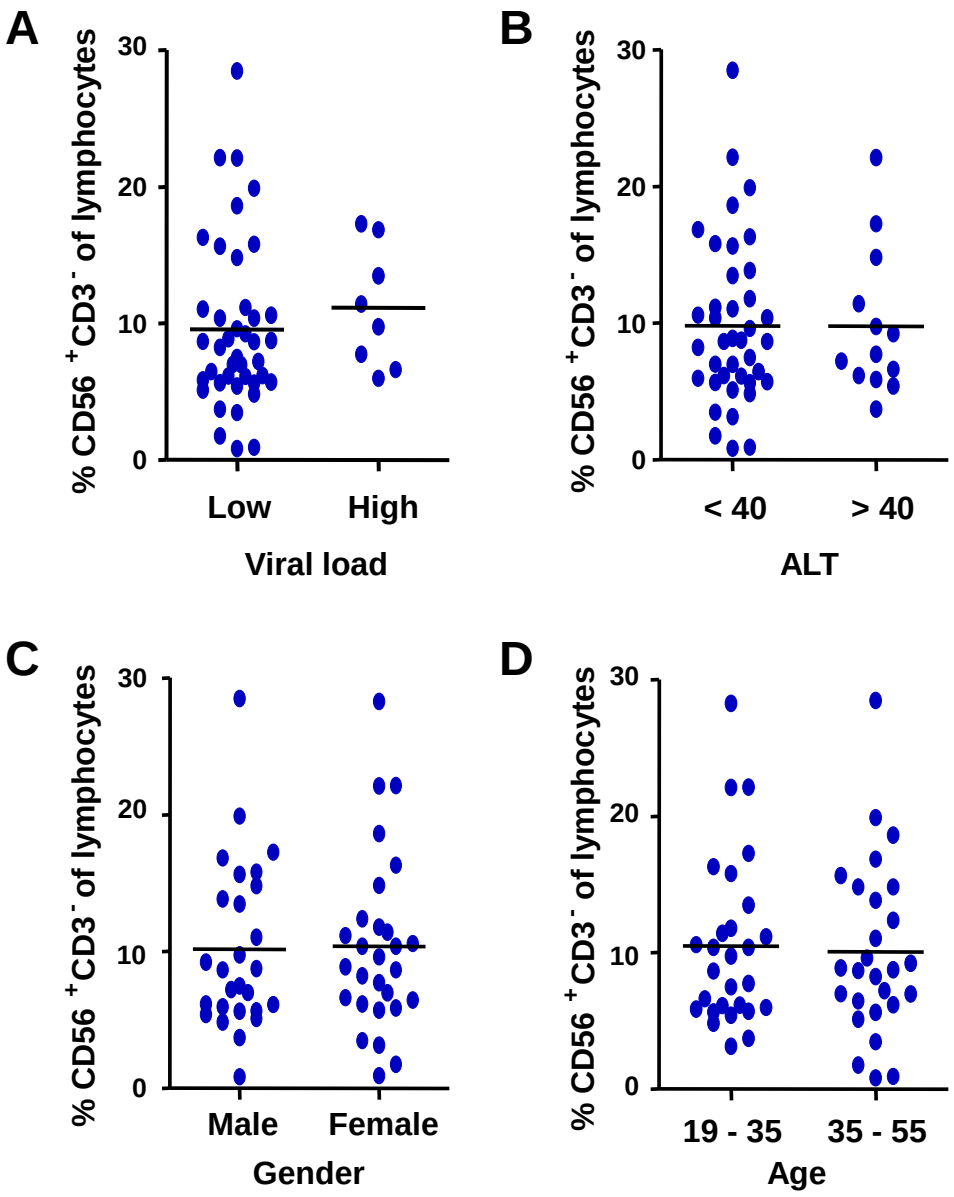

Figure 3.6: There are no significant differences in the frequencies of NK cells between patient groups within the study cohort. A, scatterplot showing frequencies of NK cells in 41 HBV patients with viral load between 10 and 10,000 copies / ml and 8 HBV patients with viral load between 300,000 and $5x10^8$ copies / ml. **B,** scatterplot showing frequencies of NK cells in 39 HBV patients with ALT below 40 IU/ml and 13 HBV patients with ALT above 40 IU/ml. **C,** scatterplot showing frequencies of NK cells in 27 male HBV patients and 28 female HBV patients. **D,** scatterplot showing frequencies of NK cells for 28 HBV patients between the age of 19 and 35 years and 27 HBV patients between the age of 35 and 55 years.

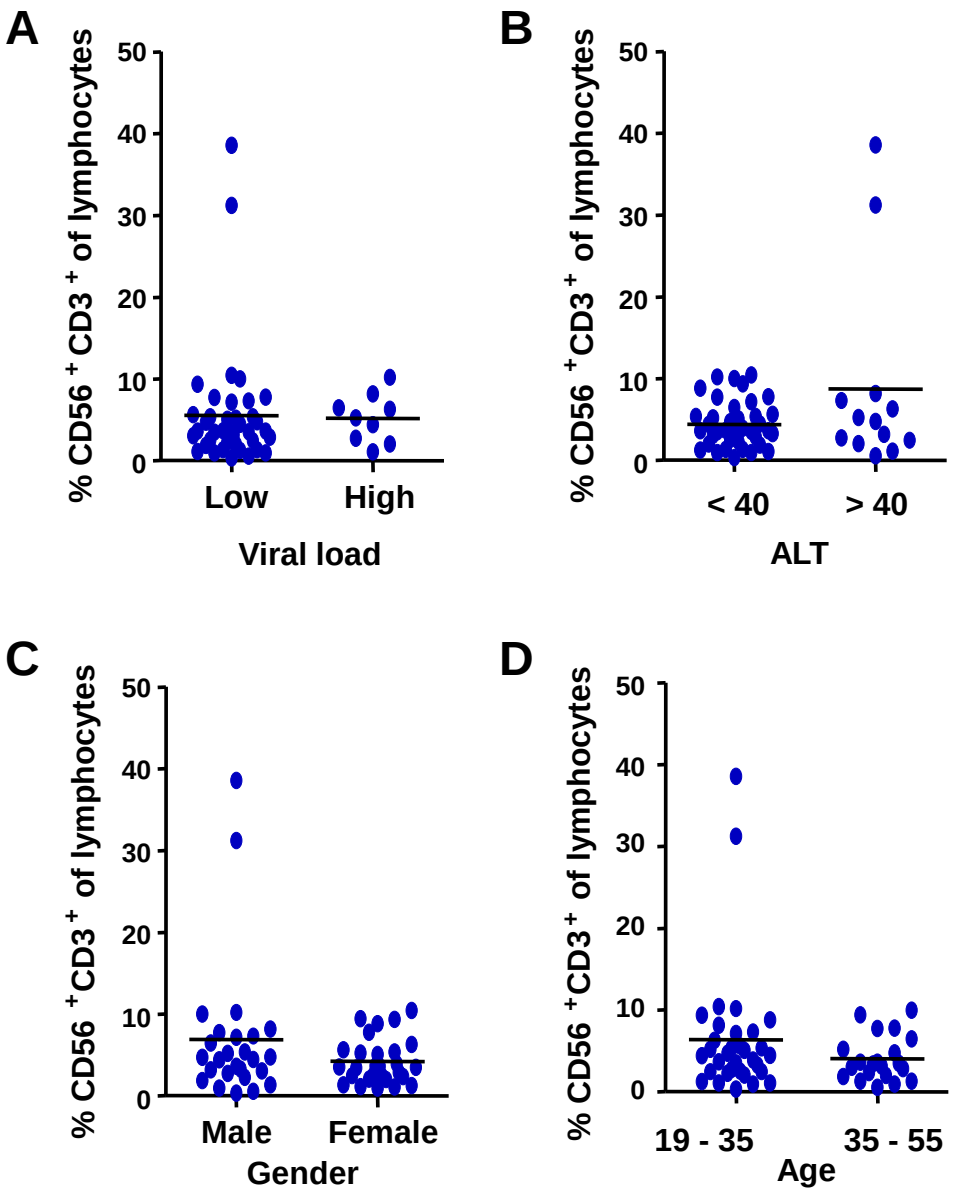

Figure 3.7: There are no significant differences in the frequencies of NT cells between patient groups within the study cohort. A, scatterplot showing frequencies of NT cells in 40 HBV patients with viral load between 10 and 10,000 copies / ml and 9 HBV patients with viral load between 300,000 and $5x10^8$ copies / ml. **B,** scatterplot showing frequencies of NT cells in 38 HBV patients with ALT below 40 IU/ml and 13 HBV patients with ALT above 40 IU/ml. **C,** scatterplot showing frequencies of NT cells in 26 male HBV patients and 28 female HBV patients. **D,** scatterplot showing frequencies of NT cells for 33 HBV patients between the age of 19 and 35 years and 21 HBV patients between the age of 35 and 55 years.

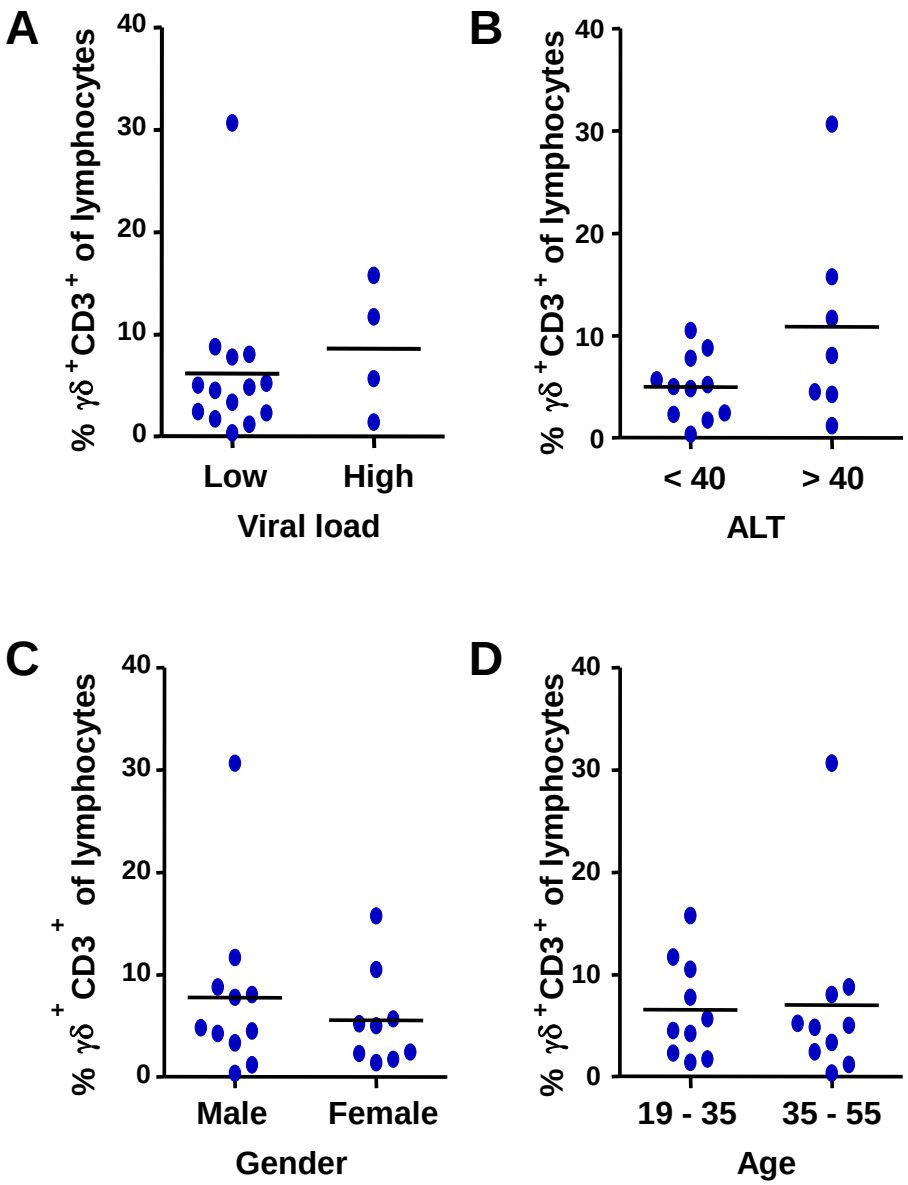

Figure 3.8: There are no significant differences in the frequencies of γδ T cells between patient groups within the study cohort. A, scatterplot showing frequencies of γδ T cells in 40 HBV patients with viral load between 10 and 10,000 copies / ml and 9 HBV patients with viral load between 300,000 and $5x10^8$ copies / ml. **B,** scatterplot showing frequencies of γδ T cells in 38 HBV patients with ALT below 40 IU/ml and 13 HBV patients with ALT above 40 IU/ml. **C,** scatterplot showing frequencies of γδ T cells in 26 male HBV patients and 28 female HBV patients. **D,** scatterplot showing frequencies of γδ T cells for 33 HBV patients between the age of 19 and 35 years and 21 HBV patients between the age of 35 and 55 years.

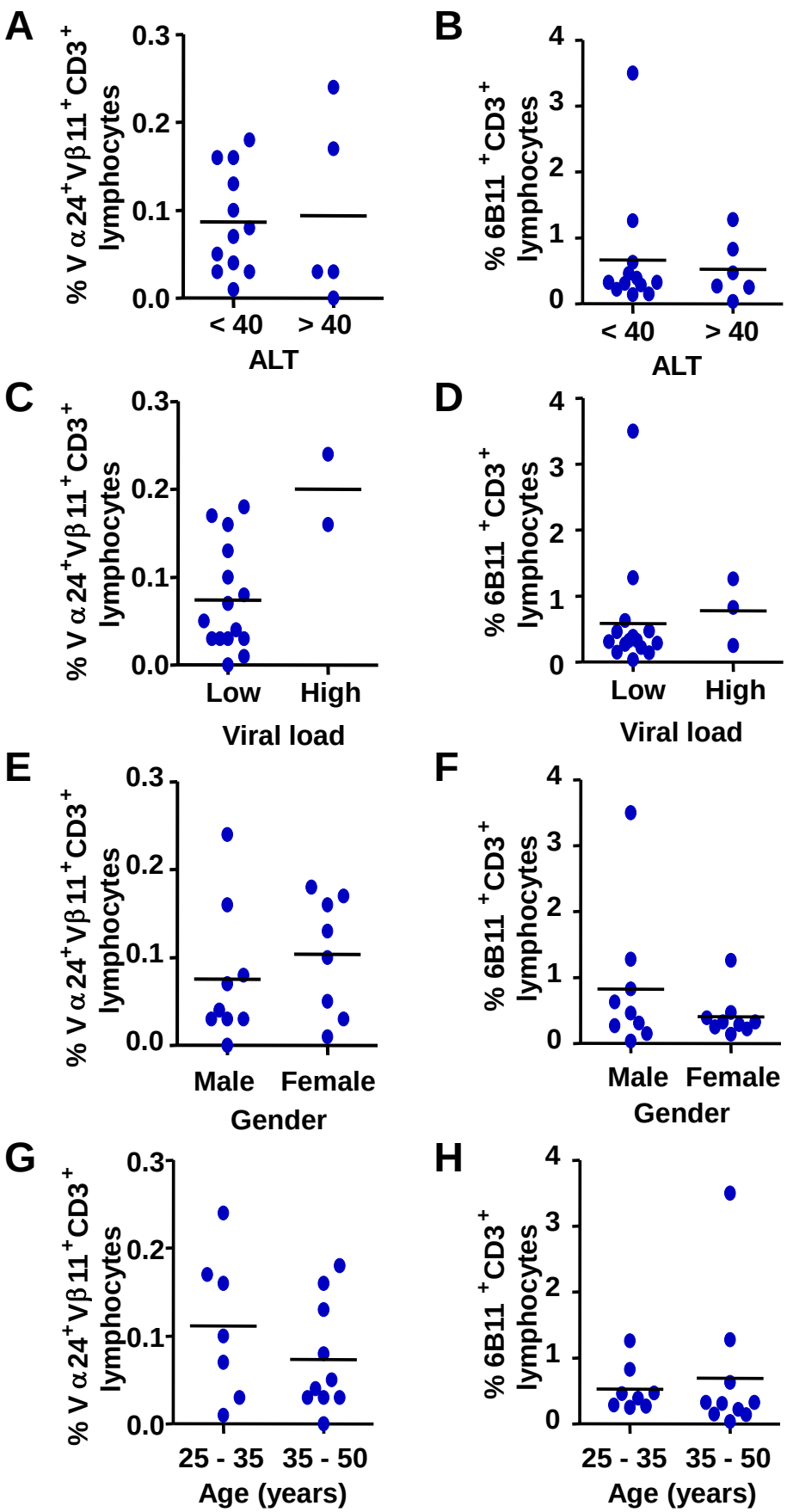
A
% V α24+Vβ11+CD3+ lymphocytes
0.3
0.2
0.1
0.0
< 40
> 40
ALT
B
% 6B11+CD3+ lymphocytes
4
3
2
1
0
< 40
> 40
ALT
C
% V α24+Vβ11+CD3+ lymphocytes
0.3
0.2
0.1
0.0
Low
High
Viral load
D
% 6B11+CD3+ lymphocytes
4
3
2
1
0
Low
High
Viral load
E
% V α24+Vβ11+CD3+ lymphocytes
0.3
0.2
0.1
0.0
Male
Female
Gender
F
% 6B11+CD3+ lymphocytes
4
3
2
1
0
Male
Female
Gender
G
% V α24+Vβ11+CD3+ lymphocytes
0.3
0.2
0.1
0.0
25 - 35
35 - 50
Age (years)
H
% 6B11+CD3+ lymphocytes
4
3
2
1
0
25 - 35
35 - 50
Age (years)

Figure 3.9: There are no significant differences in the frequencies of iNKT cells between patient groups within the study cohort.
A, scatterplot showing frequencies of $V\alpha24^{+}V\beta11^{+}CD3^{+}$ lymphocytes in 12 HBV patients with ALT below 40 IU/ml and 5 HBV patients with ALT above 40 IU/ml. **B,** scatterplot showing frequencies of $V\alpha24^{+}V\beta11^{+}CD3^{+}$ lymphocytes in 15 HBV patients with viral load below 10,000 copies / ml and 2 HBV patients with viral load between 300,000 and $5x10^{8}$ copies / ml. **C,** scatterplot showing frequencies of $V\alpha24^{+}V\beta11^{+}CD3^{+}$ lymphocytes in 9 male HBV patients and 8 female HBV patients. **D,** scatterplot showing frequencies of $V\alpha24^{+}V\beta11^{+}CD3^{+}$ lymphocytes for 7 HBV patients under the age of 35 years and 10 HBV patients between the age of 35 and 55 years. **E,** scatterplot showing frequencies of $6B11^{+}CD3^{+}$ lymphocytes in 12 HBV patients with ALT below 40 IU/ml and 6 HBV patients with ALT above 40 IU/ml. **F,** scatterplot showing frequencies of $6B11^{+}CD3^{+}$ lymphocytes in 15 HBV patients with viral load below 10,000 copies / ml 3 HBV patients with viral load between 300,000 and $5x10^{8}$ copies / ml. **G,** scatterplot showing frequencies of $6B11^{+}CD3^{+}$ lymphocytes in 9 male HBV patients and 9 female HBV patients. **H,** scatterplot showing frequencies of $6B11^{+}CD3^{+}$ lymphocytes for 8 HBV patients under the age of 35 years and 10 HBV patients between the age of 35 and 55 years.

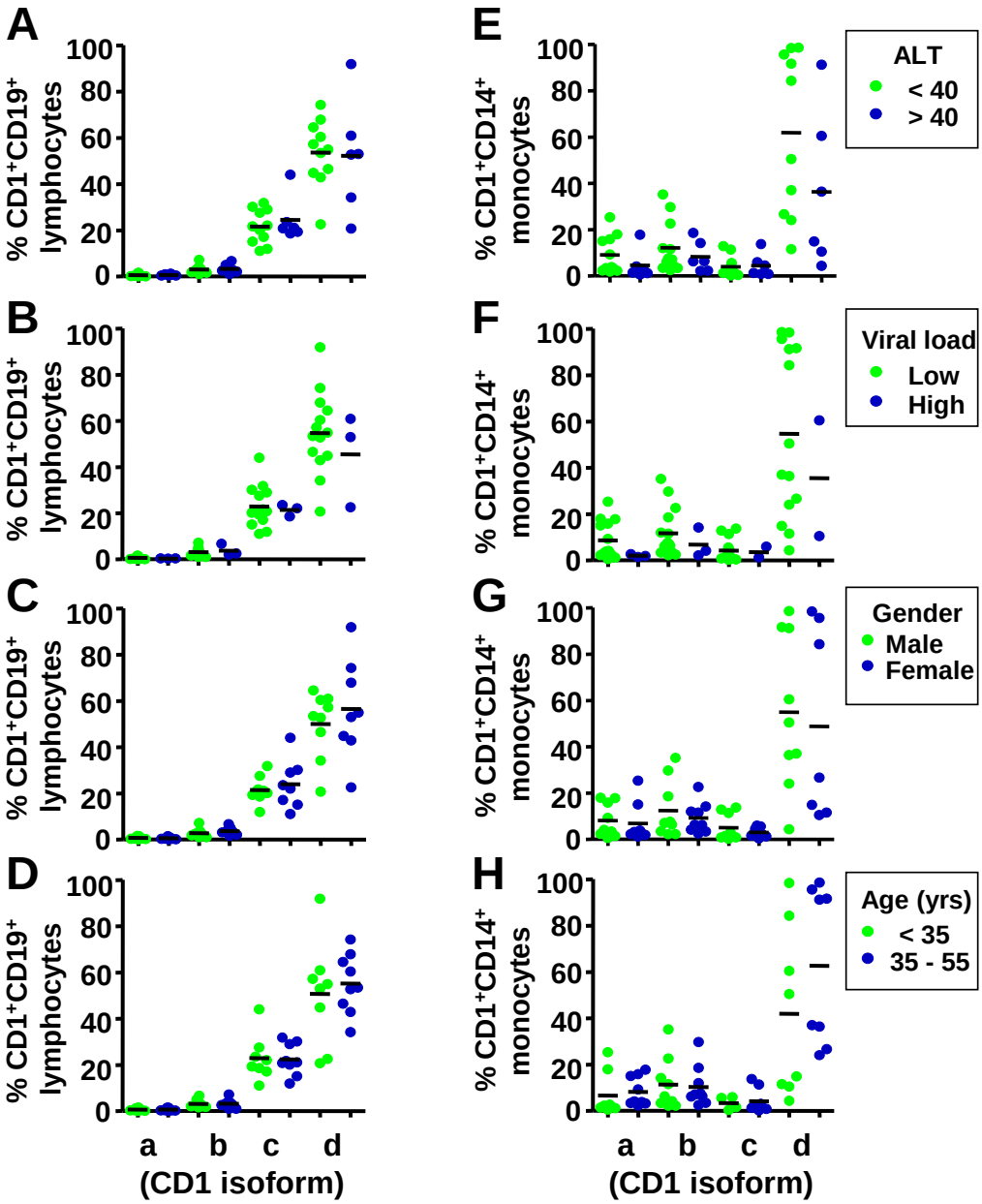

Figure 3.10: There are no significant differences in the frequencies of CD1a, b, c or CD1d$^+$ B cells or monocytes between patient groups within the study cohort. A, E, scatterplots showing frequencies of CD1$^+$CD19$^+$ lymphocytes **(A)** or CD1$^+$CD14$^+$ monocytes **(E)** in 12 HBV patients with ALT below 40 IU/ml and 6 HBV patients with ALT above 40 IU/ml. **B, F,** scatterplots showing frequencies of CD1$^+$CD19$^+$ lymphocytes **(B)** or CD1$^+$CD14$^+$ monocytes **(F)** in 15 HBV patients with viral load below 10,000 copies / ml and 3 HBV patients with viral load between 300,000 and 5x10^8 copies / ml. **C, G,** scatterplots showing frequencies of CD1$^+$CD19$^+$ lymphocytes **(C)** or CD1$^+$CD14$^+$ monocytes **(G)** in 9 male HBV patients and 9 female HBV patients. **D, H,** scatterplots showing frequencies of CD1$^+$CD19$^+$ lymphocytes **(D)** or CD1$^+$CD14$^+$ monocytes **(H)** in 8 HBV patients under the age of 35 years and 10 HBV patients between the age of 35 and 55 years.

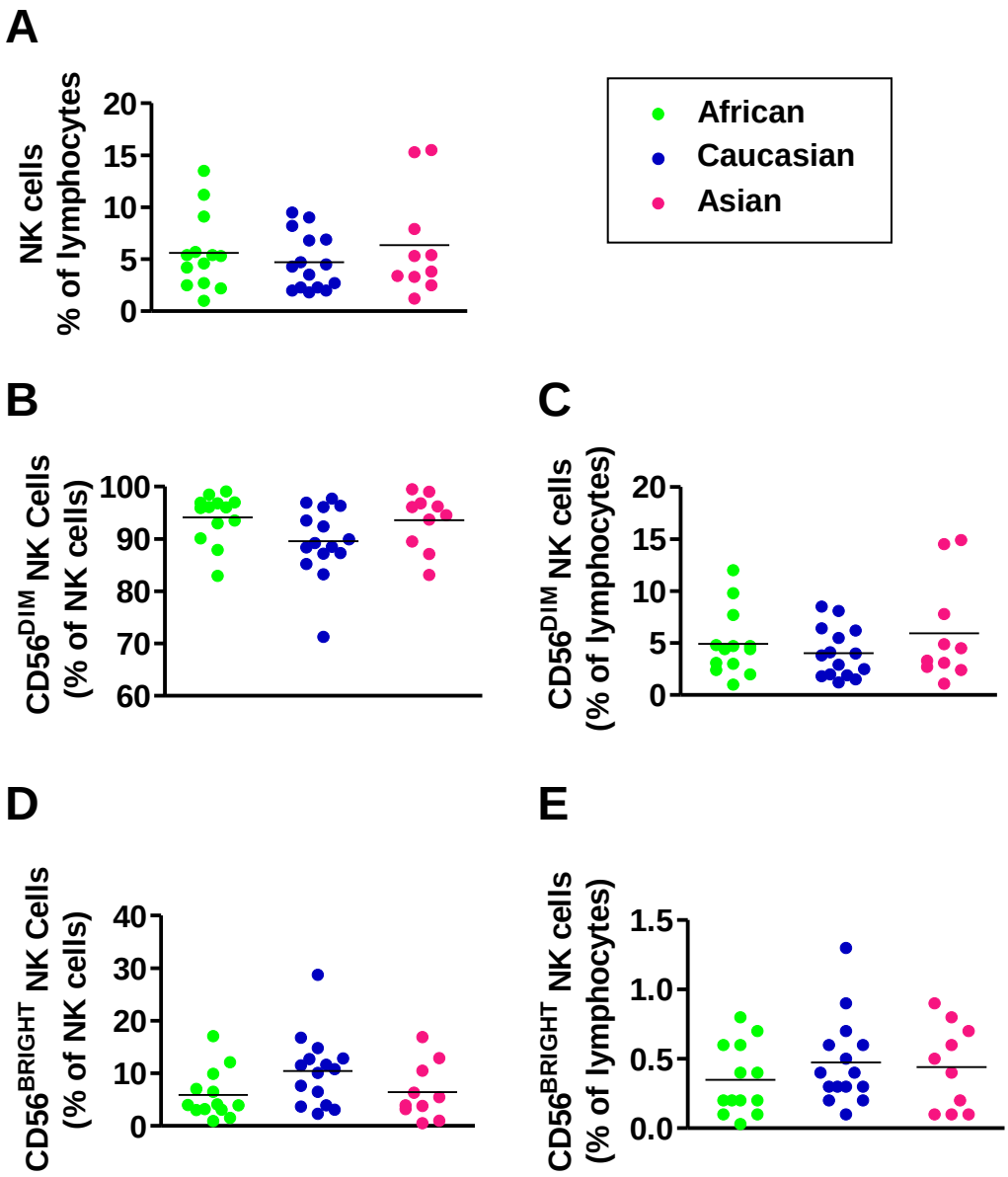

Figure 3.11: Frequencies of circulating total NK cells, CD56^{DIM} NK cells and CD56^{BRIGHT} NK cells are similar in african, caucasian and asian healthy control subjects. A, scatterplot showing the frequencies of circulating NK cells in 15 african (green), 15 caucasian (blue) and 10 asian (pink) healthy control subjects. **B, C, D and E,** scatterplots showing the frequencies of circulating CD56^{DIM} **(B,C)** and CD56^{BRIGHT} NK cells **(D,E),** as a percentage of NK cells **(B,D)** and as a percentage of lymphocytes **(C,E)** in 15 african (green), 15 caucasian (blue) and 10 asian (pink) healthy control subjects.

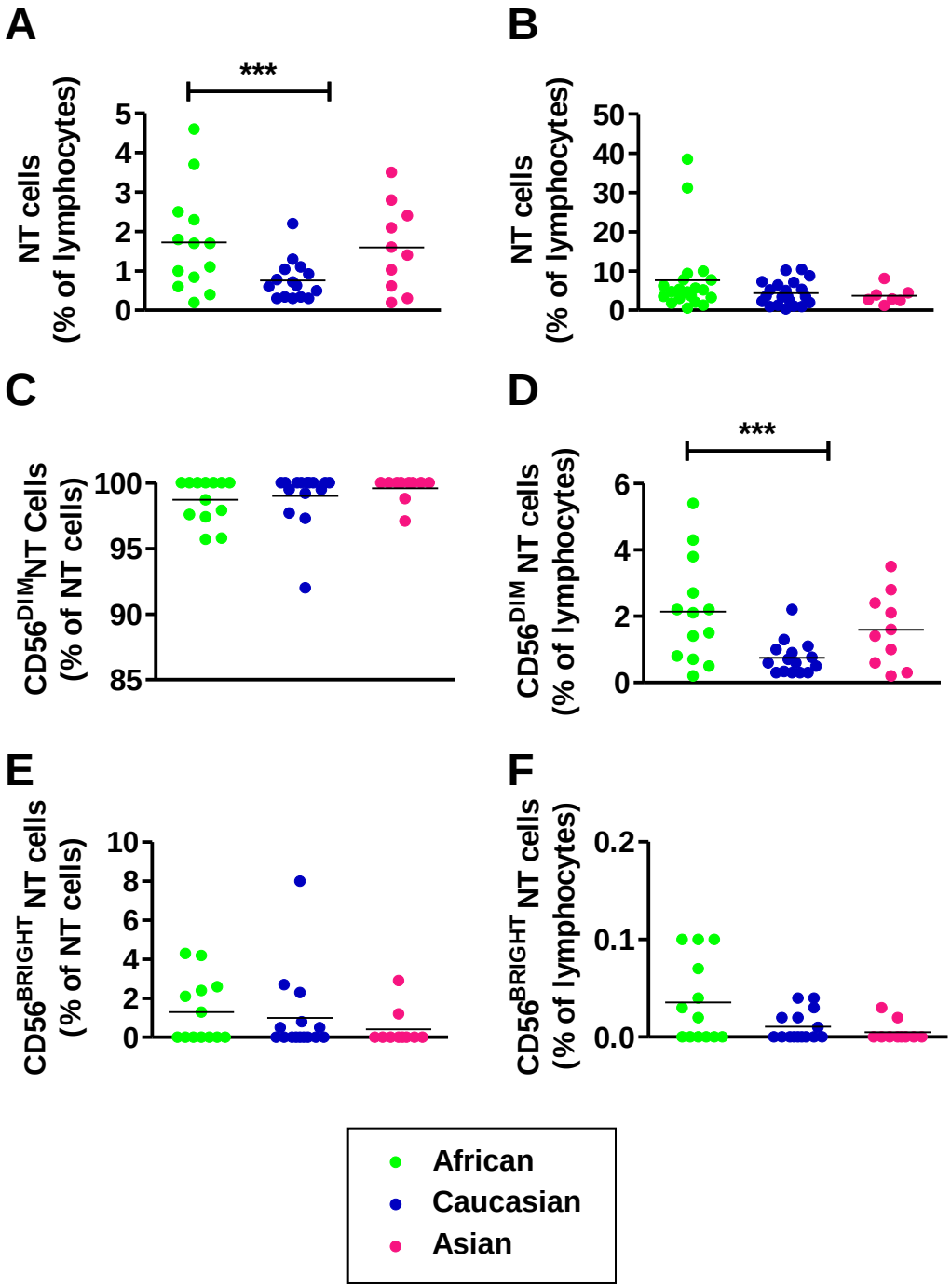

Figure 3.12: Differences in the frequencies of circulating total NT cells between african and caucasian control subjects but not between african and caucasian patients. A, scatterplots showing the frequencies of circulating NT cells in 15 african (green), 15 caucasian (blue) and 10 asian (pink) healthy control subjects **(A)** and, in 21 african (green), 21 caucasian (blue) and 7 asian (pink) HBV-infected subjects **(B). C, D, E and F,** scatterplots showing the frequencies of circulating $CD56^{DIM}$ **(C, D)** and $CD56^{BRIGHT}$ NT cells **(E, F),** as a percentage of NT cells **(C, E)** and as a percentage of lymphocytes **(D, F)** in 15 african (green), 15 caucasian (blue) and 10 asian (pink) healthy control subjects. (*p=0.05,**p=0.008).

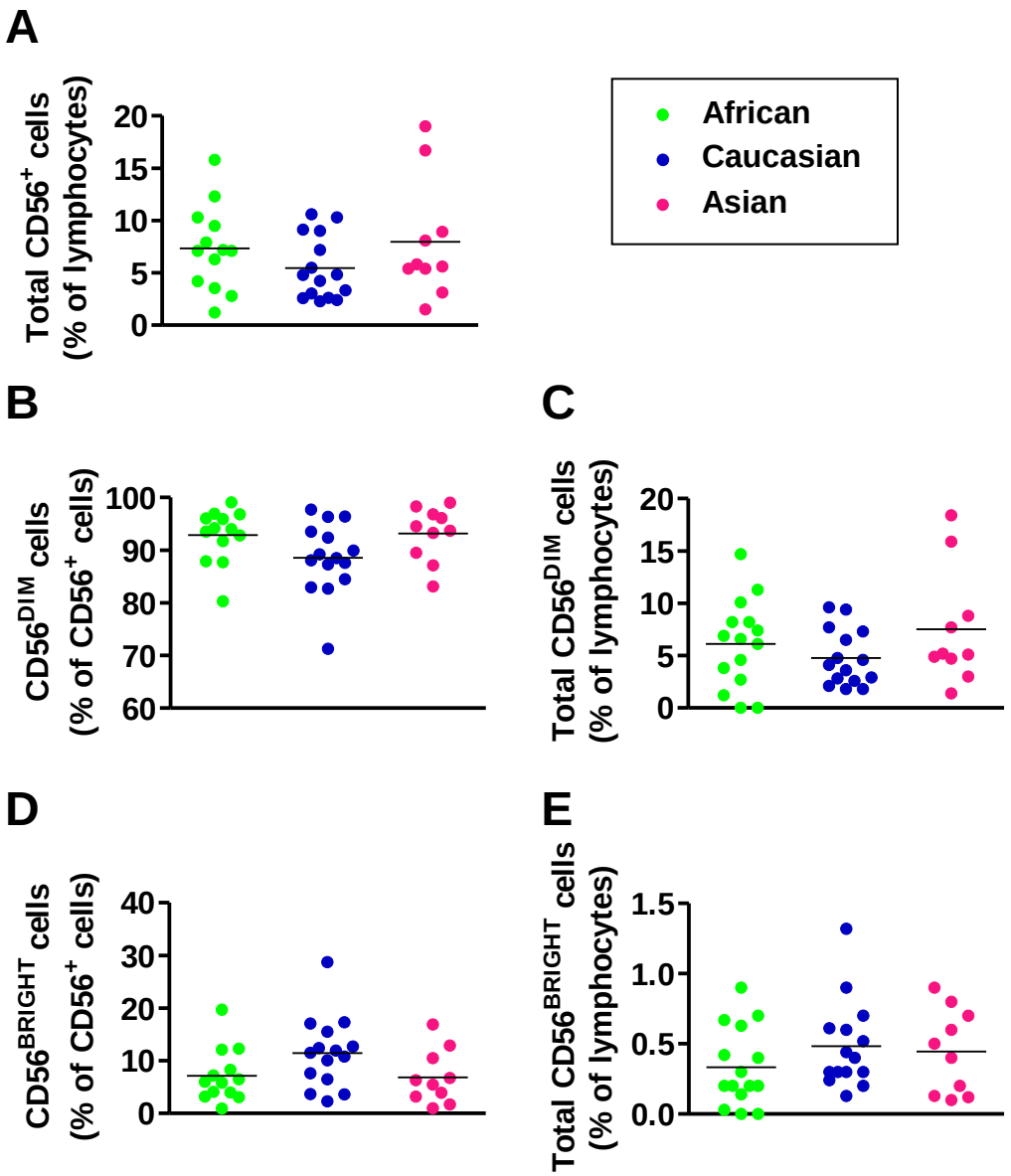

Figure 3.13: Frequencies of circulating total CD56^{+} cells, CD56^{DIM} cells and CD56^{BRIGHT} cells are similar in african, caucasians and asian healthy control subjects. A, scatterplot showing the frequencies of circulating total CD56^{+} cells in 15 african (green), 15 caucasian (blue) and 10 asian (pink) healthy control subjects. **B, C, D and E,** scatterplots showing the frequencies of circulating CD56^{DIM} **(B,C)** and CD56^{BRIGHT} cells **(D,E),** as a percentage of total CD56^{+} cells **(B,D)** and as a percentage of lymphocytes **(C,E)** in 15 african (green), 15 caucasian (blue) and 10 asian (pink) healthy control subjects.

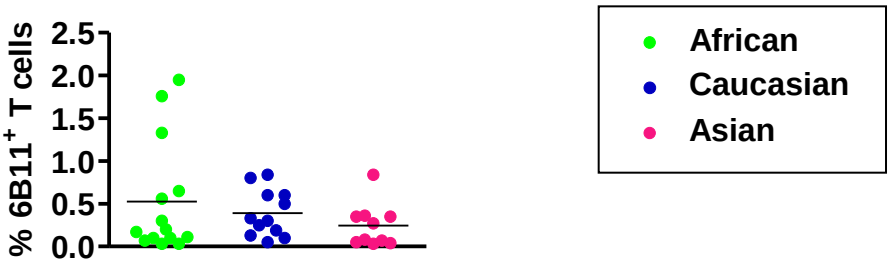

Figure 3.14: Frequencies of circulating invariant NKT cells are similar in african, caucasian and asian healthy control subjects. Scatterplot showing the frequencies of circulating iNKT cells, as a percentage of total T cells, in 15 african (green), 15 caucasian (blue) and 10 asian (pink) healthy control subjects.

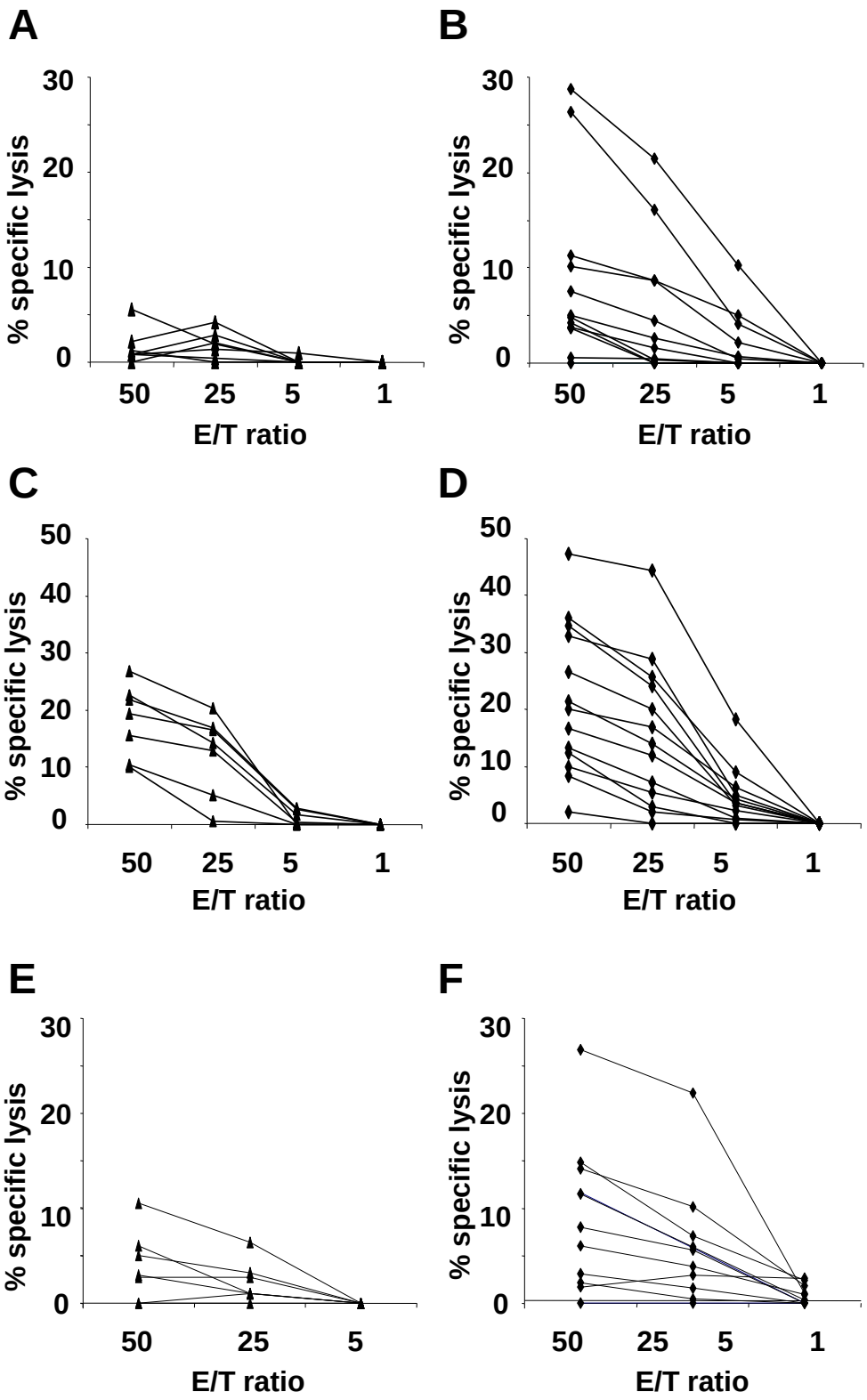
A
B
C
D
E
F
% specific lysis
E/T ratio
50
25
5
1
0
10
20
30
40

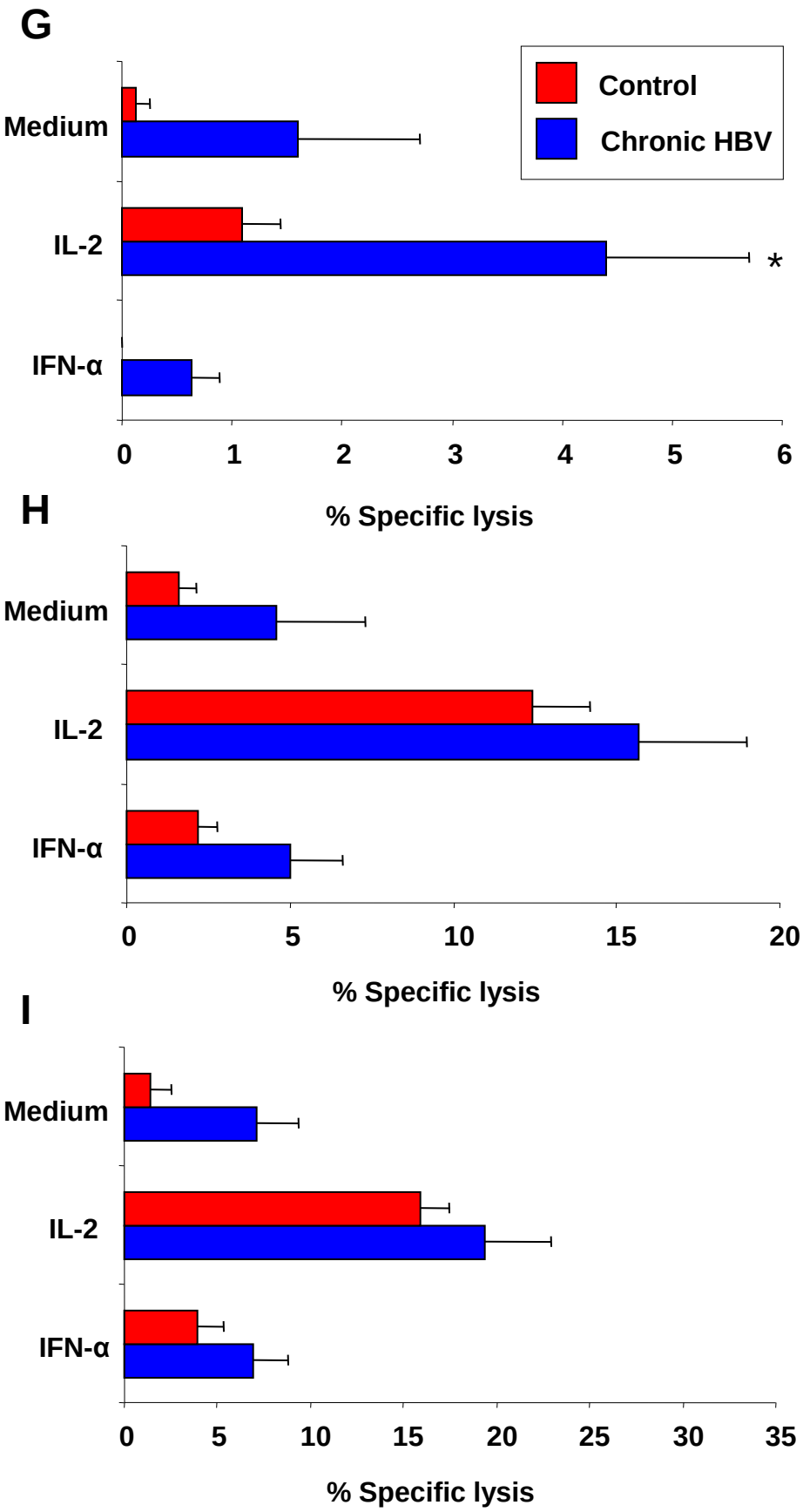
G
Control
Chronic HBV
Medium
IL-2
IFN-α
*
0
1
2
3
4
5
6
% Specific lysis
H
Medium
IL-2
IFN-α
0
5
10
15
20
% Specific lysis
I
Medium
IL-2
IFN-α
0
5
10
15
20
25
30
35
% Specific lysis

Figure 3.15: Consistently higher cytotoxic capabilities of PBMC from HBV patients.

A, B, plots showing percentages of specific lysis of K562 cells by unstimulated PBMC from 7 control subjects **(A)** and 15 HBV patients **(B)** at E:T ratios of 50, 25, 5 and 1:1. **C, D,** plots showing percentages of specific lysis of K562 cells by IL-2-stimulated PBMC from 7 control subjects **(C)** and 15 HBV patients **(D)** at E:T ratios of 50, 25, 5 and 1:1.

E, F, percentages of specific lysis of K562 cells by IFN-α-stimulated PBMC from 7 – 55 control subjects **(E)** and 15 HBV patients **(F)** at E:T ratios of 50, 25 and 5:1. **G, H, I,** bar charts showing mean percentages of specific lysis of K562 cells by natural, IL-2-induced and IFN-α-induced cytotoxicity carried out by PBMC from 7 control subjects (red) and 15 HBV patients (blue), at E:T ratios of 5:1 **(G)** and 25:1 **(H),** and PBMC from 55 control subjects (red) and 15 HBV patients (blue) at an E:T ratio of 50:1 **(I)** (*$p<0.05$).

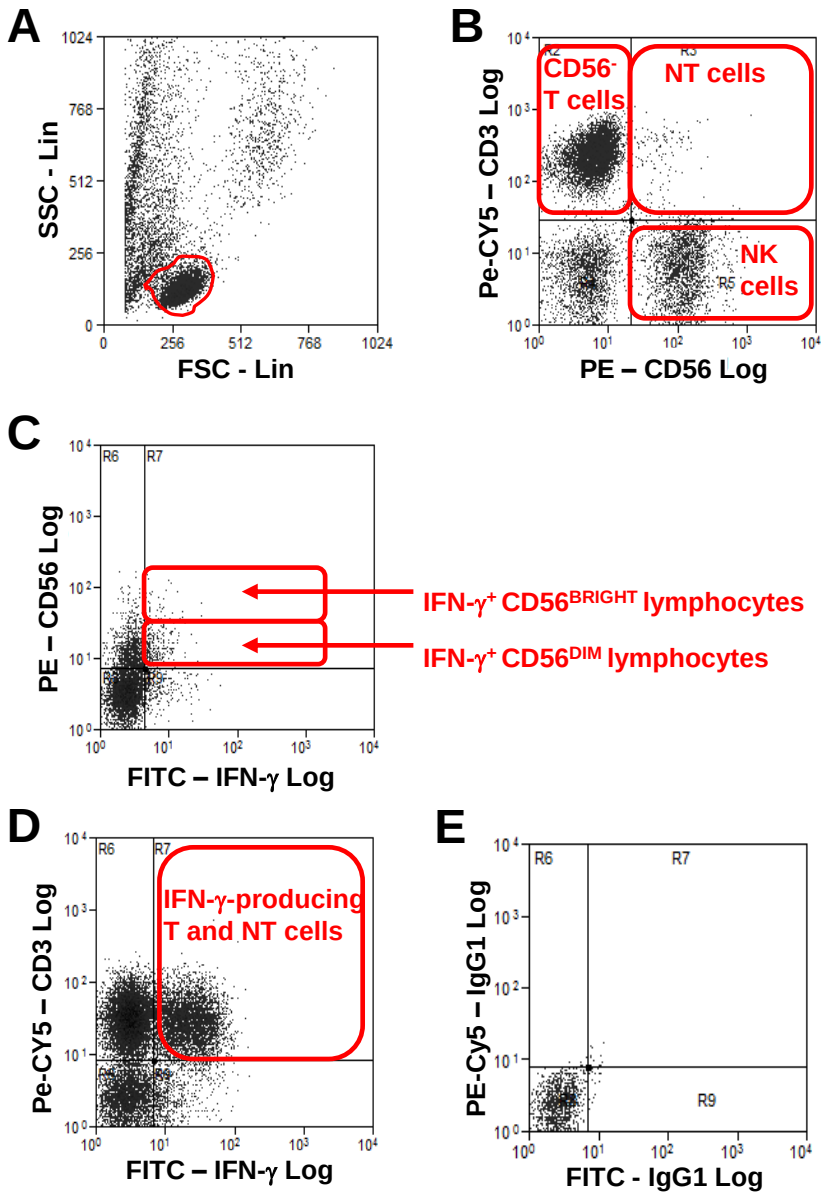

Figure 4.1: Representative dot plots of IFN-γ-producing NK, NT and CD56$^-$ T cells. A, representative dot plot of whole PBMC with region R1 gated around lymphocytes. **B, C,** dot plots of whole PBMC gated on lymphocytes and showing further gating on NK cell, NT and CD56$^-$ T cell populations **(B)** and gating on IFN-γ$^+$ CD56^{DIM} and CD56^{BRIGHT} NK cell populations **(C). D,** dot plot of whole PBMC gated on lymphocytes and showing further gating on IFN-γ-producing T and NT cell populations. **E,** dot plot of isotype control used to gate on IFN-γ$^+$ population

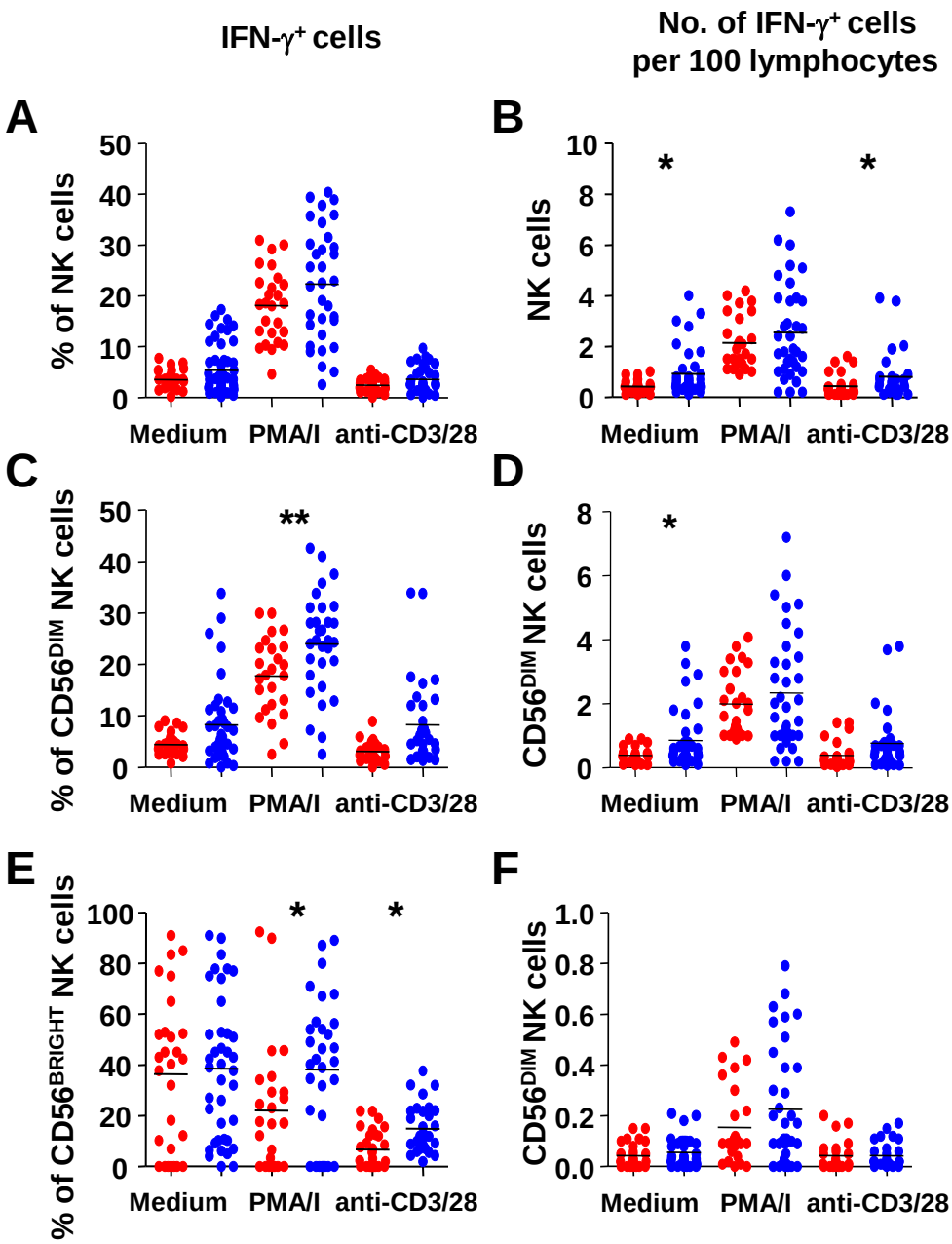

Figure 4.2: Higher frequencies of IFN-γ-producing CD56^{DIM} and CD56^{BRIGHT} NK cells and total NK cells in HBV infection. A, B, scatterplots showing frequencies of IFN-γ-producing NK cells quantified as a percentage of total NK cells **(A)** and total lymphocytes **(B)** in 23 controls (red) and 32 HBV patients (blue), following incubation in medium conditioned with and without PMA/I or anti-CD3 and anti-CD28 mAb. **C, D, E, F,** scatterplots showing frequencies of IFN-γ-producing CD56^{DIM} **(C, D)** and CD56^{BRIGHT} NK cells **(E, F)** quantified as a percentage of total CD56^{DIM} NK cells **(C)** or CD56^{BRIGHT} NK cells **(E)** and as a percentage of total lymphocytes **(D, F)** in 23 controls (red) and 26 HBV patients (blue), following incubation in medium conditioned with and without PMA/I or anti-CD3 and anti-CD28 mAb (*$p<0.05$, **$p<0.005$).

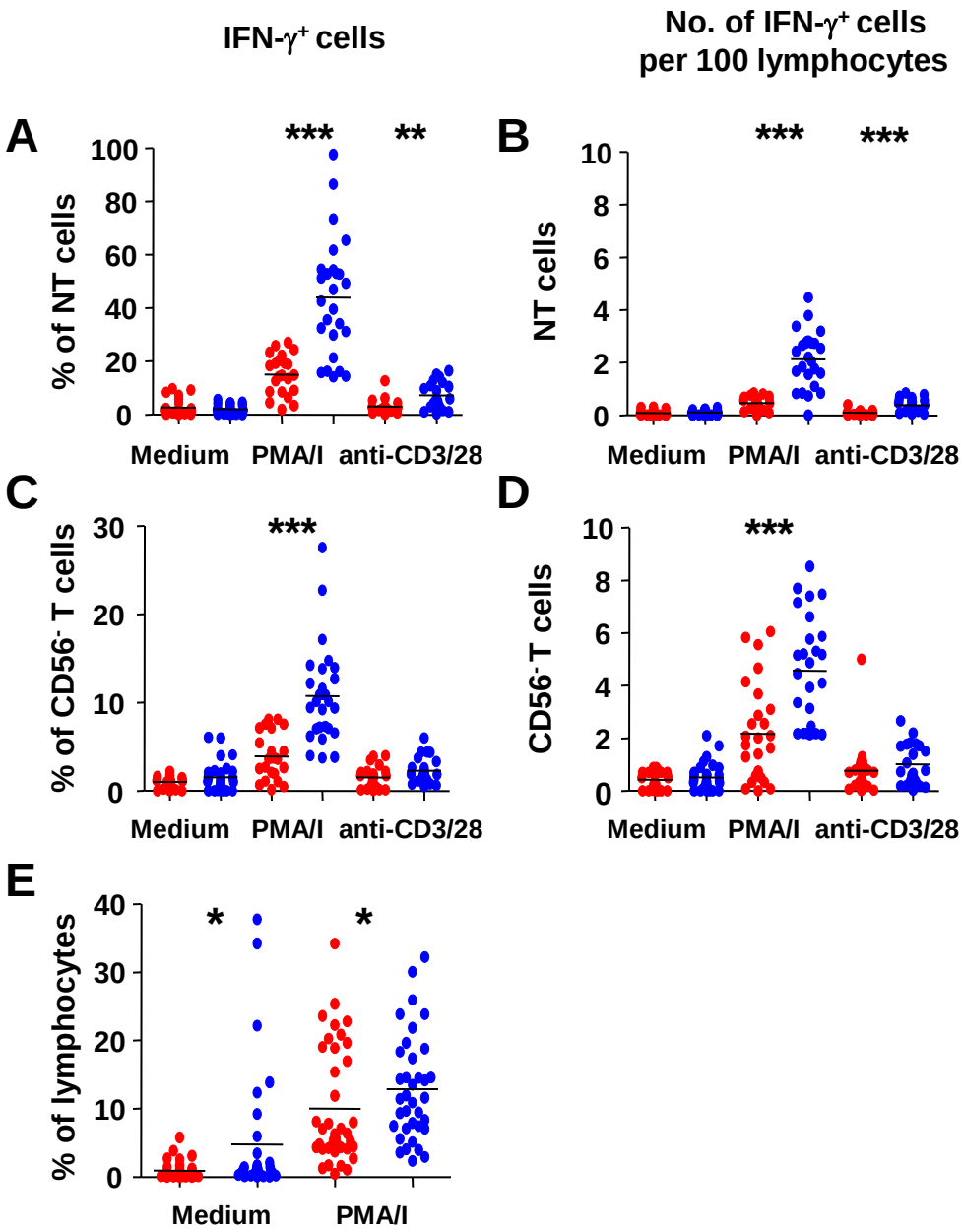

Figure 4.3: The frequencies of IFN-γ-producing NT, CD56$^-$ T and total lymphocytes are higher in chronic HBV infection. A, B, C, D, scatterplots showing frequencies of IFN-γ-producing NT **(A, B)** and CD56$^-$ T cells **(C, D)** quantified as a percentage of total NT cells **(A)** or total CD56$^-$ T cells **(C)** and as a percentage of total lymphocytes **(B, D)** in 23 controls (red) and 26 HBV patients (blue), following incubation in medium conditioned with and without PMA/I or anti-CD3 and anti-CD28 mAb. **E,** scatterplot showing frequencies of undtimulated and PMA/I-stimulated IFN-γ-producing lymphocytes in 34-39 controls (red) and 34-36 HBV patients (blue) (* $p<0.05$,** $p<0.005$, ***$p<0.0001$).

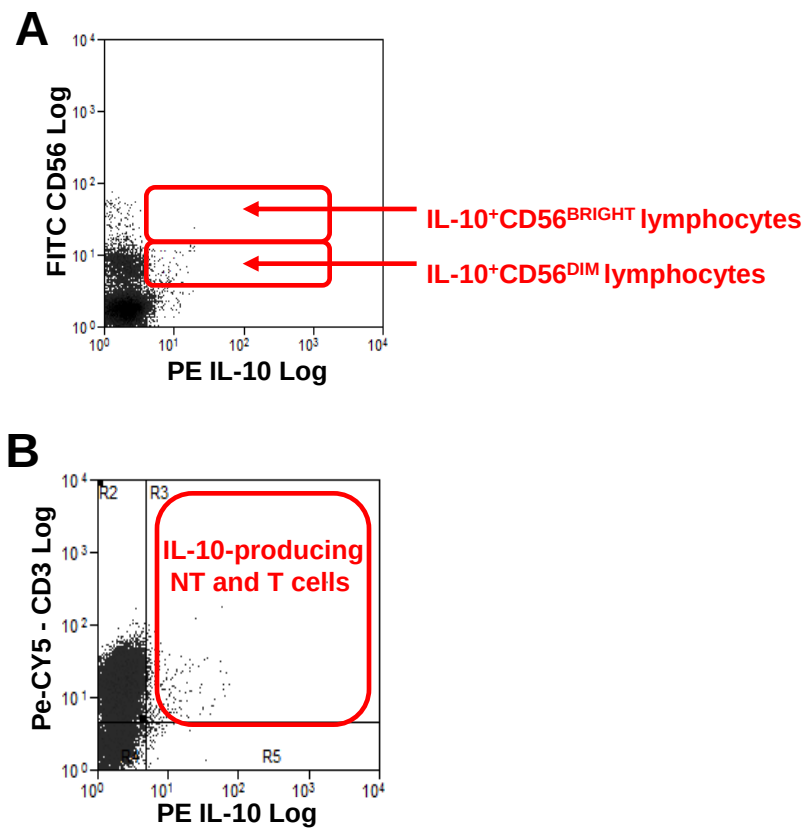

Figure 4.4: Representative dot plots of IL-10-producing NK, NT and CD56$^-$ T cells. A, representative dot plot of whole PBMC gated on lymphocytes and showing further gating on IL-10$^+$ CD56^{DIM} and CD56^{BRIGHT} NK cell populations. **B,** dot plot of whole PBMC gated on lymphocytes and showing further gating on IL-10-producing T and NT cell populations.

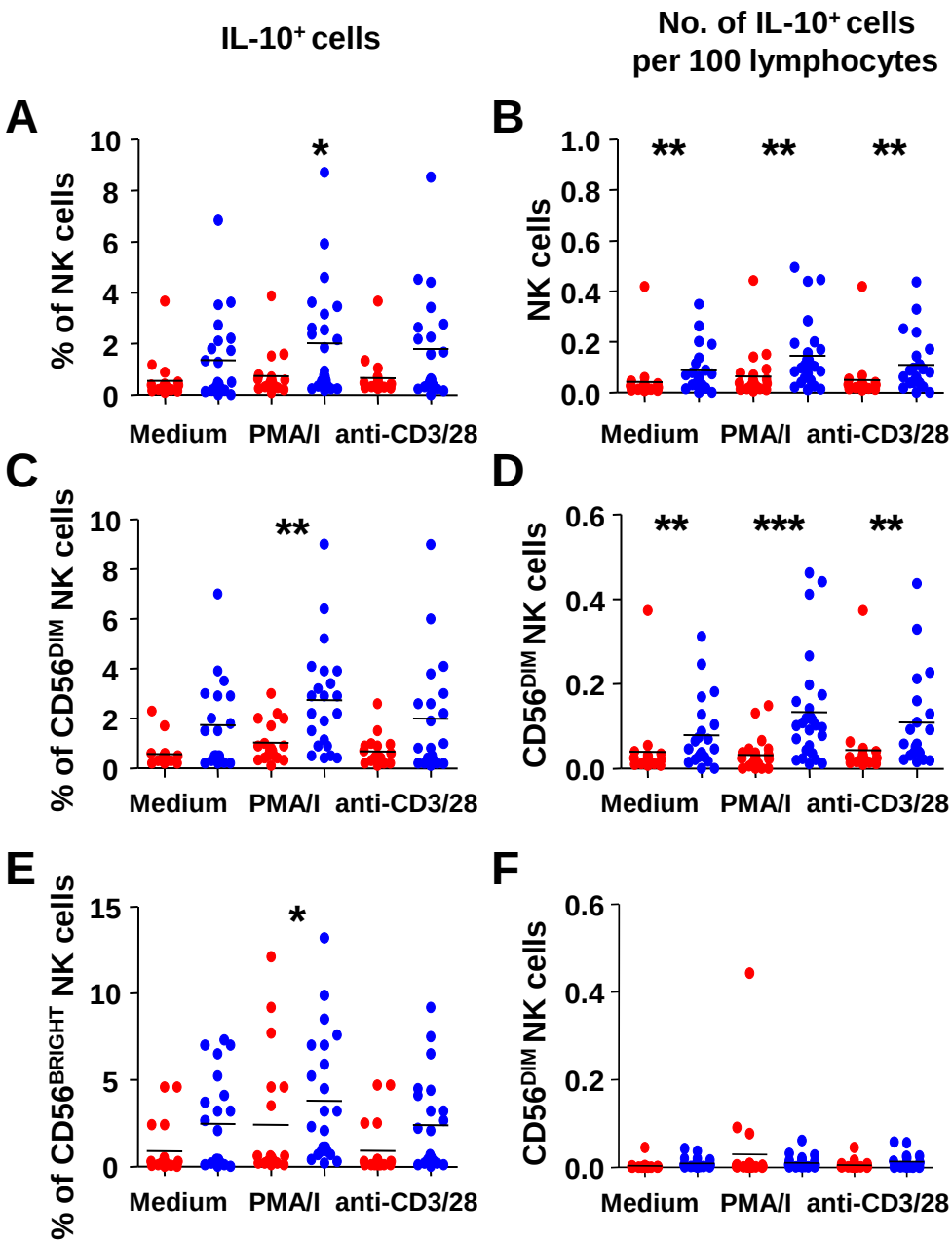

Figure 4.5: Higher frequencies of IL-10-producing CD56^{DIM} and CD56^{BRIGHT} NK cells and total NK cells in HBV infection. A, B, scatterplots showing frequencies of IL-10-producing NK cells quantified as a percentage of total NK cells **(A)** and total lymphocytes **(B)** in 23 controls (red) and 26 HBV patients (blue), following incubation in medium conditioned with and without PMA/I or anti-CD3 and anti-CD28 mAb. **C, D, E, F,** scatterplots showing frequencies of IL-10-producing CD56^{DIM} **(C, D)** and CD56^{BRIGHT} NK cells **(E, F)** quantified as a percentage of total CD56^{DIM} NK cells **(C)** or CD56^{BRIGHT} NK cells **(E)** and as a percentage of total lymphocytes **(D, F)** in 23 controls (red) and 26 HBV patients (blue), following incubation in medium conditioned with and without PMA/I or anti-CD3 and anti-CD28 mAb (*p<0.05,**p<=0.005,***p<0.0001).

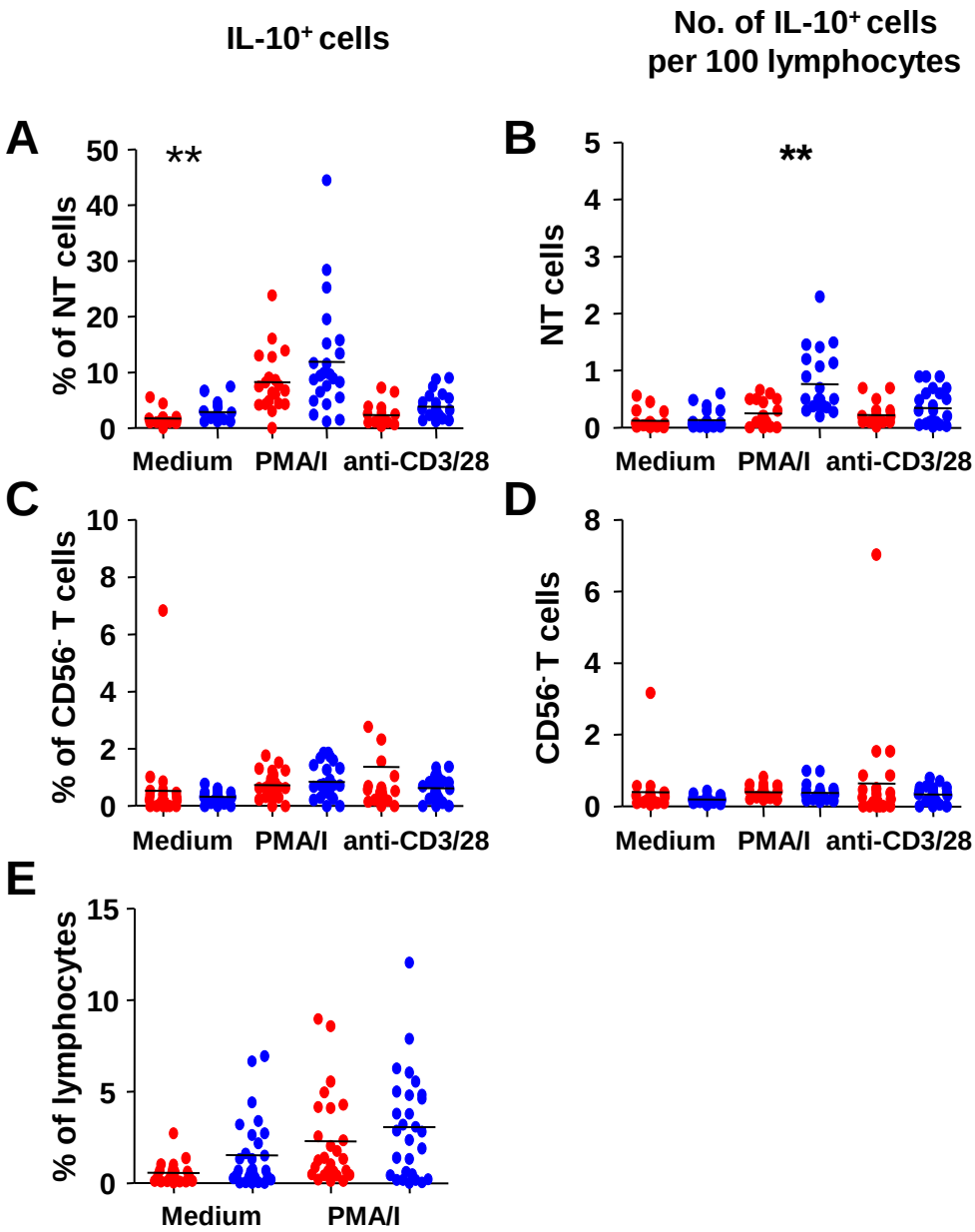

Figure 4.6: The frequencies of IL-10-producing NT cells are slightly higher in HBV infection but frequencies of CD56$^-$ T cells and total lymphocytes are unchanged. A, B, C, D, scatterplots showing frequencies of IL-10-producing NT **(A, B)** and CD56$^-$ T cells **(C, D)** quantified as a percentage of total NT cells **(A)** or total CD56$^-$ T cells **(C)** and as a percentage of total lymphocytes **(B, D)** in 23 controls (red) and 26 HBV patients (blue), following incubation in medium conditioned with and without PMA/I or anti-CD3 and anti-CD28 mAb. **E,** scatterplot showing frequencies of undtimulated and PMA/I-stimulated IL-10-producing lymphocytes in 21-26 controls (red) and 28 HBV patients (blue) (**p<0.005).

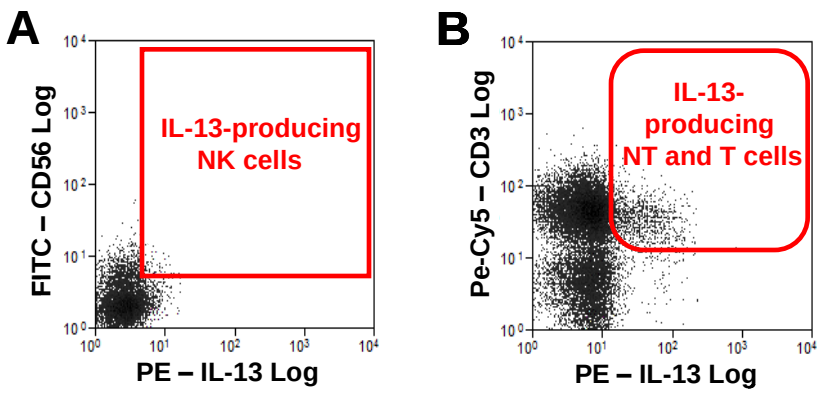

Figure 4.7: Representative dot plots of IL-13-producing NK, NT and CD56$^-$ T cells. A, representative dot plot of whole PBMC gated on lymphocytes and showing further gating on IL-13$^+$ NK cells**. B,** representative dot plot of whole PBMC gated on lymphocytes and showing further gating on IL-13-producing T and NT cell populations.

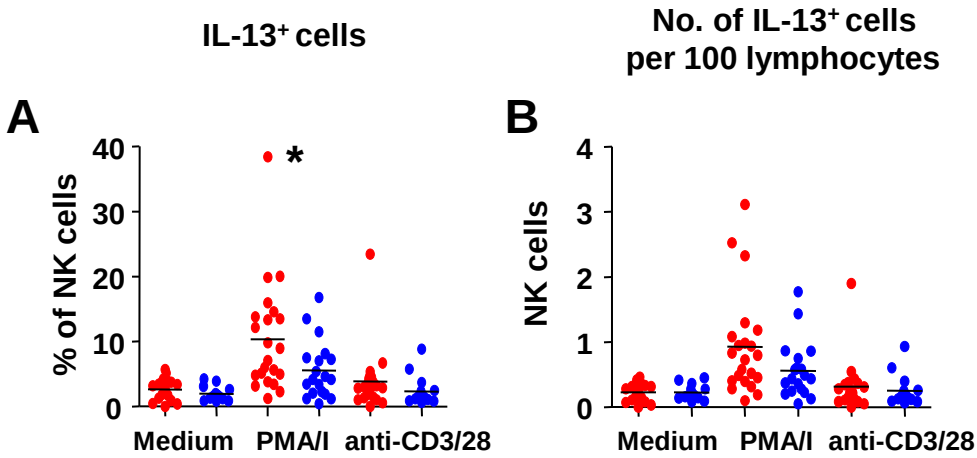

Figure 4.8: Responses of IL-13-producing NK cells to *in vitro* stimulation are lower in HBV infection. A, B, scatterplots showing frequencies of IL-13-producing NK cells quantified as a percentage of total NK cells **(A)** and total lymphocytes **(B)** in 18-22 controls (red) and 11-19 HBV patients (blue), following incubation in medium conditioned with and without PMA/I or anti-CD3 and anti-CD28 mAb (*$p<0.05$).

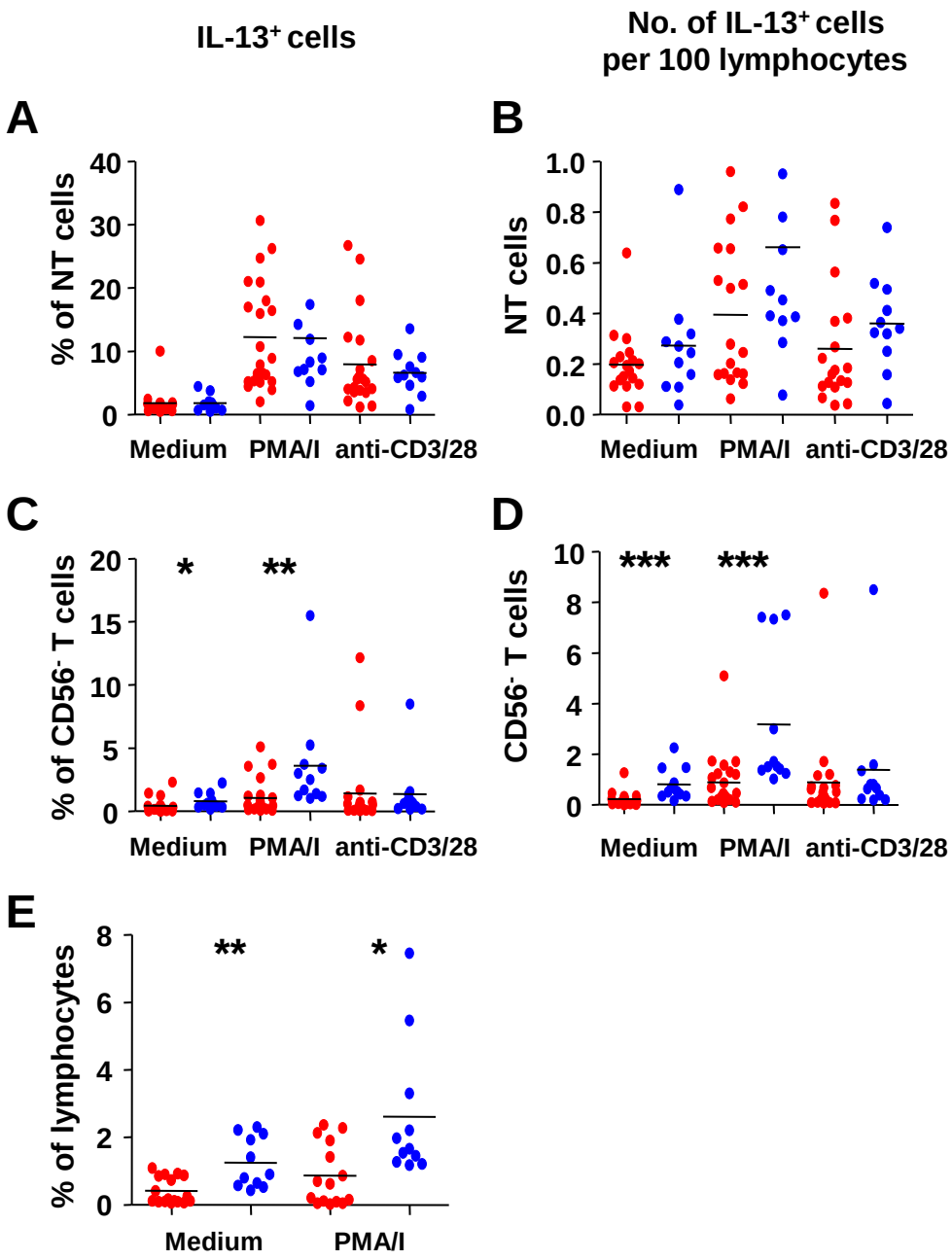

Figure 4.9: Altered frequencies of IL-13-producing CD56$^-$ T cells and total lymphocytes in HBV infection. A, B, C, D, scatterplots showing frequencies of IL-13-producing NT **(A, B)** and CD56$^-$ T cells **(C, D)** quantified as a percentage of total NT cells **(A)** or CD56$^-$ T cells **(C)** and as a percentage of total lymphocytes **(B, D)** in 18-22 controls (red) and 11-19 HBV patients (blue), following incubation in medium conditioned with and without PMA/I or anti-CD3 and anti-CD28 mAb. **E,** scatterplot showing frequencies of unstimulated and PMA/I-stimulated IL-13-producing lymphocytes in 15-17 controls (red) and 11 HBV patients (blue) (*p<0.05, **p<0.005, ***P<=0.0008).

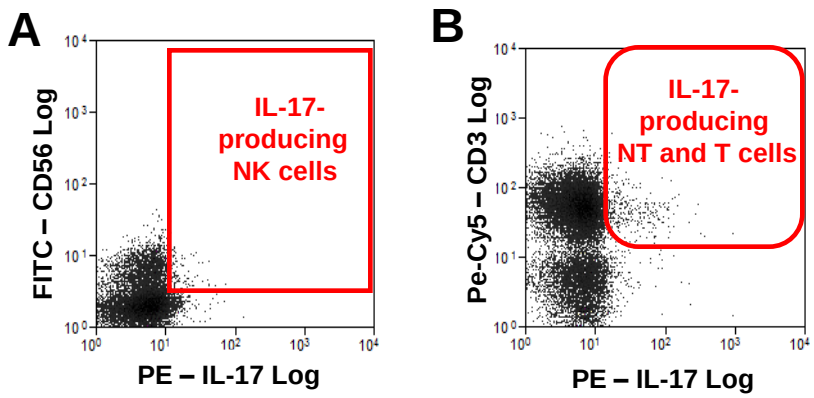

Figure 4.10: Representative dot plots of IL-17-producing NK, NT and CD56$^-$ T cells. A, representative dot plot of whole PBMC gated on lymphocytes and showing further gating on IL-17$^+$ NK cells**. B,** representative dot plot of whole PBMC gated on lymphocytes and showing further gating on IL-17-producing T and NT cell populations.

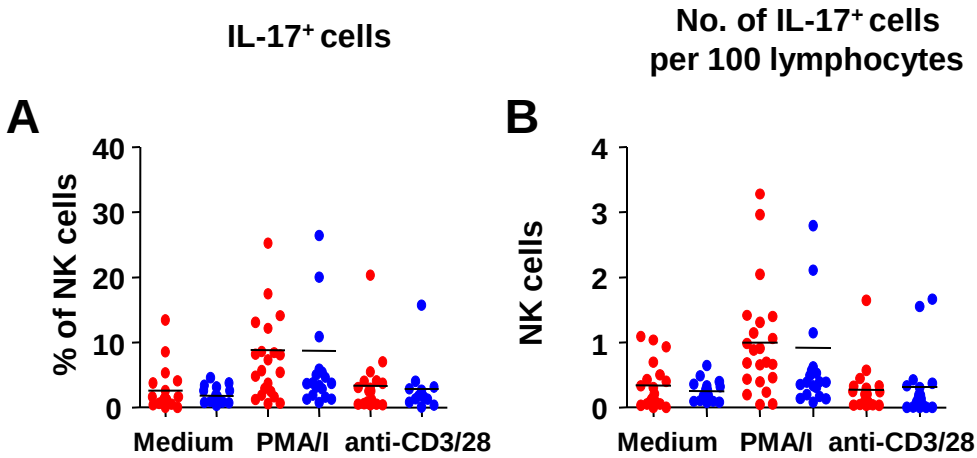

Figure 4.11: Frequencies of IL-17-producing NK cells are similar in HBV patients and control subjects. A, B, scatterplots showing frequencies of IL-17-producing NK cells quantified as a percentage of total NK cells **(A)** and total lymphocytes **(B)** in 19-22 controls (red) and 11-19 HBV patients (blue), following incubation in medium conditioned with and without PMA/I or anti-CD3 and anti-CD28 mAb.

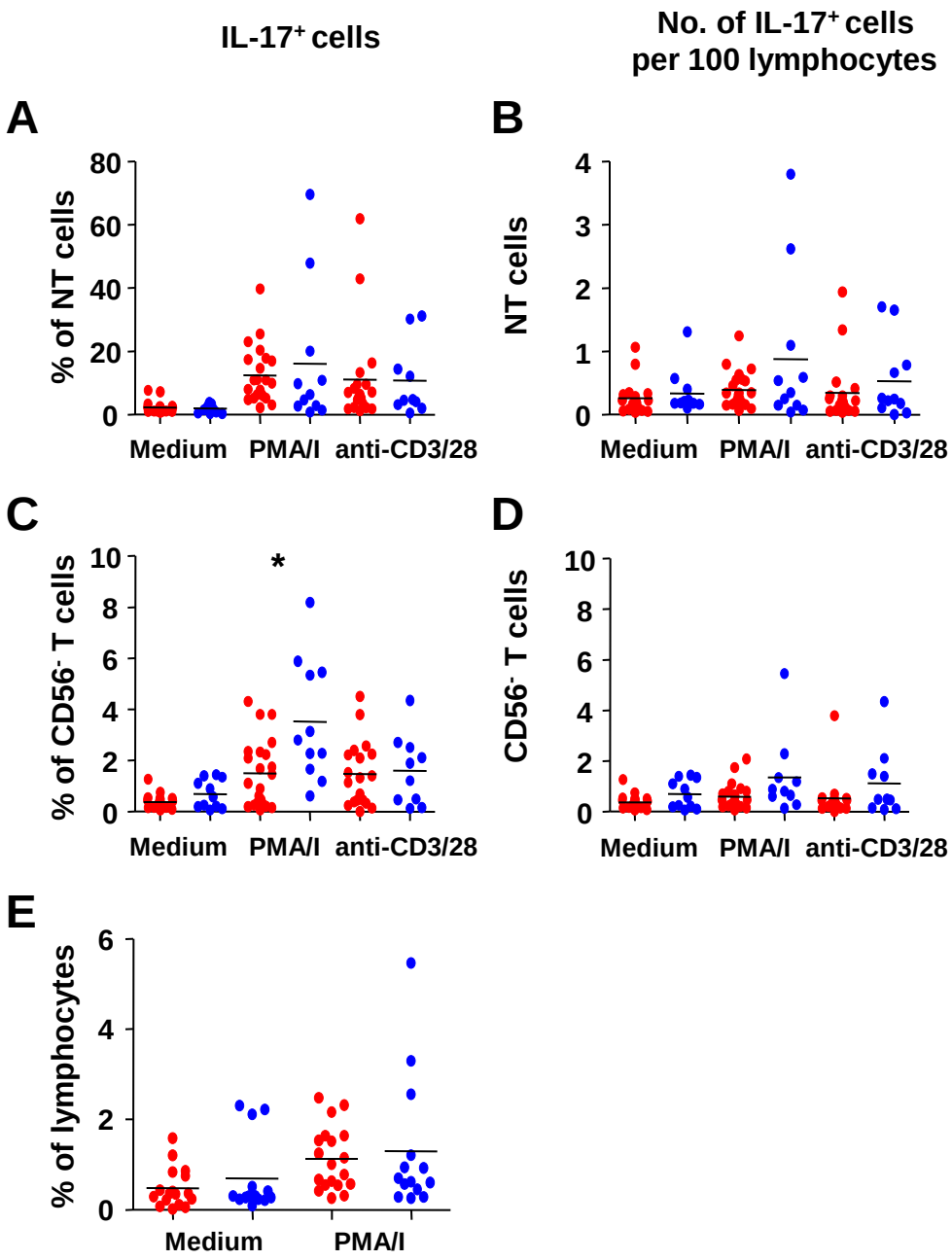

Figure 4.12: Slightly higher frequencies of IL-17-producing CD56$^-$ T cells and total lymphocytes in HBV infection. A, B, C, D, scatterplots showing frequencies of IL-17 producing NT **(A, B)** and CD56$^-$ T cells **(C, D)** quantified as a percentage of total NT cells **(A)** or CD56$^-$ T cells **(C)** and as a percentage of total lymphocytes **(B, D)** in 18-22 controls (red) and 11-19 HBV patients (blue), following incubation in medium conditioned with and without PMA/I or anti-CD3 and anti-CD28 mAb. **E,** scatterplot showing frequencies of unstimulated and PMA/I-stimulated IL-17-producing lymphocytes in 17-19 controls (red) and 14 HBV patients (blue) (*$p<0.01$).

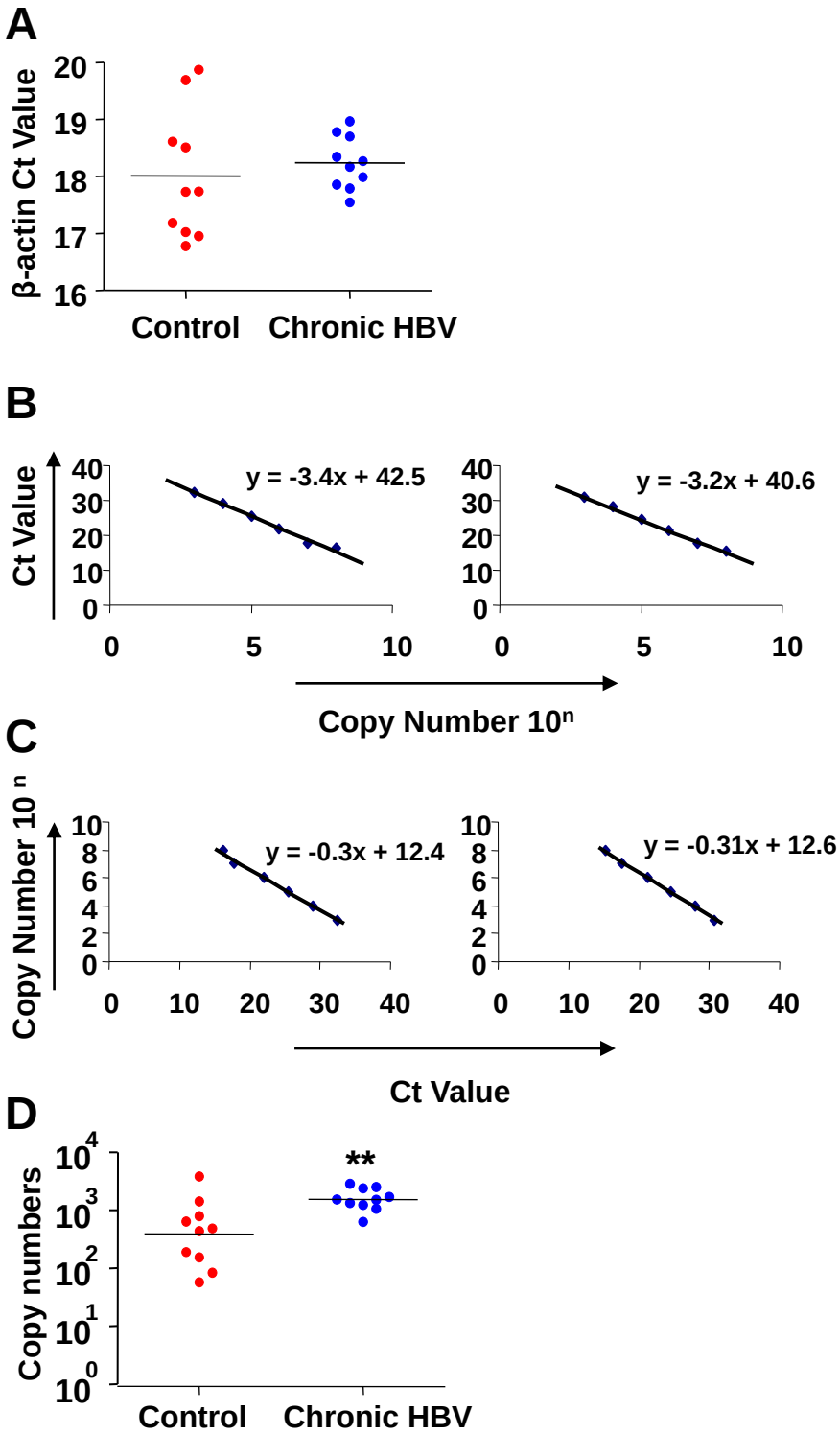

Figure 4.13: The levels of IFN-γ RNA are higher in PBMC from HBV patients. Scatterplots showing **(A)** β-actin Ct values in control subjects (red) and HBV patients (blue). **C, D,** line graphs showing standard curves for β-actin **(top)** and IFN-γ **(bottom)** with Ct Values on the y-axis and copy numbers on the x-axis **(C)** and, with copy numbers on the y-axis and Ct Values on the x-axis **(D)**. **E,** scatterplot showing the copy numbers of IFN-γ RNA in 10 control subjects (red) and 10 HBV patients (blue), (** p=0.008).

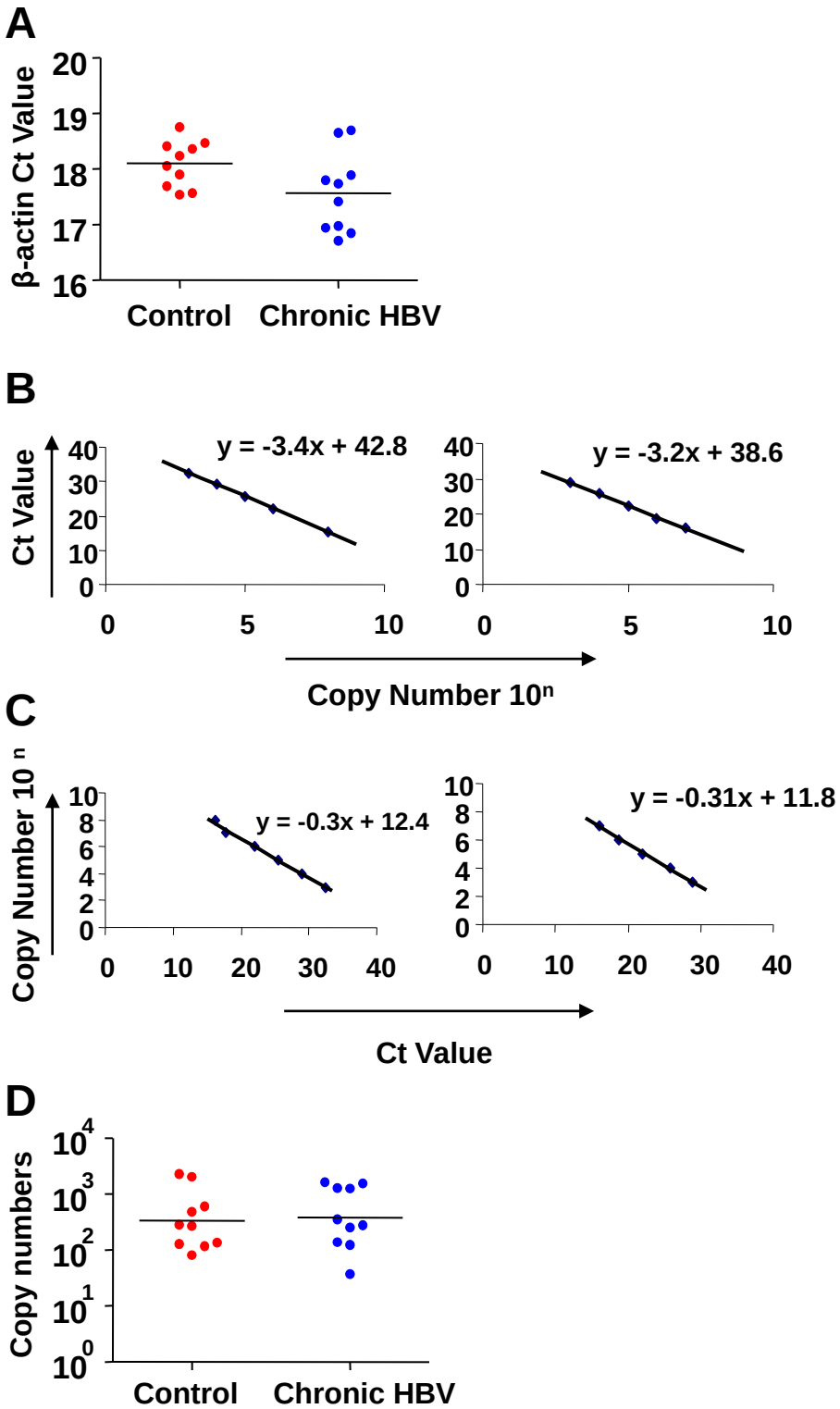

Figure 4.14: No significant difference in the level of IL-10 RNA in PBMC from HBV patients. A, Scatterplot showing β-actin Ct values in control subjects (red) and HBV patients (blue). **B, C,** line graphs showing standard curves for β-actin **(top)** and IL-10 **(bottom)** with Ct Values on the y-axis and copy numbers on the x-axis **(B)** and, with copy numbers on the y-axis and Ct Values on the x-axis **(C)**. **D,** scatterplot showing the copy numbers of IL-10 RNA in 10 control subjects (red) and 10 HBV patients (blue).

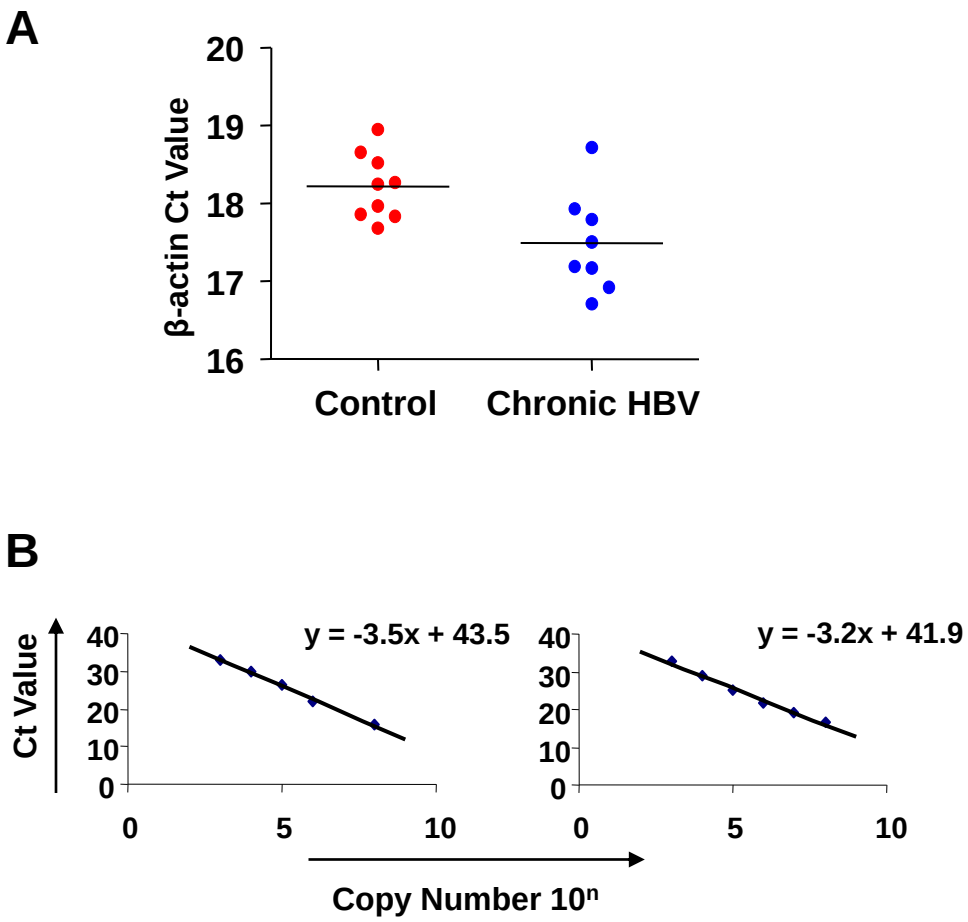

Figure 4.15: Undetectable levels of IL-17A RNA in PBMC from HBV patients and healthy control subjects. A, Scatterplot showing β-actin Ct values in control subjects (red) and HBV patients (blue). **B,** line graphs showing standard curves for β-actin **(top)** and IL-17A **(bottom)** with Ct Values on the y-axis and copy numbers on the x-axis.

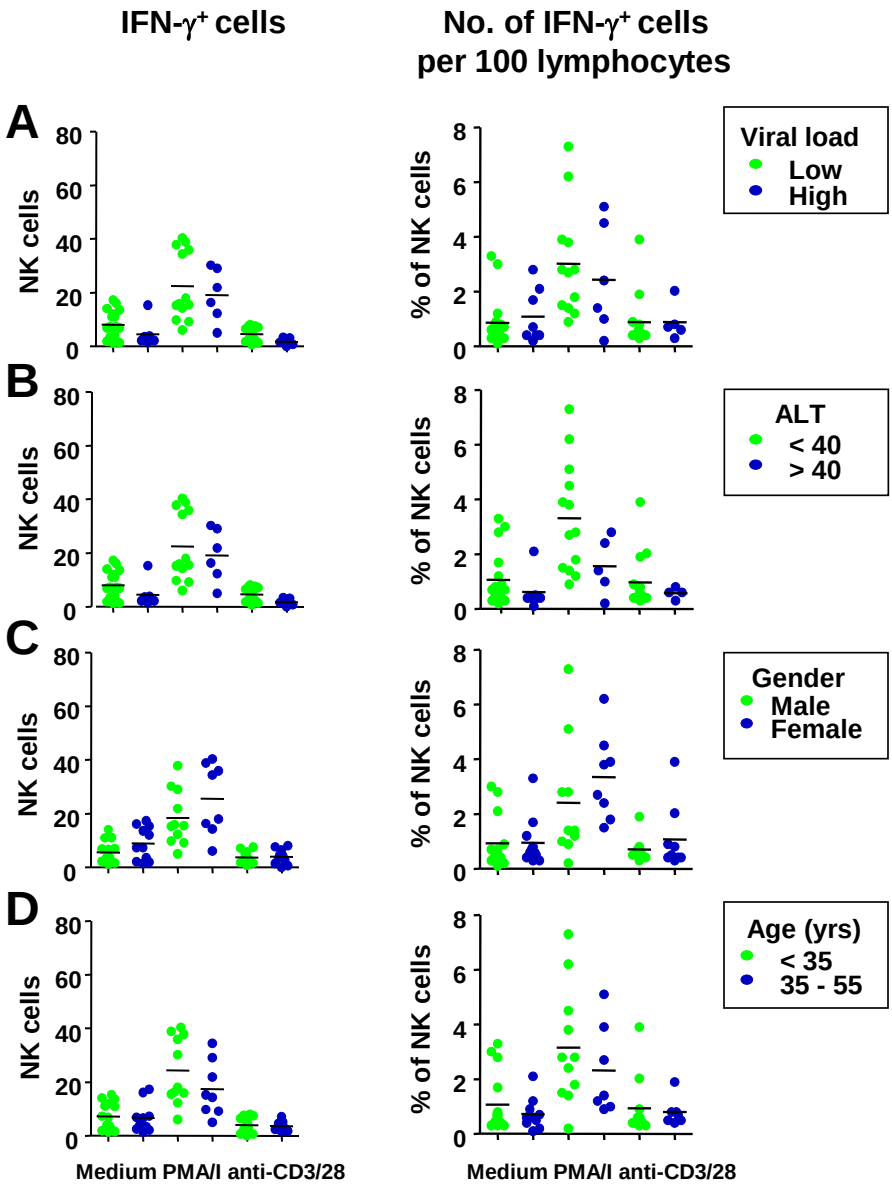

Figure 4.16: Frequencies of IFN-γ-producing NK cells in subgroups of HBV patients. A, B, C, D (left), scatterplots showing frequencies of IFN-γ-producing NK cells as a percentage of the total NK cell population in 13-17 HBV patients with viral load below 10,000 copies / ml and 5-8 patients with viral load between 100,000 and $3.2x10^8$ copies / ml **(A)**, 13-18 HBV patients with ALT below 40 IU/ml and 5-7 patients with ALT above 40 IU/ml **(B)**, 10-14 male HBV patients and 8-11 female patients **(C)** and, 10 HBV patients under the age of 35 years and 8 patients between the age of 35 and 55 years **(D)**. **A, B, C, D (right),** scatterplots showing frequencies of IFN-γ-producing NK cells as a percentage of total lymphocytes in 13-17 HBV patients with viral load below 10,000 copies / ml and 5-8 patients with viral load between 100,000 and $3.2x10^8$ copies / ml **(A)**, 13-18 HBV patients with ALT below 40 IU/ml and 5-7 patients with ALT above 40 IU/ml **(B)**, 10-14 male HBV patients and 8-11 female patients **(C)** and, 10 HBV patients under the age of 35 years and 8 patients between the age of 35 and 55 years **(D)**.

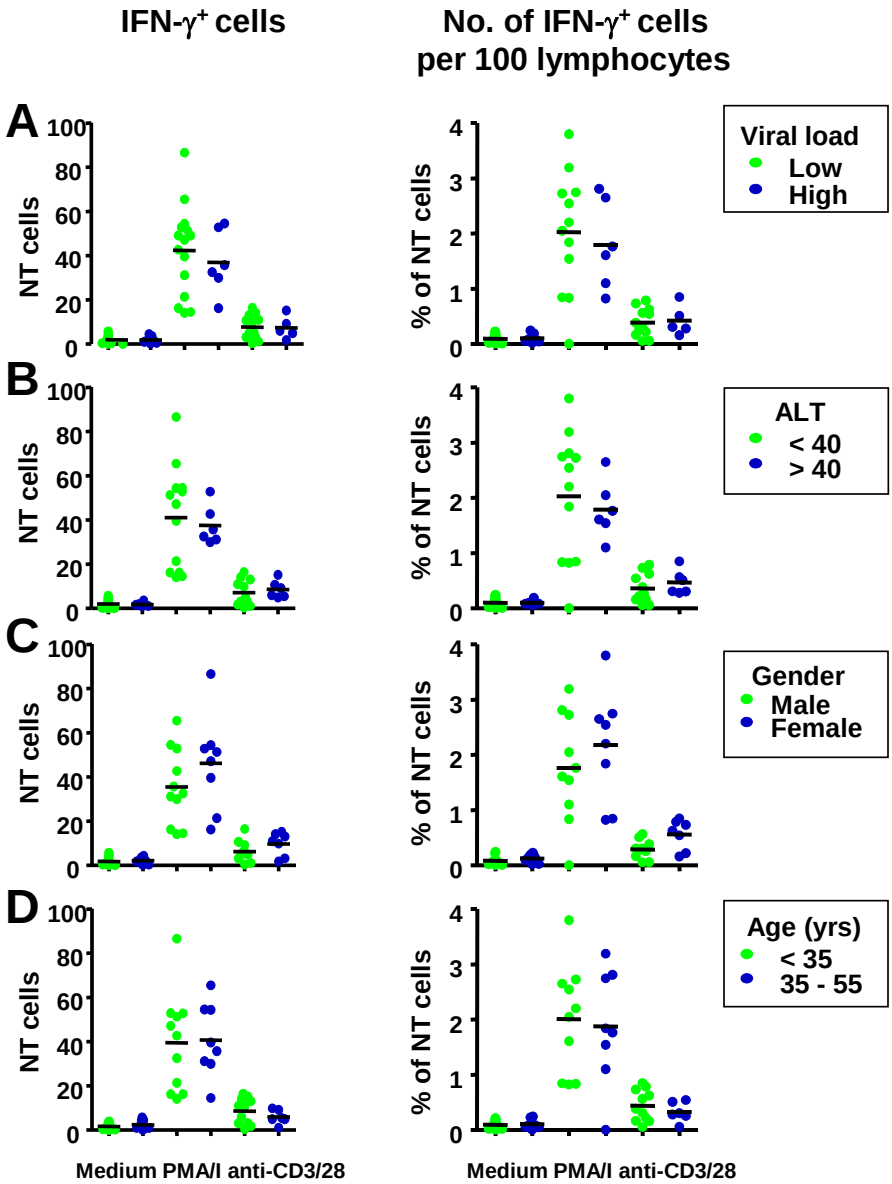

Figure 4.17: Frequencies of IFN-γ-producing NT cells in subgroups of HBV patients. A, B, C, D (left) showing frequencies of IFN-γ-producing NT cells as a percentage of the total NT cell population in 12-15 HBV patients with viral load below 10,000 copies / ml and 5-7 HBV patients with viral load between 100,000 and $3.2x10^8$ copies / ml **(A)**, 11-15 HBV patients with ALT below 40 IU/ml and 6 HBV patients with ALT above 40 IU/ml **(B)**, 10-13 male HBV patients and 7-8 female HBV patients **(C)** and, 10-12 HBV patients under the age of 35 years and 6-9 HBV patients between the age of 35 and 55 years **(D)**. **A, B, C, D (right),** scatterplots showing frequencies of IFN-γ-producing NT cells as a percentage of total lymphocytes in 12-15 HBV patients with viral load below 10,000 copies / ml and 5-7 HBV patients with viral load between 100,000 and $3.2x10^8$ copies / ml **(A)**, 11-15 HBV patients with ALT below 40 IU/ml and 6 HBV patients with ALT above 40 IU/ml **(B)**, 10-13 male HBV patients and 7-8 female HBV patients **(C)** and, 10-12 HBV patients under the age of 35 years and 6-9 HBV patients between the age of 35 and 55 years **(D)**.

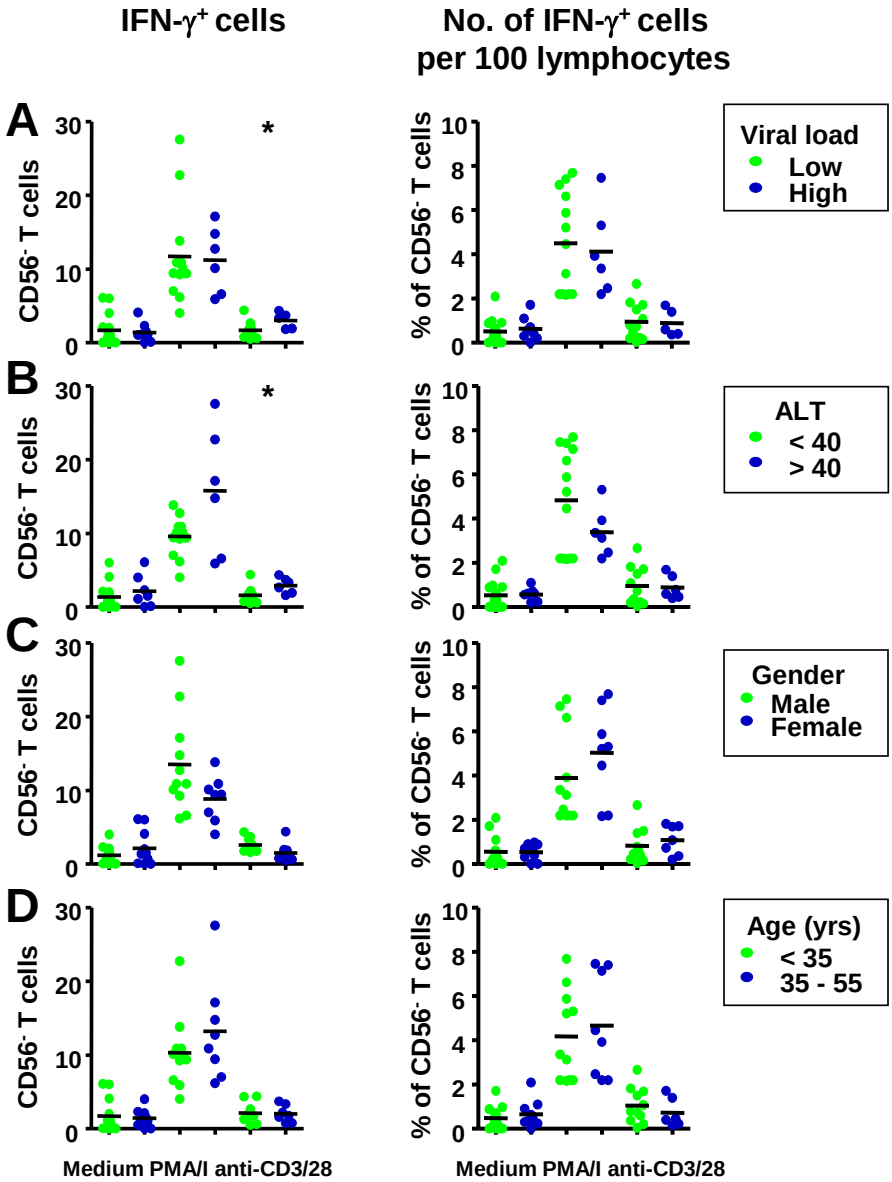

Figure 4.18: Frequencies of IFN-γ-producing CD56$^-$ T cells in subgroups of HBV patients. A, B, C, D (left), scatterplots showing frequencies of IFN-γ-producing CD56$^-$ T cells as a percentage of the total CD56$^-$ T cell population in 12-17 HBV patients with viral load below 10,000 copies / ml and 5-8 HBV patients with viral load between 100,000 and 3.2x10^8 copies / ml **(A)**, 11-17 HBV patients with ALT below 40 IU/ml and 6-8 HBV patients with ALT above 40 IU/ml **(B)**, 9-14 male HBV patients and 8-11 female HBV patients **(C)** and, 11-15 HBV patients under the age of 35 years and 6-10 HBV patients between the age of 35 and 55 years **(D)**. **A, B, C, D (right),** scatterplots showing frequencies of IFN-γ-producing CD56$^-$ T cells as a percentage of total lymphocytes in 12-17 HBV patients with viral load below 10,000 copies / ml and 5-8 HBV patients with viral load between 100,000 and 3.2x10^8 copies / ml **(A)**, 11-17 HBV patients with ALT below 40 IU/ml and 6-8 HBV patients with ALT above 40 IU/ml **(B)**, 9-14 male HBV patients and 8-11 female HBV patients **(C)** and, 11-15 HBV patients under the age of 35 years and 6-10 HBV patients between the age of 35 and 55 years **(D)** (*$p<0.05$).

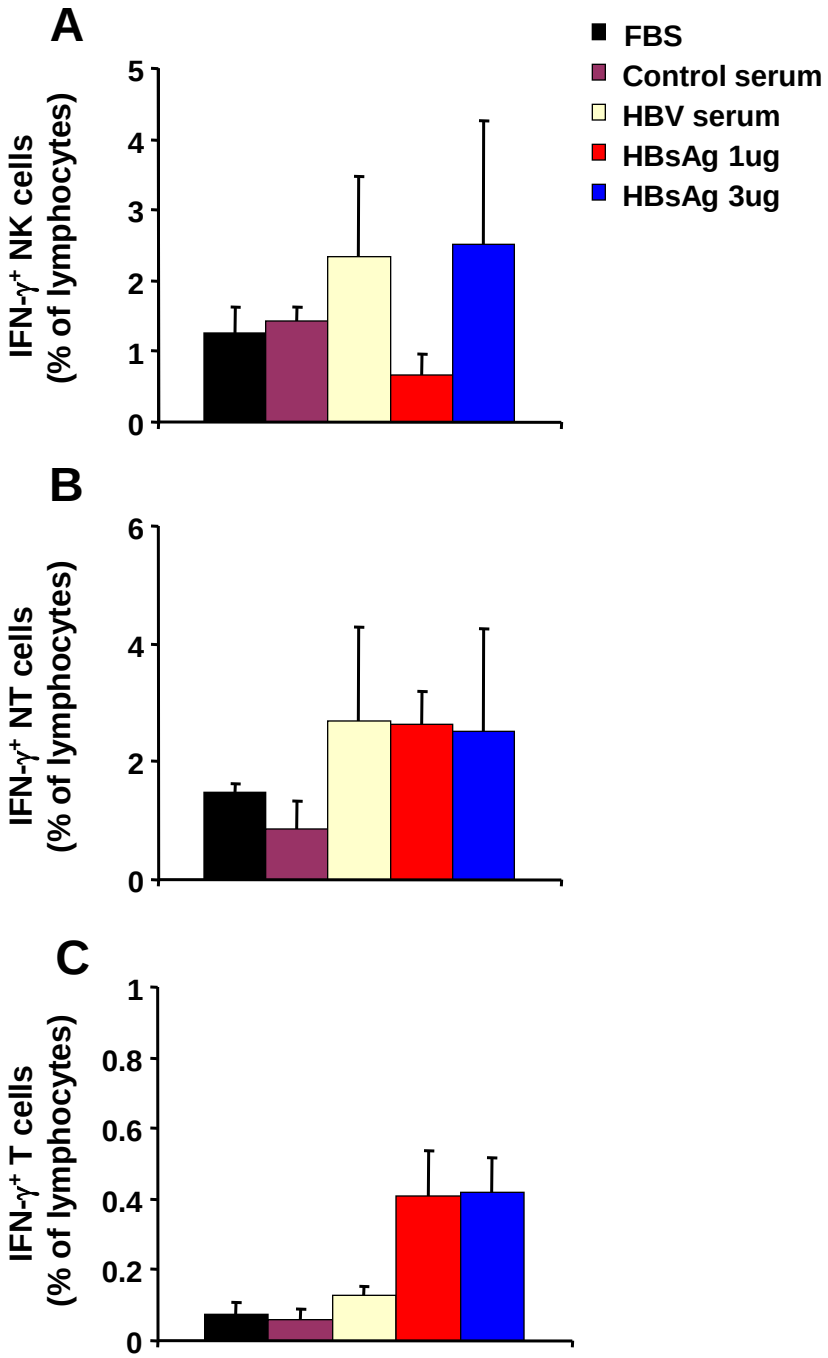

Figure 4.19: Higher frequencies of IFN-γ-producing NK and NT cells in the presence of HBsAg. A, B, C, barcharts showing frequencies of IFN-γ-producing NK **(A),** NT **(B),** and CD56- T cells **(C)** from 3 healthy donors, following a 24 hour incubation in medium supplemented with foetal bovine serum (FBS) (black), human serum from a healthy donor (purple), human serum from a HBV patient (off white), 1μg of HBsAg (red) and 3μg of HBsAg (blue) ($p>0.05$).

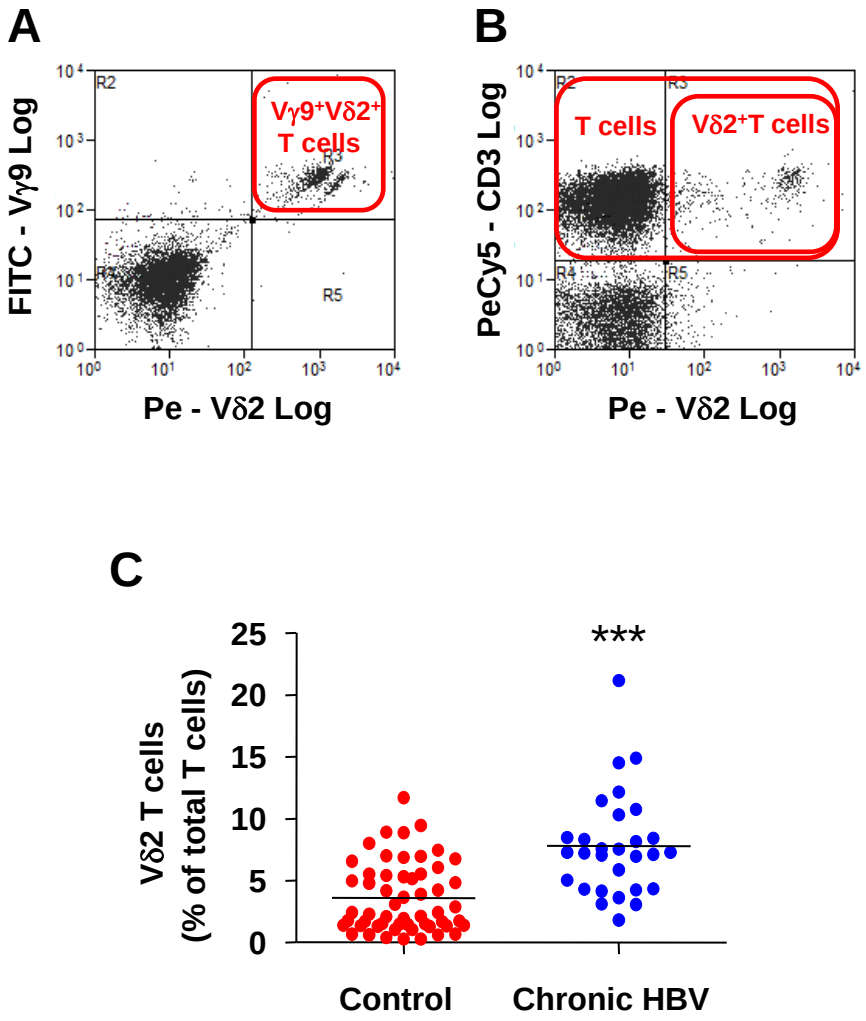

Figure 5.1: Frequencies of circulating Vδ2 T cells are significantly higher in HBV-infected subjects than in control subjects. A, representative dot plot of whole PBMC, gated on lymphocytes and stained with FITC-labelled anti-Vγ9 mAb, PE-labelled anti-Vδ2 mAb and PE-Cy5-labelled anti-CD3 mAb for identification of $Vγ9^+Vδ2^+$ T cells. Since most cells expressing Vγ9 also expressed Vδ2, analysis of Vδ2 expression alone by $CD3^+$ cells **(B)** was sufficient. **C,** scatterplot showing the frequencies of circulating Vδ2 T cells in 55 control subjects (red) and 33 HBV patients (blue) (***$p<0.0001$).

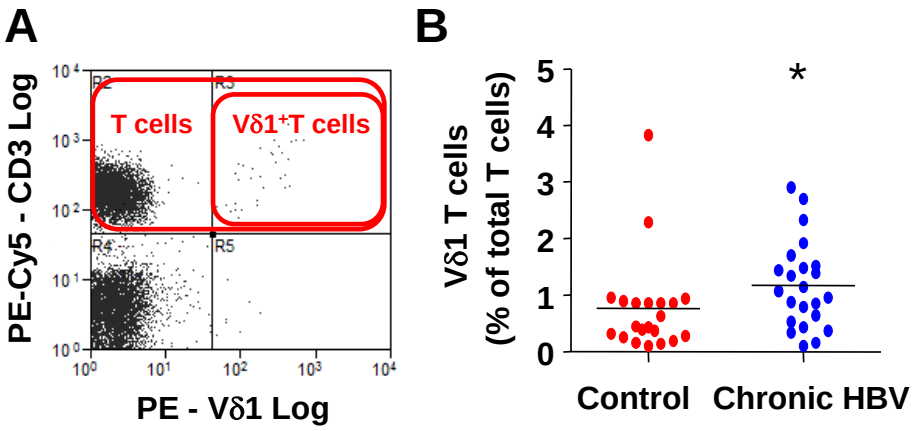

Figure 5.2: Frequencies of circulating Vδ1 T cells are significantly higher in HBV-infected subjects than in control subjects. A, representative dot plot of whole PBMC, gated on lymphocytes and stained with PE-labelled anti-mouse IgG and unconjugated anti-Vδ1 mAb, together with PE-Cy5-labelled anti-CD3 mAb for identification of Vδ1 T cells. **B,** scatterplot showing the frequencies of circulating Vδ1 T cells in 21 control subjects (red) and 23 HBV patients (blue) (*p=0.02).

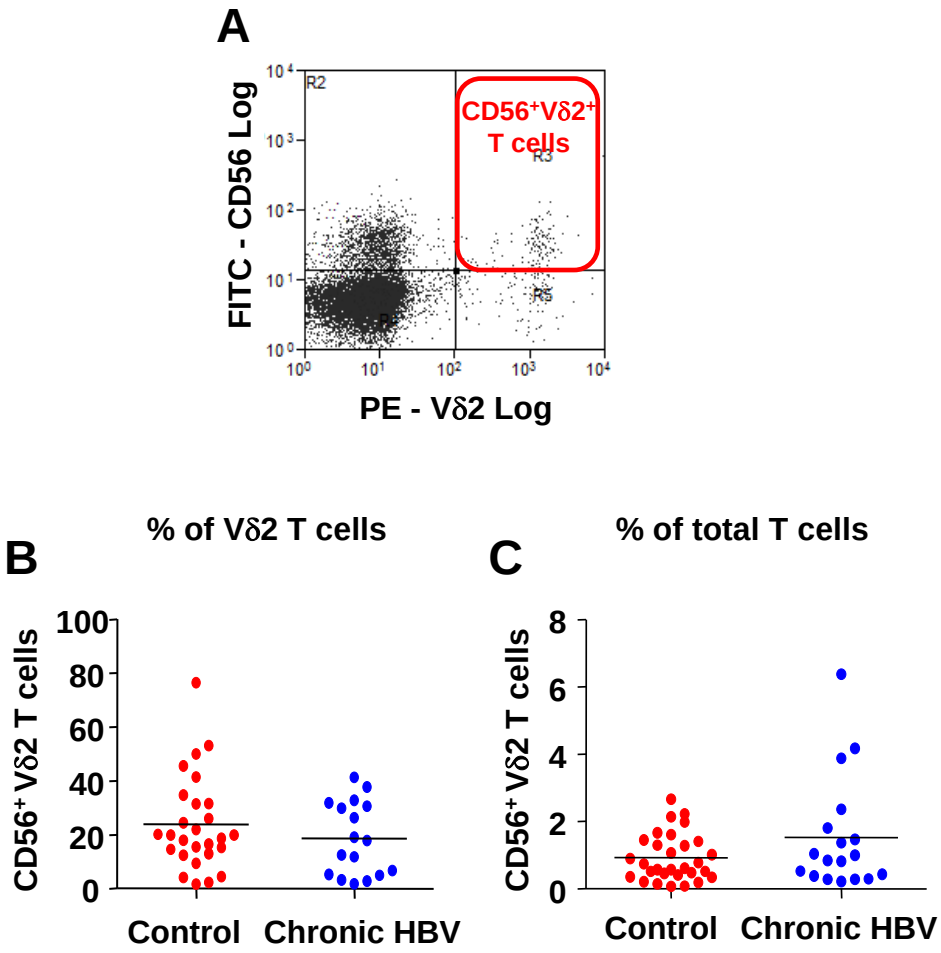

Figure 5.3: Frequencies of circulating CD56$^+$ Vδ2 T cells are similar in HBV-infected and control subjects. A, representative dot plots of whole PBMC, gated on T lymphocytes and stained with FITC-labelled anti-CD56 mAb and, PE-labelled anti-Vδ2 mAb for the identification of CD56$^+$ Vδ2 cells. **B, C,** scatterplots showing the frequencies of circulating CD56$^+$ Vδ2 as a percentage of Vδ2 T cells **(B)** and as a percentage of total T cells **(E)** in 30 control subjects (red) and 18 HBV patients (blue).

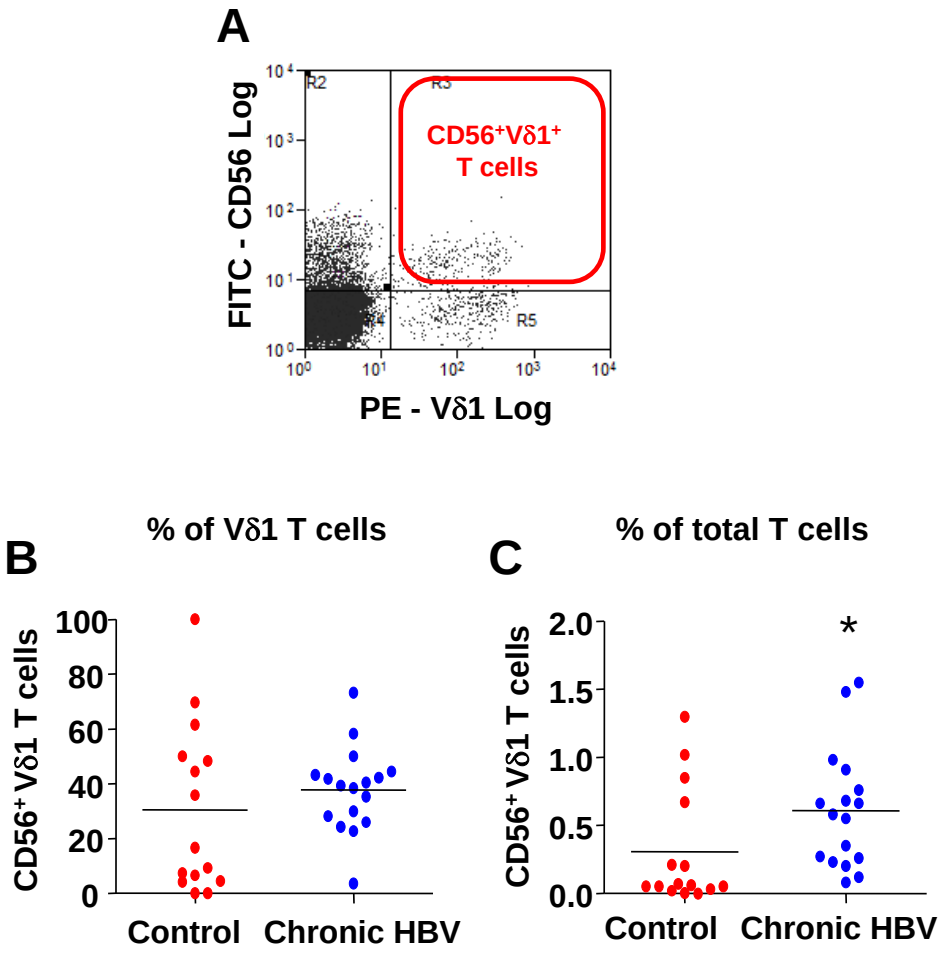

Figure 5.4: Frequencies of circulating CD56⁺ Vδ1 T cells are higher in HBV-infected subjects than in control subjects. A, representative dot plots of whole PBMC, gated on T lymphocytes and stained with FITC-labelled anti-CD56 mAb and, PE-labelled anti-mouse IgG in combination with unconjugated anti-Vδ1 mAb for the identification of CD56⁺ Vδ1 T cells. **B, C,** scatterplots showing the frequencies of CD56⁺ Vδ1 T cells as a percentage of Vδ1 T cells **(B)** and as a percentage of total T cells **(C)** in 15 control subjects (red) and 17 HBV patients (blue) (*p=0.01).

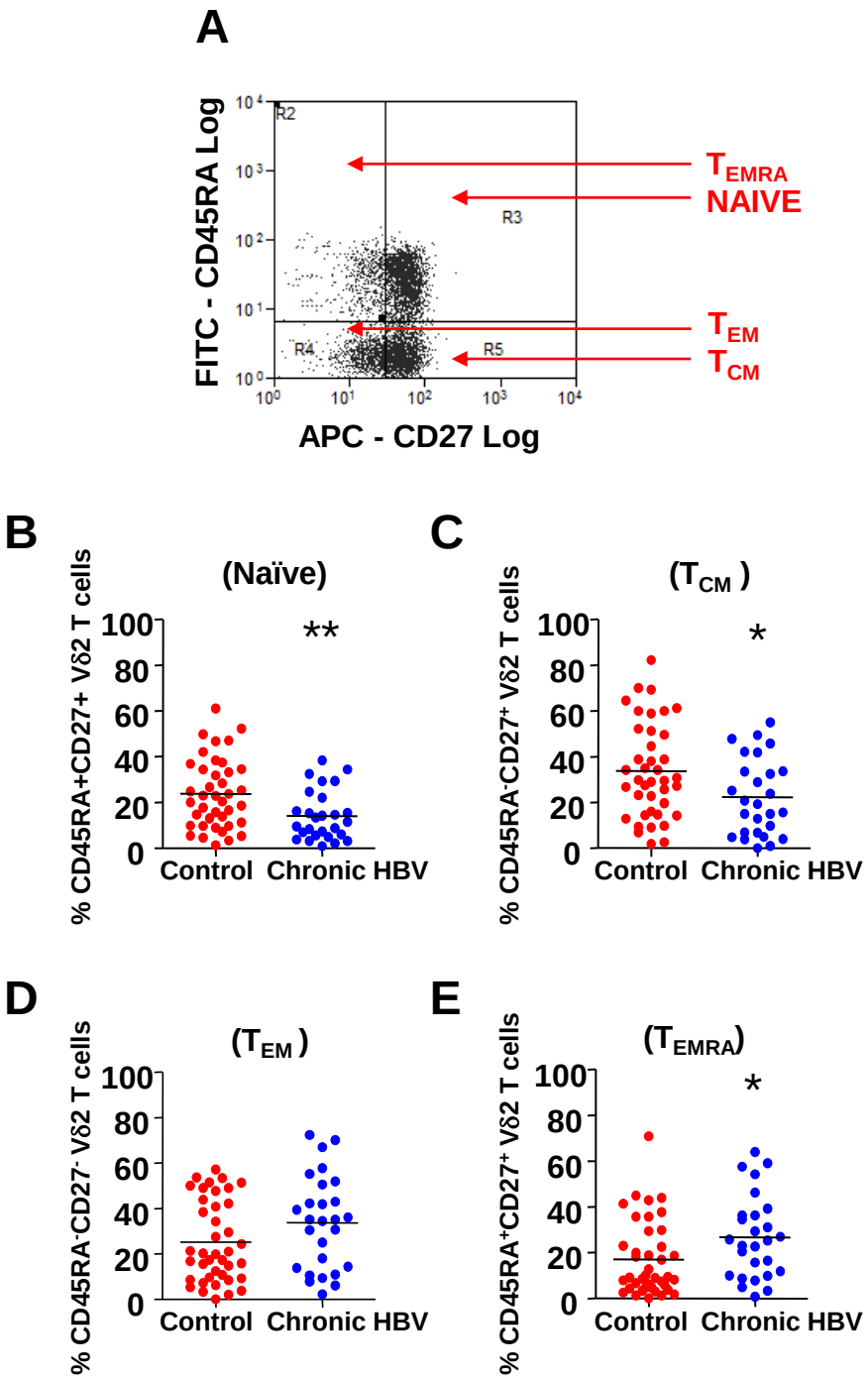

Figure 5.5: Effector-memory Vδ2$^+$ T cells are expanded in HBV infection. A, representative dot plot of whole PBMC stained with FITC-labelled anti-CD45RA mAb, PE-labelled anti-Vδ2 mAb, PerCP-labelled anti-CD3 mAb and APC-labelled anti-CD27 mAb and, gated on T lymphocytes for the identification of T_{EM}, T_{CM}, naïve and T_{EMRA} Vδ2$^+$ T cells. **B, C, D, E,** scatterplots showing the frequencies of circulating naïve **(B),** T_{CM} **(C),** T_{EM} **(D)** and T_{EMRA} **(E)** Vδ2$^+$ T cells as a percentage of Vδ2$^+$ T cells in 40 control subjects (red) and 27 HBV patients (blue) (*p<0.05, **p = 0.007).

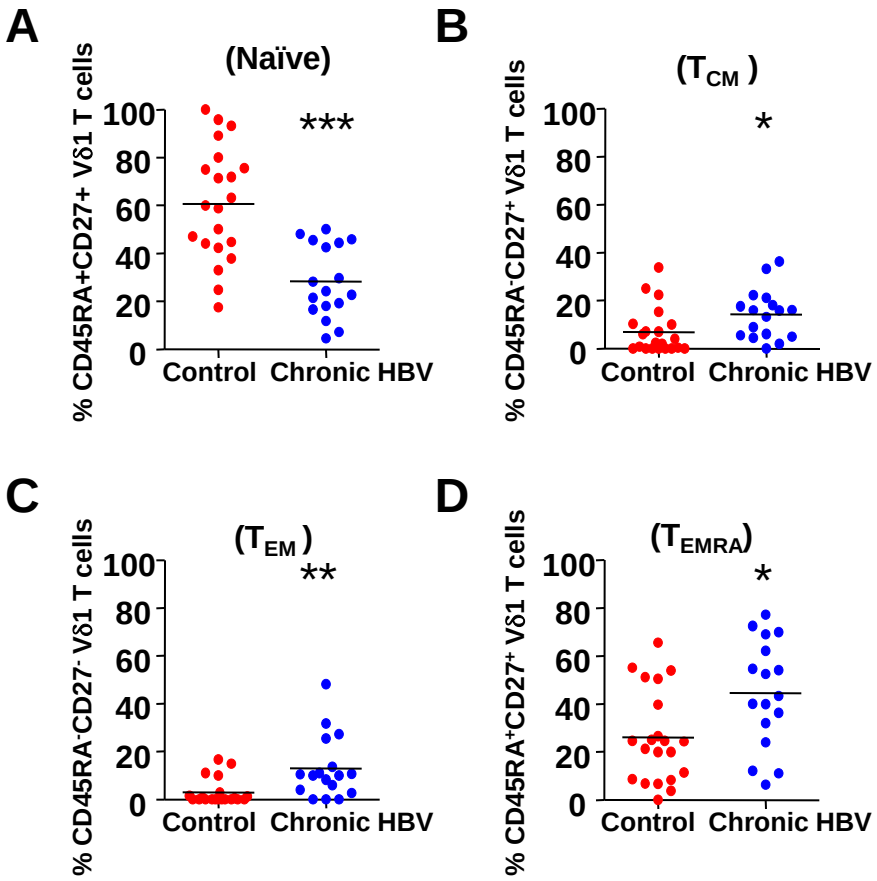

Figure 5.6: Significantly lower frequencies of naive Vδ1 T cells in HBV infection. A, B, C, D, scatterplots showing the frequencies of circulating naive **(A),** T_{CM} **(B),** T_{EM} **(C)** and T_{EMRA} **(D)** Vδ1 T cells as a percentage of Vδ1 T cells in 21 control subjects (red) and 17 HBV patients (blue) (*p<0.05, **p<0.005, ***p<0.0005).

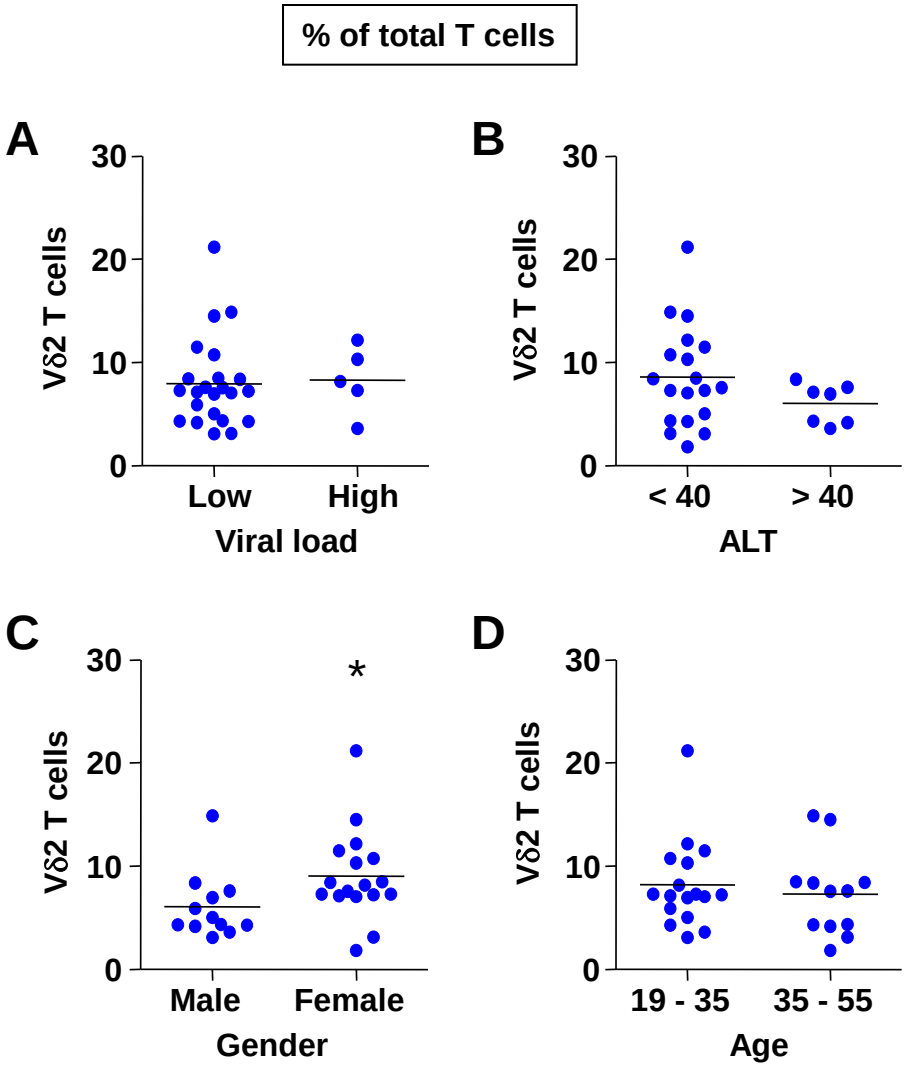

Figure 5.7: The frequencies of Vδ2 T cells in HBV patient subsets based on viral load, ALT, gender and age. A, scatterplot showing frequencies of Vδ2 T cells in 23 HBV patients with viral load between 10 and 100,000 copies/ml and 5 HBV patients with viral load between 100,000 and $5x10^8$ copies/ml. **B,** scatterplot showing frequencies of Vδ2 T cells in 19 HBV patients with ALT below 40 IU/ml and 7 HBV patients with ALT above 40 IU/ml. **C,** scatterplot showing frequencies of Vδ2 T cells in 12 male HBV patients and 17 female HBV patients. **D,** scatterplot showing frequencies of Vδ2 T cells in 17 HBV patients between the age of 19 and 35 years and 12 HBV patients between the age of 35 and 55 years (*p=0.02).

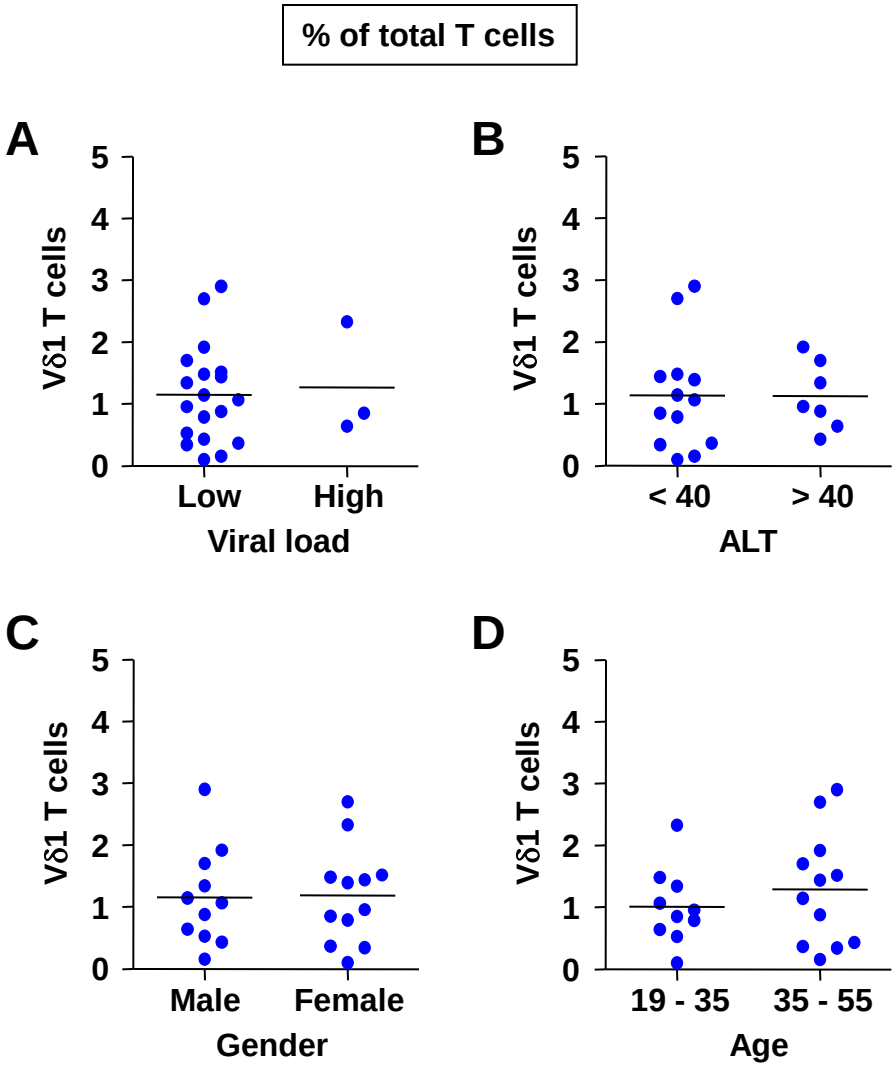

Figure 5.8: There are no significant differences in the frequencies of Vδ1 T cells between patient groups within the study cohort. A, scatterplot showing frequencies of Vδ1 T cells in 19 HBV patients with viral load between 10 and 100,000 copies/ml and 3 HBV patients with viral load between 100,000 and $5x10^8$ copies/ml. **B,** scatterplot showing frequencies of Vδ1 T cells in 13 HBV patients with ALT below 40 IU/ml and 7 HBV patients with ALT above 40 IU/ml. **C,** scatterplot showing frequencies of Vδ1 T cells in 11 male HBV patients and 12 female HBV patients. **D,** scatterplot showing frequencies of Vδ1 T cells in 10 HBV patients between the age of 19 and 35 years and 12 HBV patients between the age of 35 and 55 years.

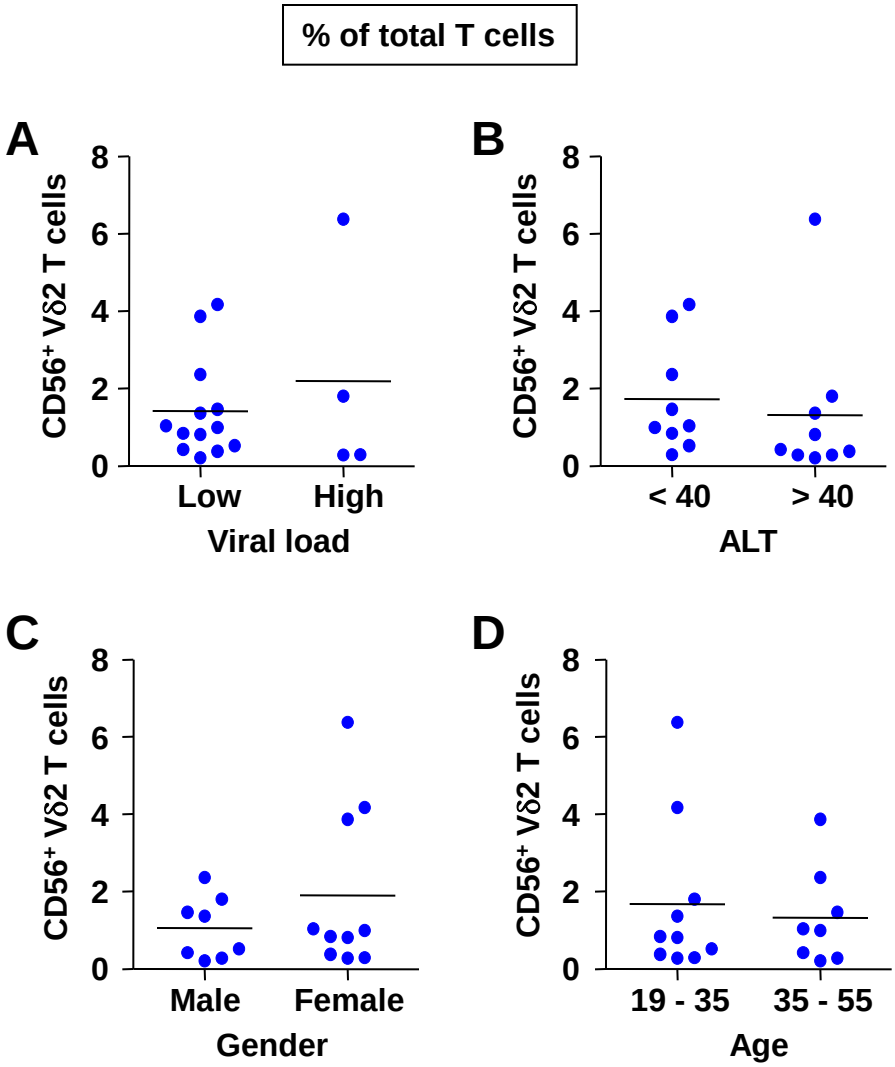

Figure 5.9: There are no significant differences in the frequencies of CD56$^+$ Vδ2 T cells between patient groups within the study cohort. A, scatterplot showing frequencies of CD56$^+$ Vδ2 T cells in 13 HBV patients with viral load between 10 and 100,000 copies/ml and 4 HBV patients with viral load between 100,000 and 5x10^8 copies/ml. **B,** scatterplot showing frequencies of CD56$^+$ Vδ2 T cells in 9 HBV patients with ALT below 40 IU/ml and 9 HBV patients with ALT above 40 IU/ml. **C,** scatterplot showing frequencies of CD56$^+$ Vδ2 T cells in 8 male HBV patients and 10 female HBV patients. **D,** scatterplot showing frequencies of CD56$^+$ Vδ2 T cells in 10 HBV patients between the age of 19 and 35 years and 8 HBV patients between the age of 35 and 55 years.

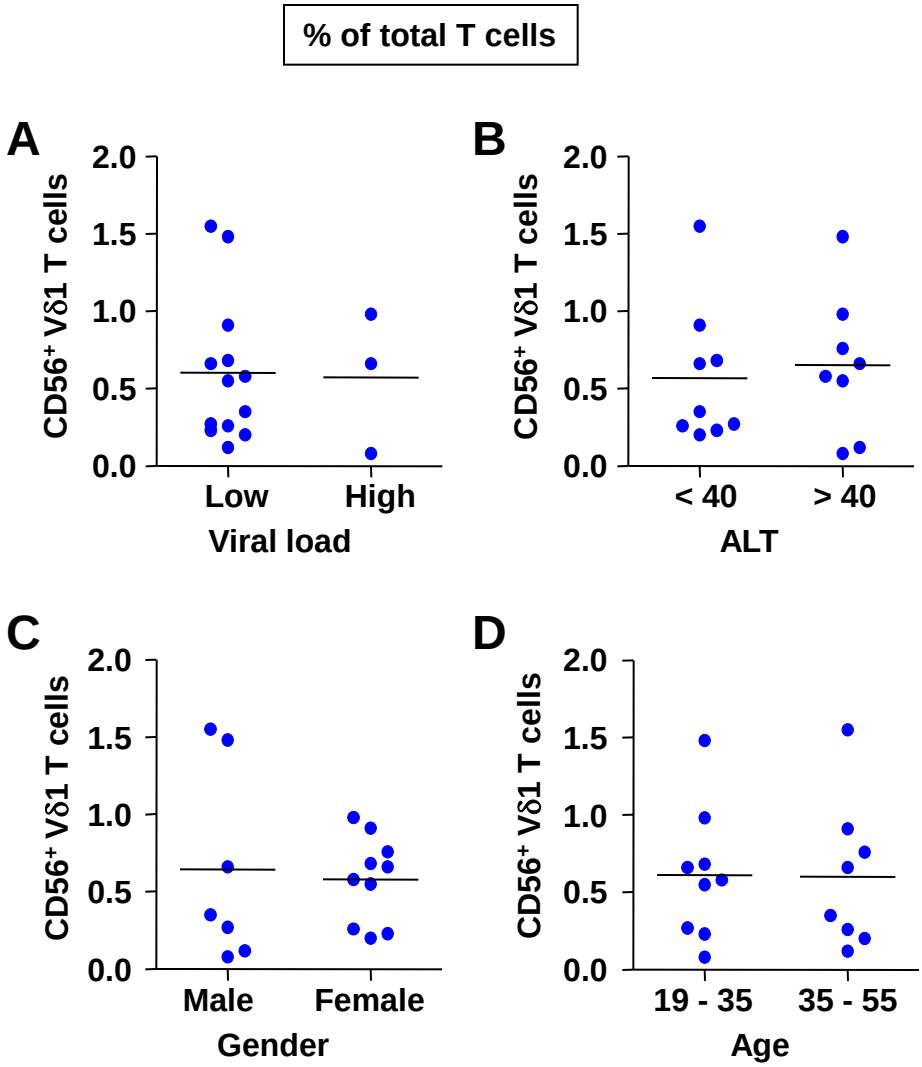

Figure 5.10: There are no significant differences in the frequencies of CD56$^+$ Vδ1 T cells between patient groups within the study cohort. A, scatterplot showing frequencies of CD56$^+$ Vδ1 T cells in 13 HBV patients with viral load between 10 and 100,000 copies/ml and 3 HBV patients with viral load between 100,000 and 5x10^8 copies/ml. **B,** scatterplot showing frequencies of CD56$^+$ Vδ1 T cells in 9 HBV patients with ALT below 40 IU/ml and 8 HBV patients with ALT above 40 IU/ml. **C,** scatterplot showing frequencies of CD56$^+$ Vδ1 T cells in 7 male HBV patients and 10 female HBV patients. **D,** scatterplot showing frequencies of CD56$^+$Vδ1 T cells in 9 HBV patients between the age of 19 and 35 years and 8 HBV patients between the age of 35 and 55 years.

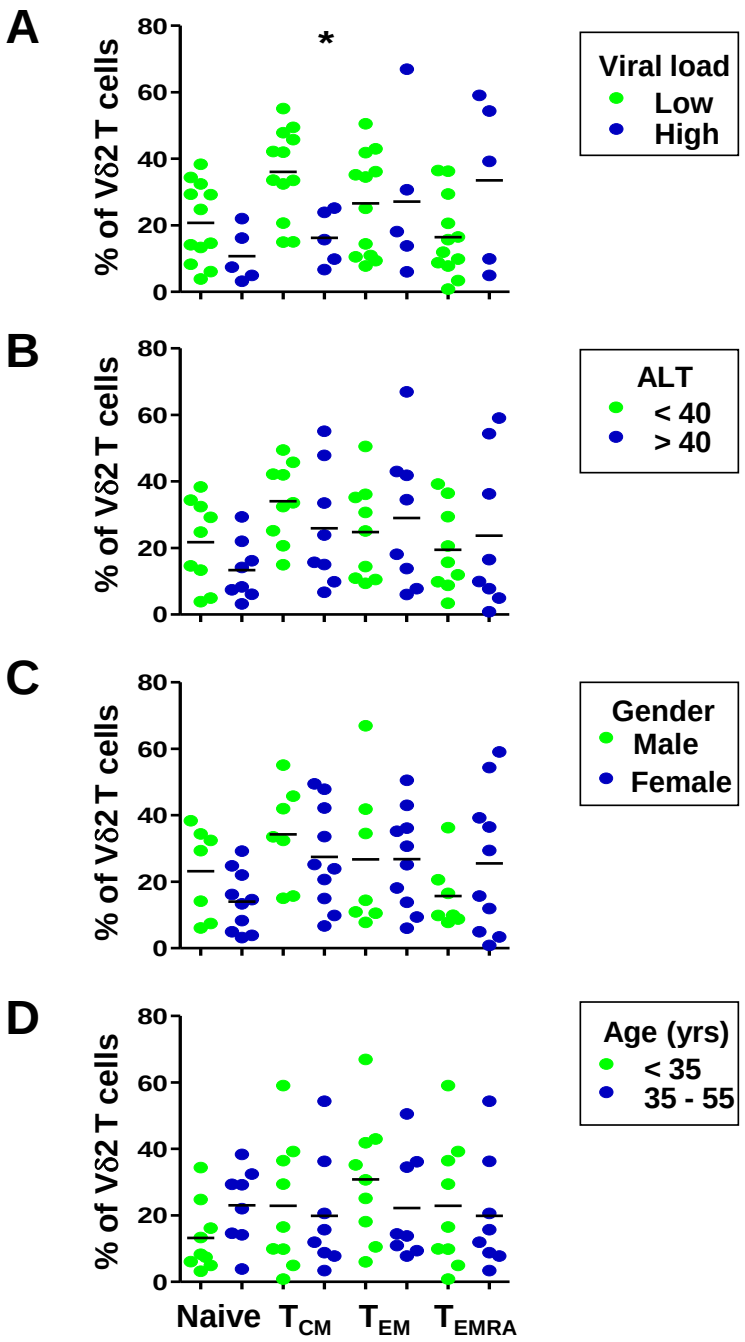

Figure 5.11: Differentiation status of circulating Vδ2 T cells in subgroups of HBV patients. A, B, C, D, scatterplots showing frequencies of naïve,T_{CM}, T_{EM} and T_{EMRA} Vδ2 T cells as a percentage of the total Vδ2 T cell population in 12 HBV patients with viral load below 100,000 copies/ml and 5 HBV patients with viral load between 100,000 and 1x108 copies/ml **(A)**, 9 HBV patients with ALT below 40 IU/ml and 8 HBV patients with ALT above 40 IU/ml **(B)**, 7 male HBV patients and 10 female HBV patients **(C)** and, 10 HBV patients under the age of 35 years and 8 HBV patients between the age of 35 and 55 years **(D)**, (*p=0.02).

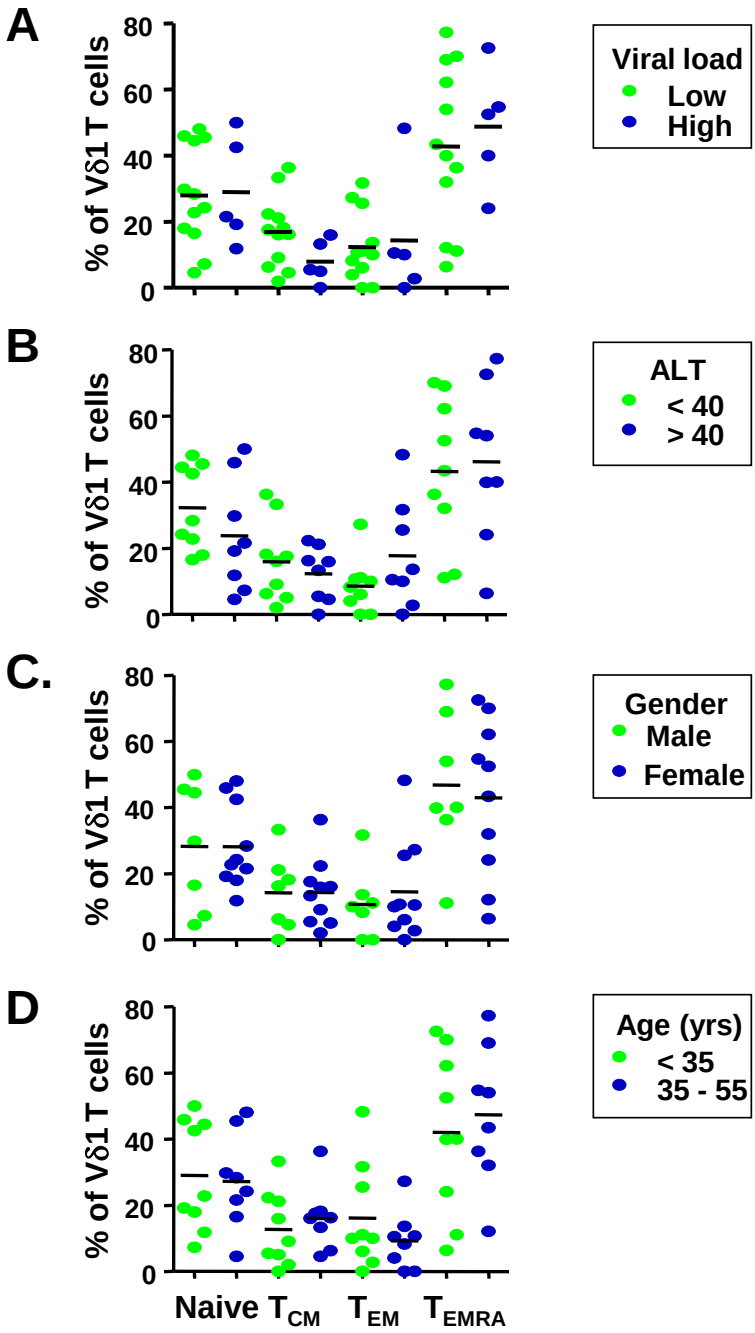

Figure 5.12: No correlation between the memory phenotype of Vδ1 T cells and viral load, disease severity, gender or age in HBV infection. **A, B, C, D,** scatterplots showing frequencies of naïve, T_{CM}, T_{EM} and T_{EMRA} Vδ1 T cells as a percentage of the total Vδ1 T cell population in 12 HBV patients with viral load below 100,000 copies/ml and 5 HBV patients with viral load between 100,000 and 1x108 copies/ml **(A)**, 9 HBV patients with ALT below 40 IU/ml and 8 HBV patients with ALT above 40 IU/ml **(B)**, 7 male HBV patients and 10 female HBV patients **(C)** and, 10 HBV patients under the age of 35 years and 8 HBV patients between the age of 35 and 55 years **(D)**.

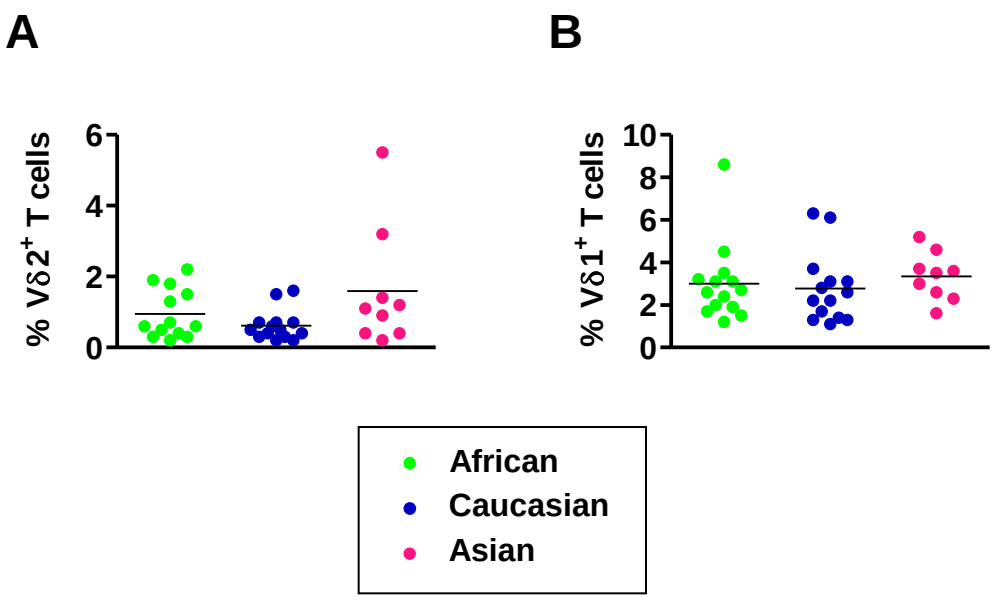

Figure 5.13: Frequencies of circulating Vδ2 and Vδ1 cells are similar in african, caucasian and asian healthy control subjects. A, B, scatterplots showing the frequencies of circulating Vδ2 T cells **(A)** and Vδ1 T cells **(B)**, as a percentage of total T cells, in 13 african, 14 caucasian and 9 asian healthy control subjects.

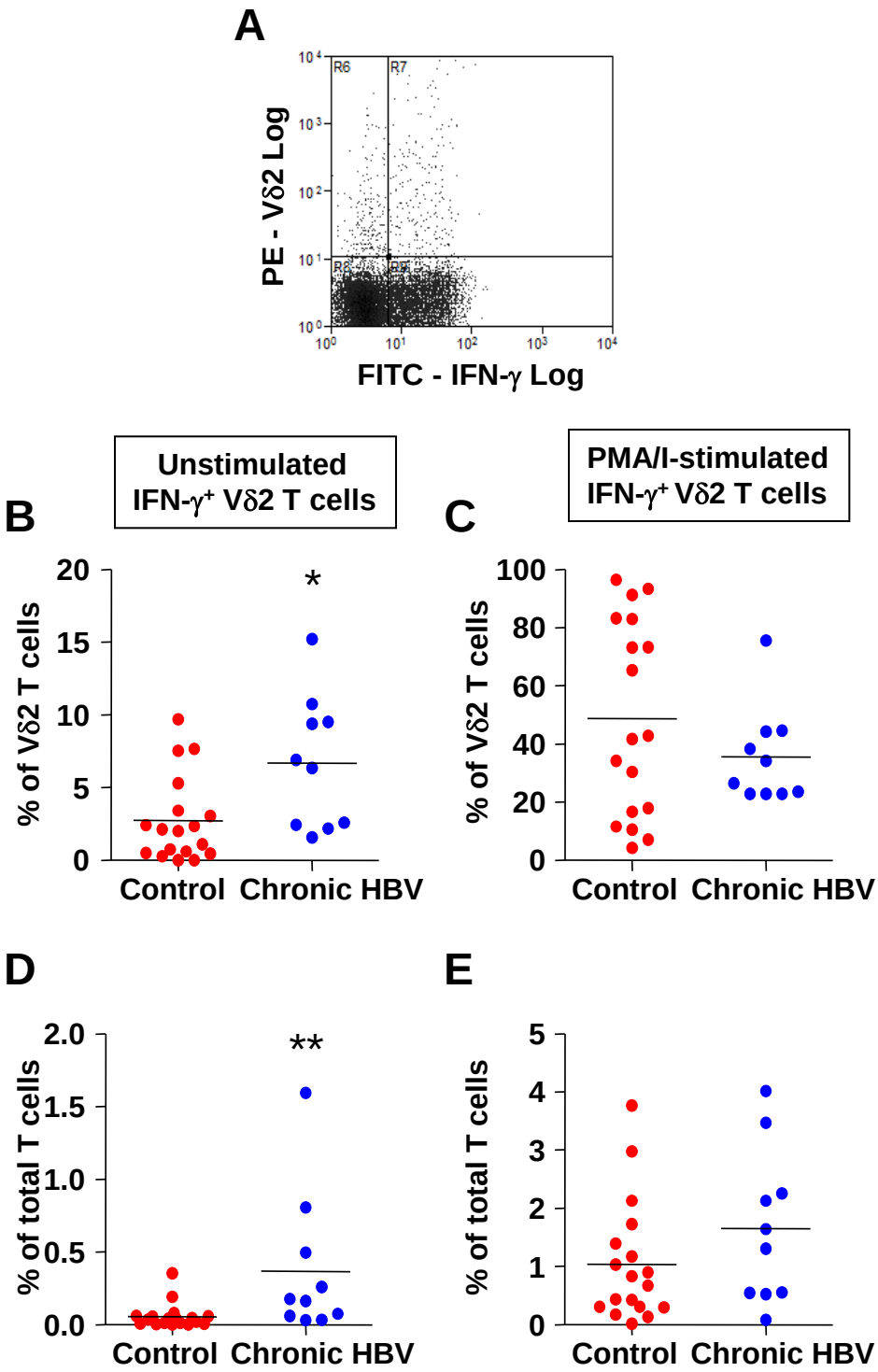

Figure 5.14: Frequencies of circulating IFN-γ-producing Vδ2 T cells are higher in HBV-infected subjects than in control subjects. A, representative dot plot of whole PBMC stained with FITC-labelled anti-IFN-γ mAb, PE-labelled anti-Vδ2 mAb and PE-Cy5-labelled anti-CD3 mAb for the identification of IFN-γ-producing Vδ2 T cells. **B, C, D, E,** scatterplots showing the frequencies of IFN-γ-producing Vδ2 T cells as a percentage of total Vδ2 T cells **(B,C)** and as a percentage of total T lymphocytes **(D,E),** following incubation in medium alone **(B,D)** and following incubation in medium conditioned with PMA/I **(C, E)** in 18 control subjects (red) and 10 HBV patients (blue) (*p=0.01, **p=0.005).

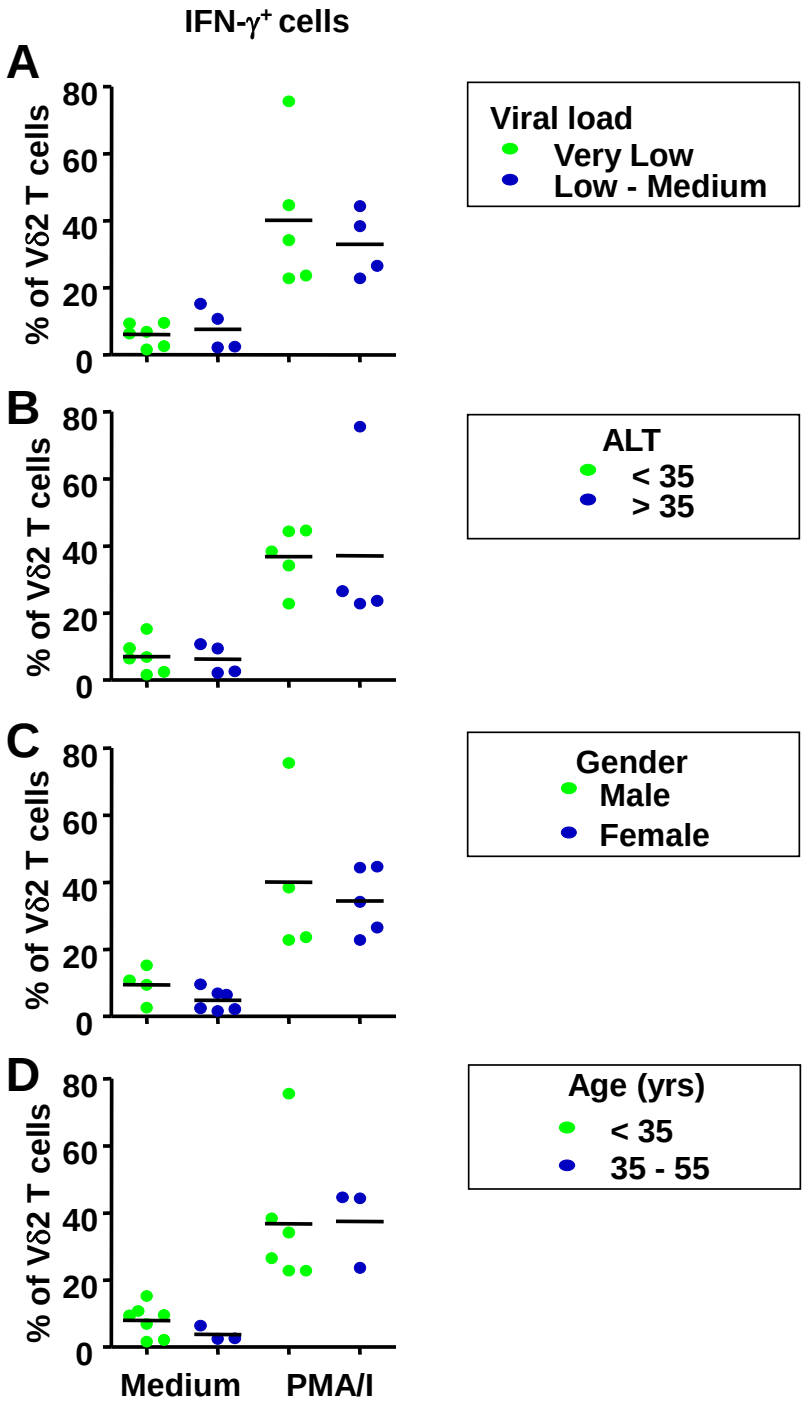

Figure 5.15: No correlation between the frequencies of IFN-γ-producing Vδ2 T cells and viral load, disease severity, gender or age in HBV infection. A, B, C, D, scatterplots showing frequencies of IFN-γ-producing Vδ2 T cells, as a percentage of total Vδ2 T cells, in 5 - 6 HBV patients with viral load below 1,000 copies/ml and 4 HBV patients with viral load between 1,000 and 100,000 copies/ml **(A)**, 5 - 6 HBV patients with ALT below 35 IU/ml and 4 HBV patients with ALT above 35 IU/ml **(B)**, 4 male HBV patients and 5 - 6 female HBV patients **(C)** and, 6 - 7 HBV patients under the age of 35 years and 3 HBV patients between the age of 35 and 55 years **(D)**. All frequencies of IFN-γ-producing Vδ2 T cells are shown after a 4 hour incubation in medium alone and, medium conditioned with PMA/I.

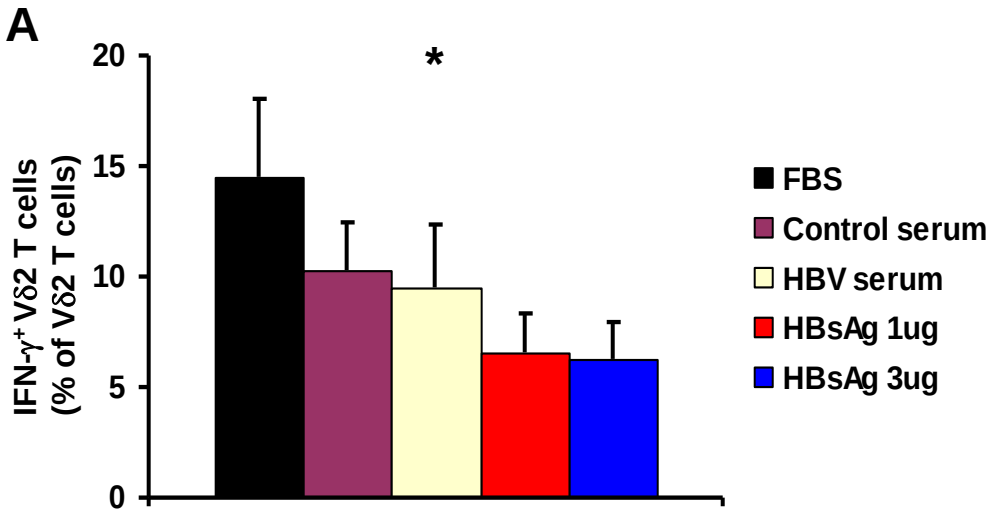

Figure 5.16: Lower frequencies of IFN-γ-expressing Vδ2 T cells in the presence of HBsAg. A, barchart showing the frequencies of circulating IFN-γ-expressing Vδ2 T cells as a percentage of total Vδ2 T cells in 3 healthy donors following a 24 hour incubation in medium supplemented with FBS (black), human serum from a healthy donor (purple), human serum from a HBV patient (off white), 1μg of HBsAg (red) and 3μg of HBsAg (blue) (*p=0.04).

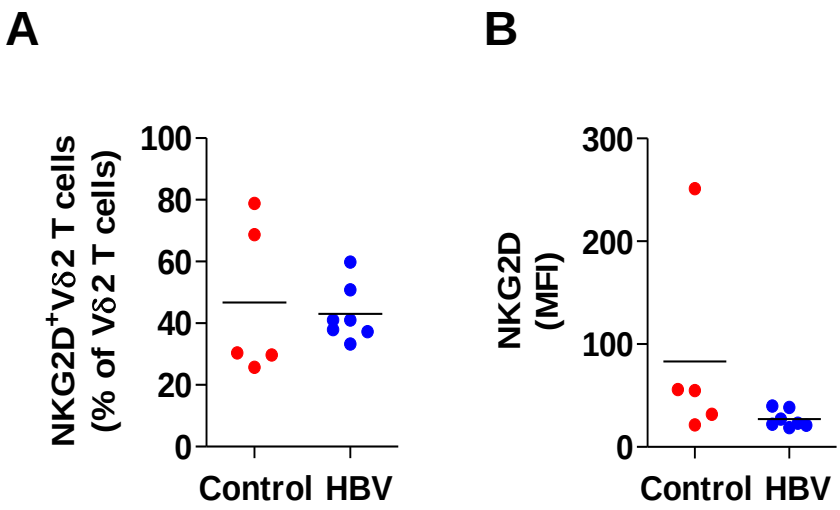

Figure 5.17: Lower NKG2D expression on Vδ2 T cells in HBV infection. A, scatterplot showing the frequencies of circulating NKG2D-expressing Vδ2 T cells as a percentage of total Vδ2 T cells in 5 control subjects (red) and 7 HBV patients (blue). B, scatterplot showing the mean fluorescence intensity (MFI) of NKG2D expression by Vδ2 T cells in 5 control subjects (red) and 7 HBV patients (blue).

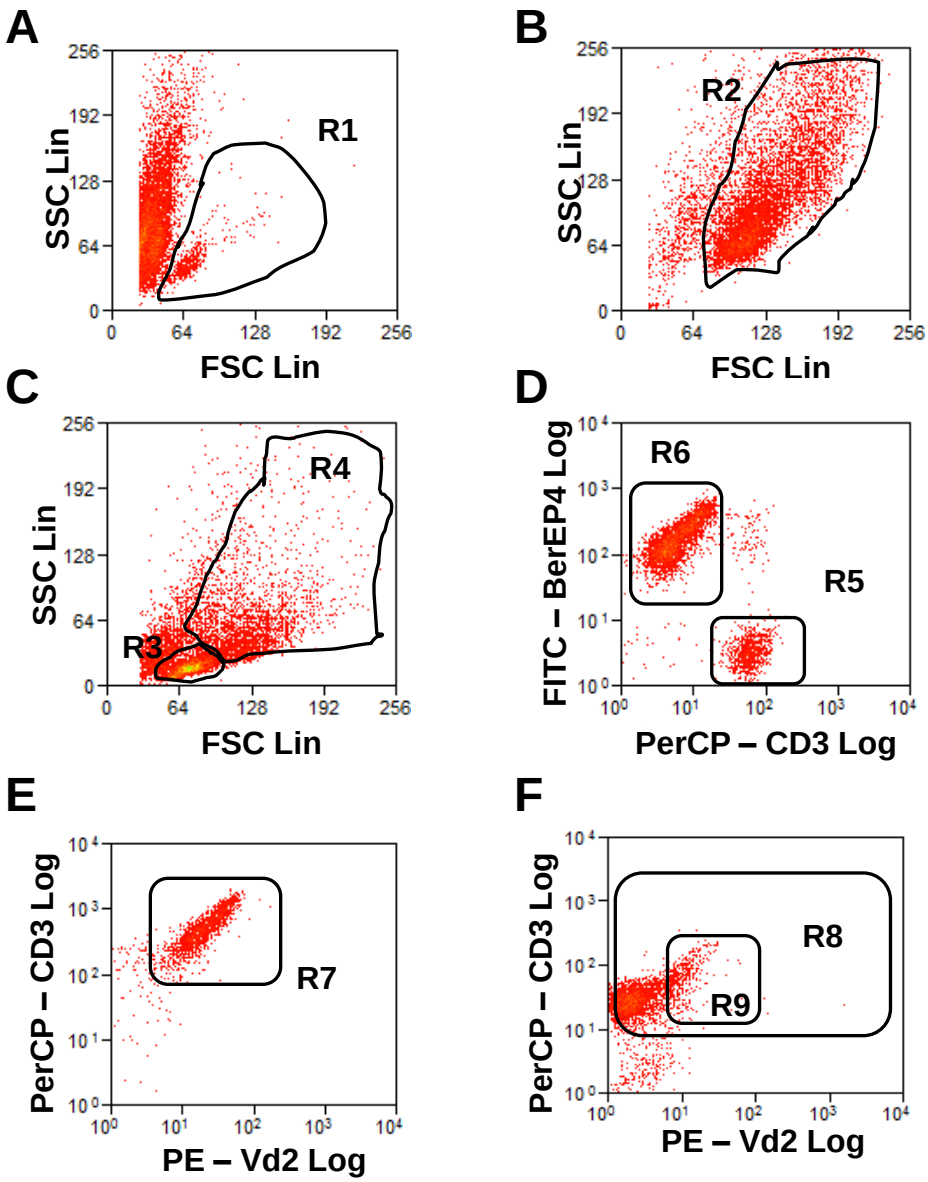

Figure 6.1: Gating technique for analysis of surface expression on HMBPP and IL-2-expanded Vδ2 T cells, PHA and IL-2-expanded T cells and epithelial cells. A, representative dot plot of 14-day old HMBPP-expanded PBMC, showing lymphocytes are the predominant living cell type, gated in R1 to exclude dead cell debris. **B,** representative dot plot of Hep3B cells, gated in R2 to exclude unwanted cell debris from subsequent analysis. **C,** representative dot plot of 14-day old HMBPP-expanded PBMC (gated in R3) co-cultured with GRM cells (gated in R4). **D,** representative dot plot showing that gating on R5 can exclude the BerEP4^{+} epithelial cells or that gating in R6 can exclude the T cells. **E**, representative dot plot of HMBPP-expanded PBMC previously gated in R5 to exclude epithelial cells and now gated in R7 to identify Vδ2 T cells only. **F,** representative dot plot of PHA and IL-2-expanded PBMC showing all T cells in R8 and showing that Vδ2 T cells gated in R9 are not the predominant T cell population.

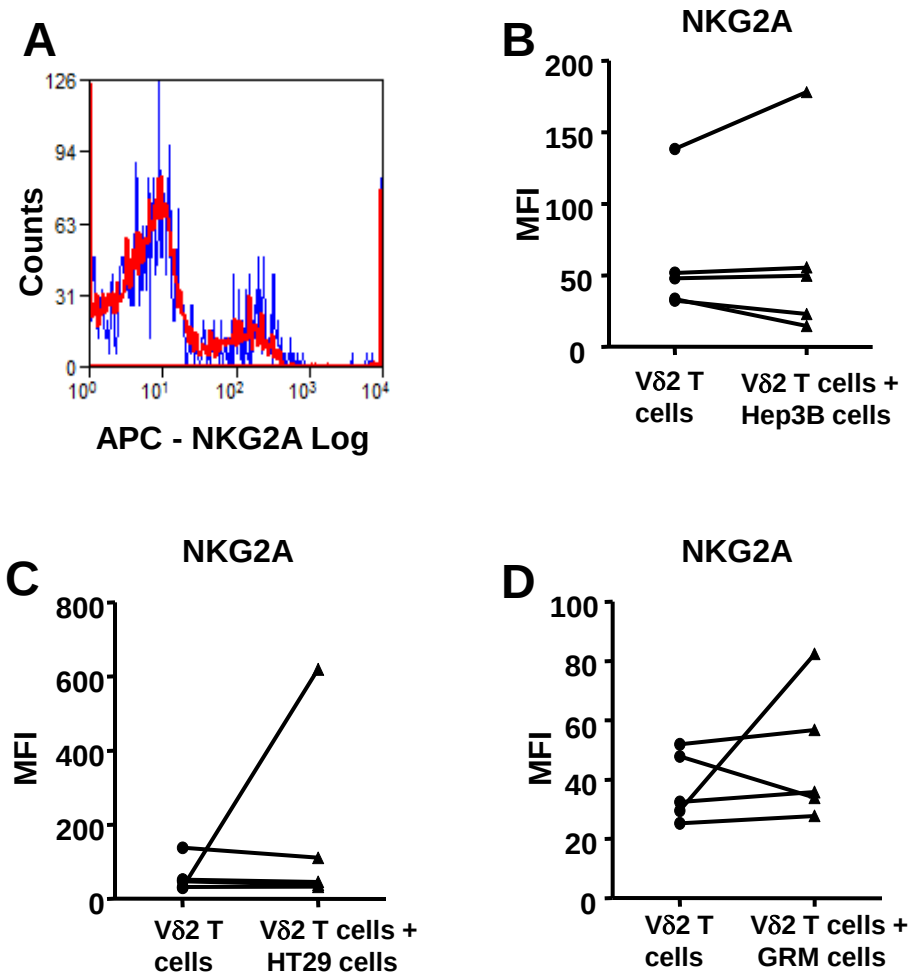

Figure 6.2: The surface expression of NKG2A by Vδ2 T cells is not altered following co-culture with Hep3B, HT29 or GRM cells. A, representative histogram showing NKG2A expression by Vδ2 T cells in 14-day old HMBPP-expanded PBMC after 24 hours of culture in the presence (blue) and absence (red) of Hep3B cells. **B, C, D,** scatterplot showing the MFI of NKG2A expression by HMBPP-expanded Vδ2 T cells from 5 donors following a 24 hour incubation in the absence (circle) and presence (triangle) of Hep3B, HT29 or GRM cells, respectively.

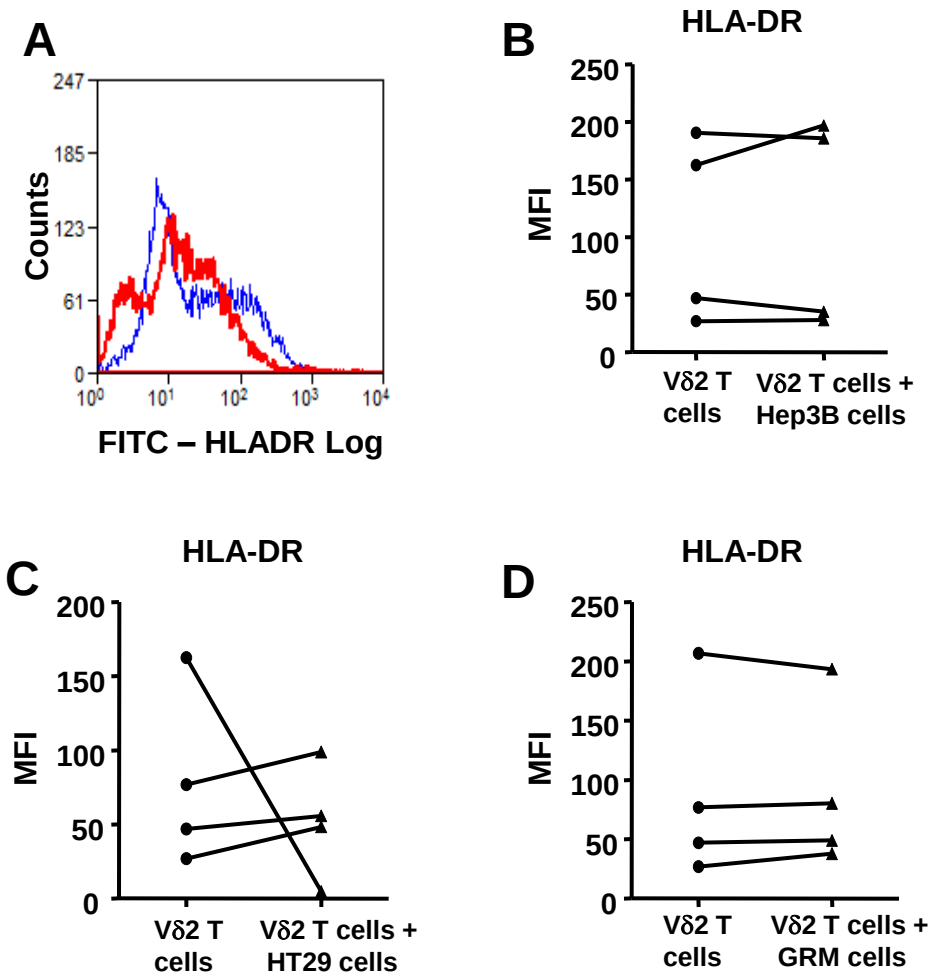

Figure 6.3: The surface expression of HLA-DR by Vδ2 T cells is not altered following co-culture with Hep3B, HT29 or GRM cells. A, representative histogram showing HLA-DR expression by Vδ2 T cells in 14-day old HMBPP-expanded PBMC after 24 hours of culture in the presence (blue) and absence (red) of HT29 cells. **B, C, D,** scatterplot showing the MFI of HLA-DR expression by HMBPP-expanded Vδ2 T cells from 4-5 donors following a 24 hour incubation in the absence (circle) and presence (triangle) of Hep3B, HT29 or GRM cells, respectively.

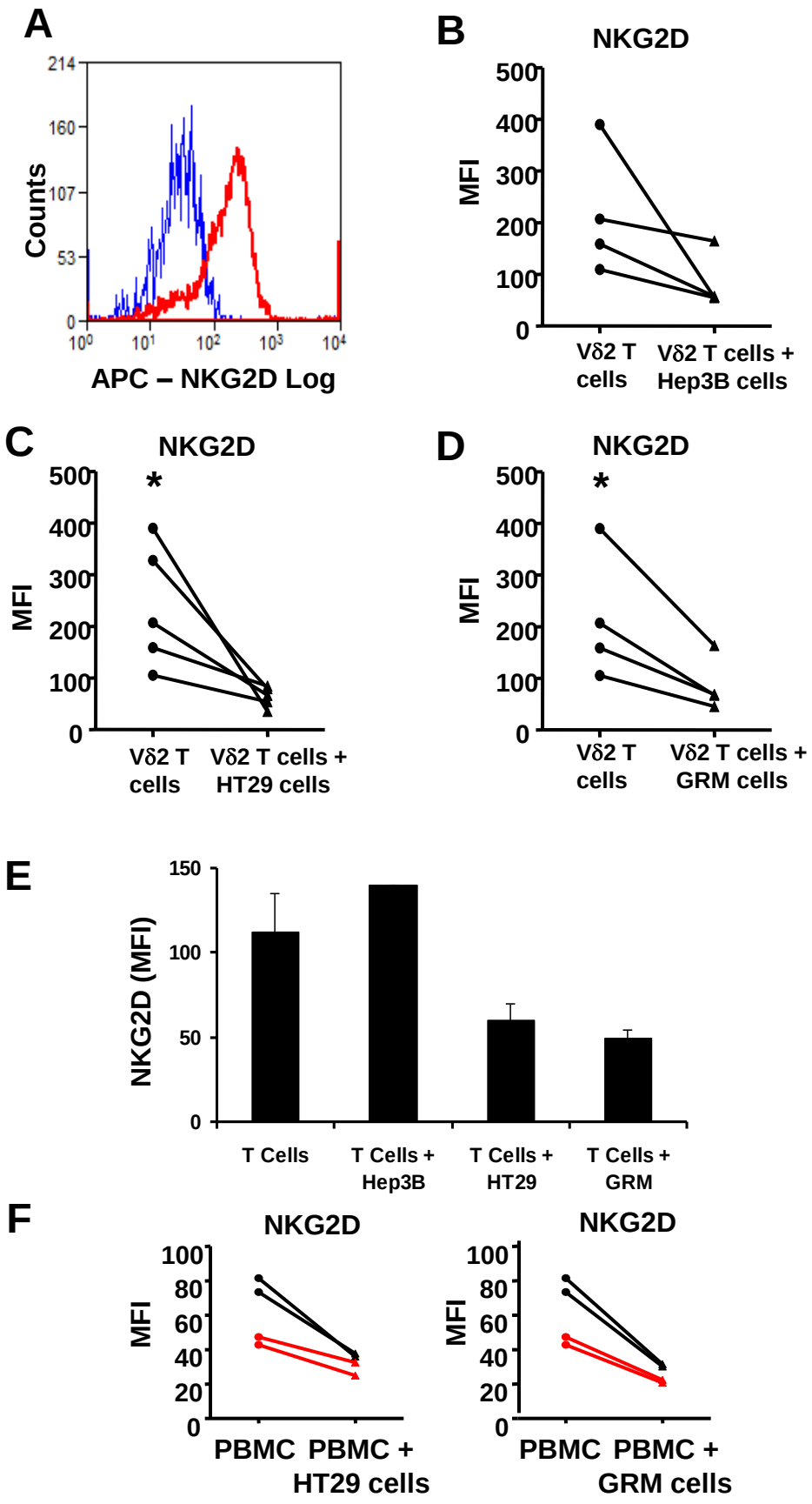
A
214
160
107
53
0
Counts
10^0 10^1 10^2 10^3 10^4
APC – NKG2D Log
B
NKG2D
500
400
300
200
100
0
MFI
Vδ2 T cells
Vδ2 T cells + Hep3B cells
C
NKG2D
*
MFI
Vδ2 T cells
Vδ2 T cells + HT29 cells
D
NKG2D
*
MFI
Vδ2 T cells
Vδ2 T cells + GRM cells
E
NKG2D (MFI)
150
100
50
0
T Cells
T Cells + Hep3B
T Cells + HT29
T Cells + GRM
F
NKG2D
NKG2D
100
80
60
40
20
0
MFI
PBMC
PBMC + HT29 cells
PBMC + GRM cells

Figure 6.4: The surface expression of NKG2D by Vδ2 T cells is lower following co-culture with Hep3B, HT29 or GRM cells. A, representative histogram showing NKG2D expression by Vδ2 T cells in 14-day old HMBPP-expanded PBMC after 24 hours of culture in the presence (blue) and absence (red) of Hep3B cells. **B, C, D,** scatterplot showing the MFI of NKG2D expression by HMBPP-expanded Vδ2 T cells from 4-5 donors following a 24 hour incubation in the absence (circle) and presence (triangle) of Hep3B, HT29 or GRM cells, respectively (*$p<0.05$). **E,** barchart showing NKG2D expression by PHA and IL-2 expanded T cells from 1-2 donors following a 24 hour incubation in the absence and presence of Hep3B, HT29 and GRM cells. **F,** scatterplots showing the MFI of NKG2D expression by Vδ2 T cells (black) and αβ T cells (red) in fresh PBMC from 2 donors following a 24 hour incubation in the absence (circle) and presence (triangle) of HT29 cells **(left)** or GRM cells **(right)**.

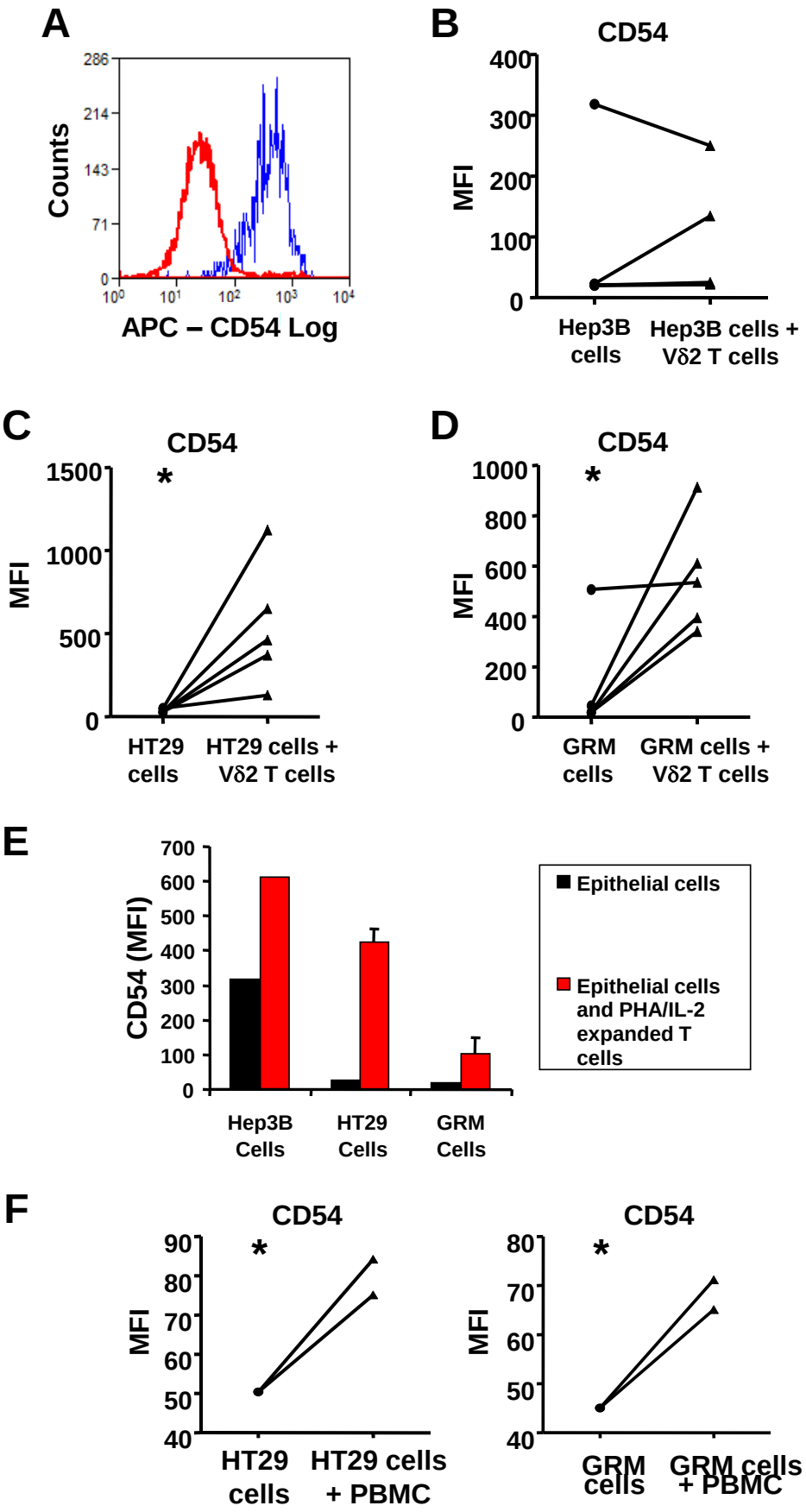
A
Counts
286
214
143
71
0
10^0
10^1
10^2
10^3
10^4
APC – CD54 Log
B
CD54
MFI
400
300
200
100
0
Hep3B cells
Hep3B cells + Vδ2 T cells
C
CD54
MFI
1500
1000
500
0
*
HT29 cells
HT29 cells + Vδ2 T cells
D
CD54
MFI
1000
800
600
400
200
0
*
GRM cells
GRM cells + Vδ2 T cells
E
CD54 (MFI)
700
600
500
400
300
200
100
0
Hep3B Cells
HT29 Cells
GRM Cells
Epithelial cells
Epithelial cells and PHA/IL-2 expanded T cells
F
CD54
MFI
90
80
70
60
50
40
*
HT29 cells
HT29 cells + PBMC
CD54
MFI
80
70
60
50
40
*
GRM cells
GRM cells + PBMC

Figure 6.5: Co-culture with HMBPP-expanded Vδ2 T cells results in significantly higher levels of CD54 expression by HT29 and GRM cells, but not by Hep3B cells. A, histogram showing CD54 expression by BerEP4^{+} GRM cells culturd alone (red) and cultured in the presence of HMBPP-expanded Vδ2 T cells (blue). **B, C, D,** scatterplots showing the MFI of CD54 expression by Hep3B **(B),** HT29 **(C)** and GRM cells **(D)** after a 24 hour incubation in the absence (circle) and presence (triangle) of HMBPP-expanded Vδ2 T cells from 5 donors. **E,** barchart showing CD54 expression by Hep3B, HT29 and GRM cells following a 24 hour incubation in the absence (black) and presence (red) of PHA and IL-2-expanded T cells from 1-2 donors. **F**, scatterplots showing the MFI of CD54 expression by HT29 **(left)** and GRM cells **(right)** after a 24 hour incubation in the absence (circle) and presence (triangle) of fresh PBMC from 2 donors (*$p<0.05$).

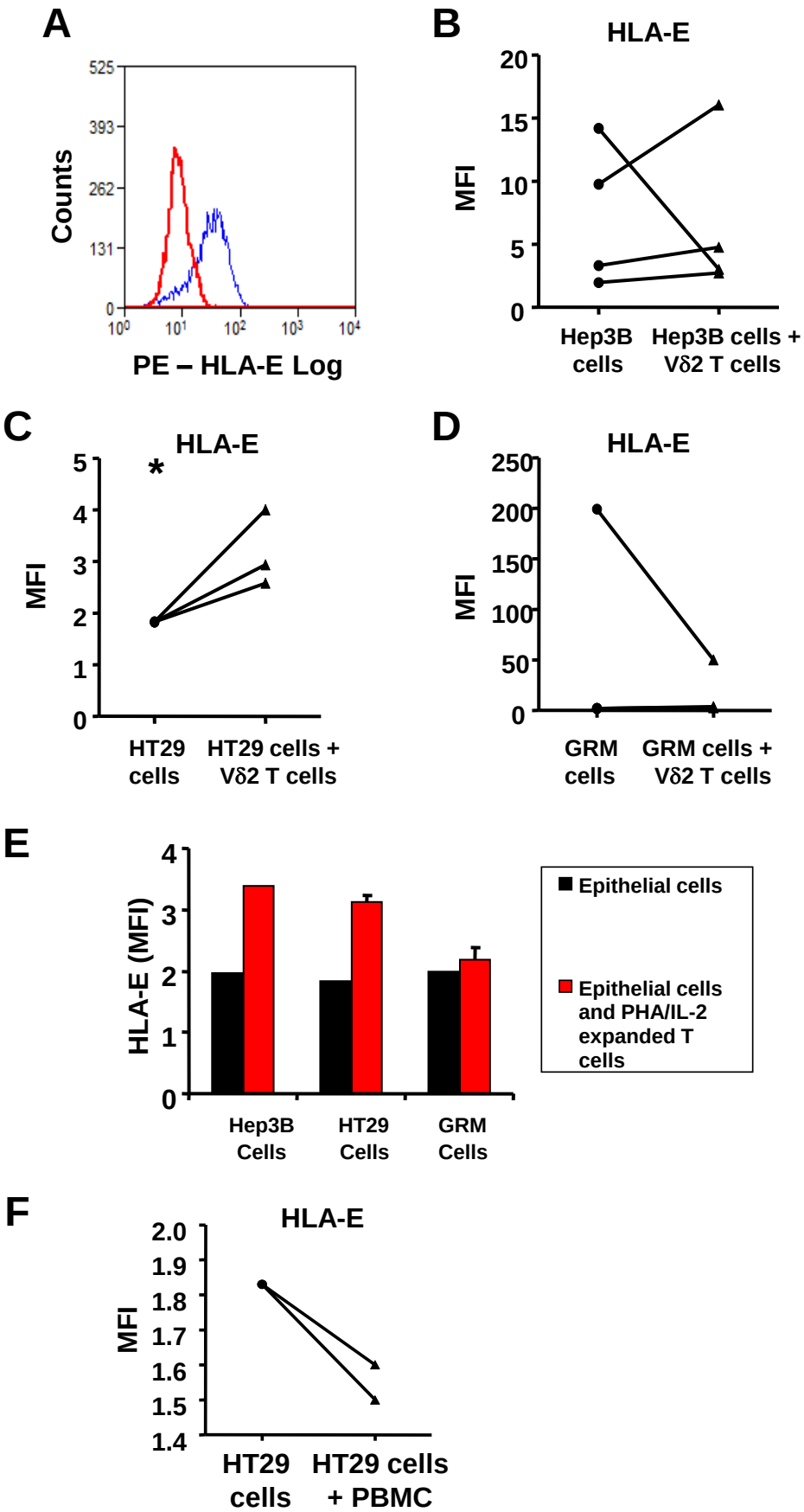
A
525
393
262
131
0
Counts
10^0 10^1 10^2 10^3 10^4
PE – HLA-E Log
B
HLA-E
20
15
10
5
0
MFI
Hep3B cells
Hep3B cells + Vδ2 T cells
C
HLA-E
*
5
4
3
2
1
0
MFI
HT29 cells
HT29 cells + Vδ2 T cells
D
HLA-E
250
200
150
100
50
0
MFI
GRM cells
GRM cells + Vδ2 T cells
E
4
3
2
1
0
HLA-E (MFI)
Hep3B Cells
HT29 Cells
GRM Cells
Epithelial cells
Epithelial cells and PHA/IL-2 expanded T cells
F
HLA-E
2.0
1.9
1.8
1.7
1.6
1.5
1.4
MFI
HT29 cells
HT29 cells + PBMC

Figure 6.6: Co-culture with HMBPP-expanded Vδ2 T cells results in higher levels of HLA-E expression by HT29 , but not by Hep3B or GRM cells. A, histogram showing HLA-E expression by BerEP4^{+} HT29 cells culturd alone (red) and cultured in the presence of HMBPP-expanded Vδ2 T cells (blue). **B, C, D,** scatterplots showing the MFI of HLA-E expression by Hep3B **(B),** HT29 **(C)** and GRM cells **(D)** after a 24 hour incubation in the absence (circle) and presence (triangle) of HMBPP-expanded Vδ2 T cells from 3-4 donors. **E,** barchart showing HLA-E expression by Hep3B, HT29 and GRM cells following a 24 hour incubation in the absence (black) and presence (red) of PHA and IL-2-expanded T cells from 1-2 donors. **F,** scatterplot showing the MFI of HLA-E expression by HT29 cells after a 24 hour incubation in the absence (circle) and presence (triangle) of fresh PBMC from 2 donors (*$p<0.05$).

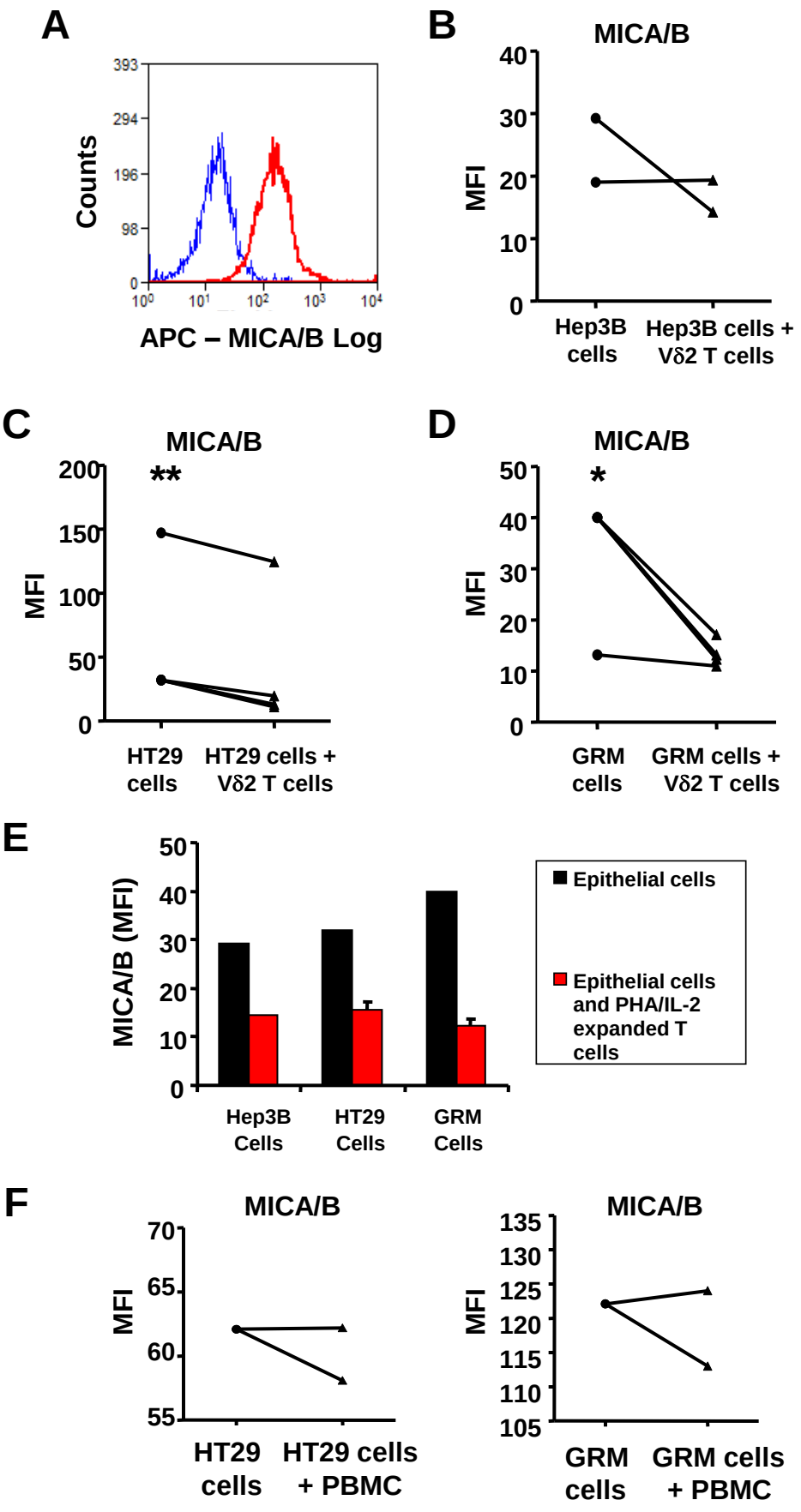
A
393
294
196
98
0
Counts
10^0
10^1
10^2
10^3
10^4
APC – MICA/B Log
B
MICA/B
40
30
20
10
0
MFI
Hep3B cells
Hep3B cells + Vδ2 T cells
C
MICA/B
**
200
150
100
50
0
MFI
HT29 cells
HT29 cells + Vδ2 T cells
D
MICA/B
*
50
40
30
20
10
0
MFI
GRM cells
GRM cells + Vδ2 T cells
E
50
40
30
20
10
0
MICA/B (MFI)
Hep3B Cells
HT29 Cells
GRM Cells
Epithelial cells
Epithelial cells and PHA/IL-2 expanded T cells
F
MICA/B
70
65
60
55
MFI
HT29 cells
HT29 cells + PBMC
MICA/B
135
130
125
120
115
110
105
MFI
GRM cells
GRM cells + PBMC

Figure 6.7: Co-culture with HMBPP-expanded Vδ2 T cells results in lower levels of MICA/B expression by epithelial cells. A, histogram showing MICA/B expression by BerEP4^{+} GRM cells cultured alone (red) and cultured in the presence of HMBPP-expanded Vδ2 T cells (blue). **B, C, D,** scatterplots showing the MFI of MICA/B expression by Hep3B **(B),** HT29 **(C)** and GRM cells **(D)** after a 24 hour incubation in the absence (circle) and presence (triangle) of HMBPP-expanded Vδ2 T cells from 3-4 donors. **E,** barchart showing MICA/B expression by Hep3B, HT29 and GRM cells following a 24 hour incubation in the absence (black) and presence (red) of PHA and IL-2-expanded T cells from 1-2 donors. **F,** scatterplots showing the MFI of MICA/B expression by HT29 **(left)** and GRM cells **(right)** after a 24 hour incubation in the absence (circle) and presence (triangle) of fresh PBMC from 2 donors (*p=0.02, **p=0.002).

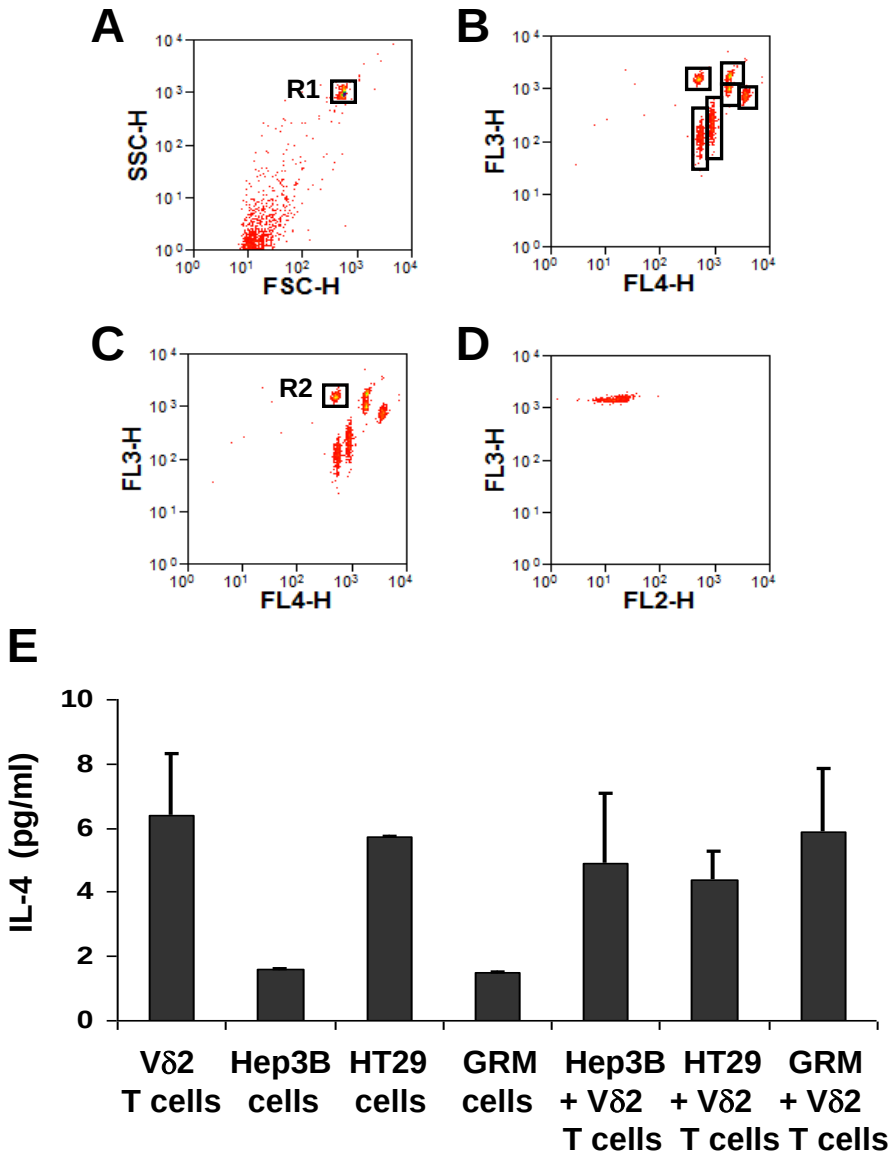

Figure 6.8: No significant difference in IL-4 expression following co-culture of epithelial cells with HMBPP-expanded Vδ2 T cells. A, representative dot plot of antibody coated beads with electronic gate R1 surrounding the antibody coated beads and excluding the debris. **B, C,** representative dot plots of all populations of cytokine beads, previously gated in R1 and now, divided by fluorescence intensity in the FL3 and FL4 channels. IL-4 conjugated beads are gated in R2 **(C). D,** dot plot showing IL-4 conjugated beads from a single sample. The plot has been gated on R2. The MFI of the population in FL2 indicates the level of IL-4 expression in the sample. **E,** barchart showing the concentration of IL-4 protein (pg/ml) in supernatants taken from HMBPP-expanded Vδ2 T cell cultures from 3-5 healthy donors, supernatants taken from Hep3B, HT29 or GRM cells and supernatants taken from co-cultures containing both HMBPP-expanded Vδ2 T cells and Hep3B, HT29 or GRM cells.

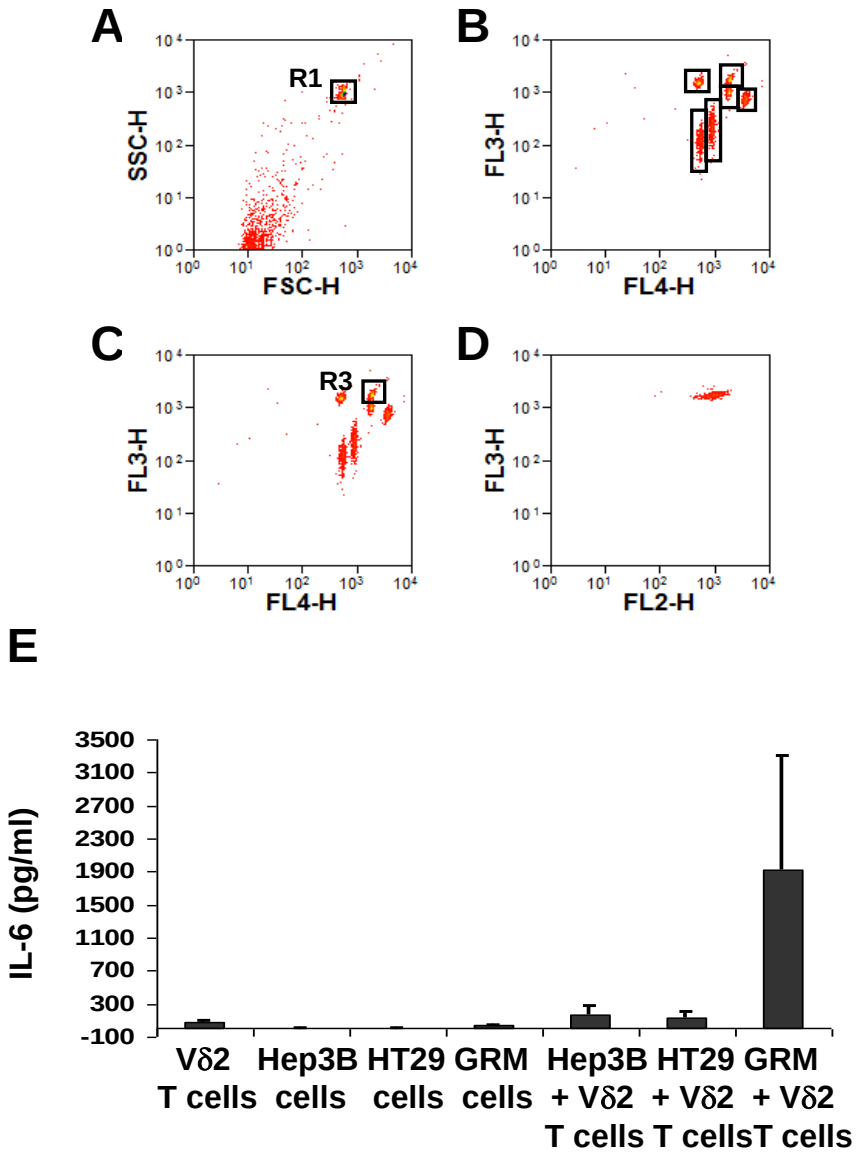

Figure 6.9: No significant difference in IL-6 expression following co-culture of epithelial cells with HMBPP-expanded Vδ2 T cells. A, representative dot plot of antibody coated beads with electronic gate R1 surrounding the antibody coated beads and excluding the debris. **B, C,** representative dot plots of all populations of cytokine beads, previously gated in R1 to and now, divided by fluorescence intensity in the FL3 and FL4 channels. IL-6 conjugated beads are gated in R3 **(C). D,** dot plot showing IL-6 conjugated beads only from a single sample, because the plot has been gated on R3. The MFI of this population in FL2 indicates the level of IL-6 expression in the sample. **E,** barchart showing the concentration of IL-6 protein (pg/ml) in supernatants taken from HMBPP-expanded Vδ2 T cell cultures from 3-5 healthy donors, supernatants taken from Hep3B, HT29 or GRM cells and supernatants taken from co-cultures containing both HMBPP-expanded Vδ2 T cells and Hep3B, HT29 or GRM cells.

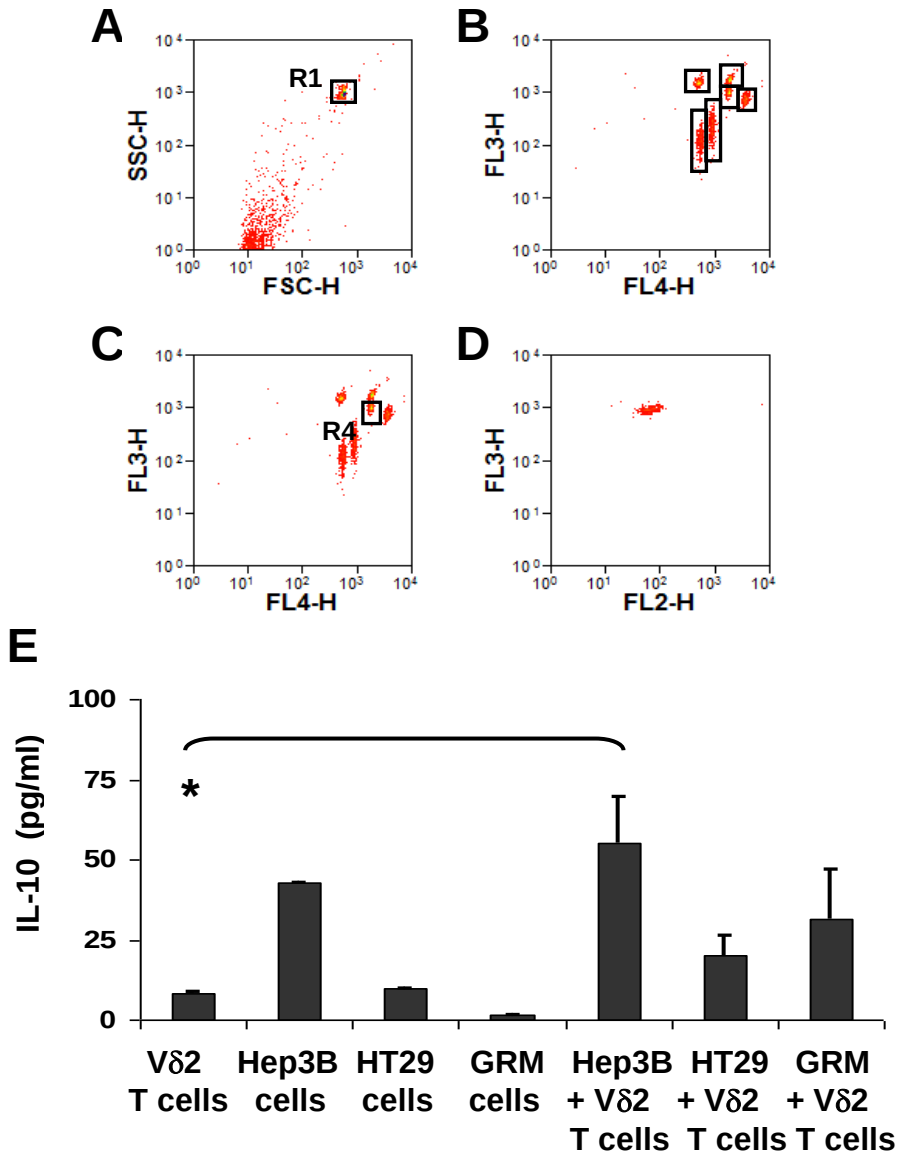

Figure 6.10: Higher IL-10 expression in epithelial and HMBPP-expanded Vδ2 T cell co-cultures, compared to HMBPP-expanded Vδ2 T cell cultures. A, representative dot plot of antibody coated beads with electronic gate R1 surrounding the antibody coated beads and excluding the debris. **B, C,** representative dot plots of all populations of cytokine beads, previously gated in R1 and now, divided by fluorescence intensity in the FL3 and FL4 channels. IL-10 conjugated beads are gated in R4 **(C). D,** dot plot showing IL-10 conjugated beads from a single sample. The plot has been gated on R4. The MFI of this population in FL2 indicates the level of IL-10 expression in the sample. **E,** barchart showing IL-10 protein concentration (pg/ml) in supernatants of HMBPP-expanded Vδ2 T cell cultures from 3-5 healthy donors, supernatants of Hep3B, HT29 or GRM cells and supernatants of co-cultures containing both HMBPP-expanded Vδ2 T cells and Hep3B, HT29 or GRM cells (*p=0.03).

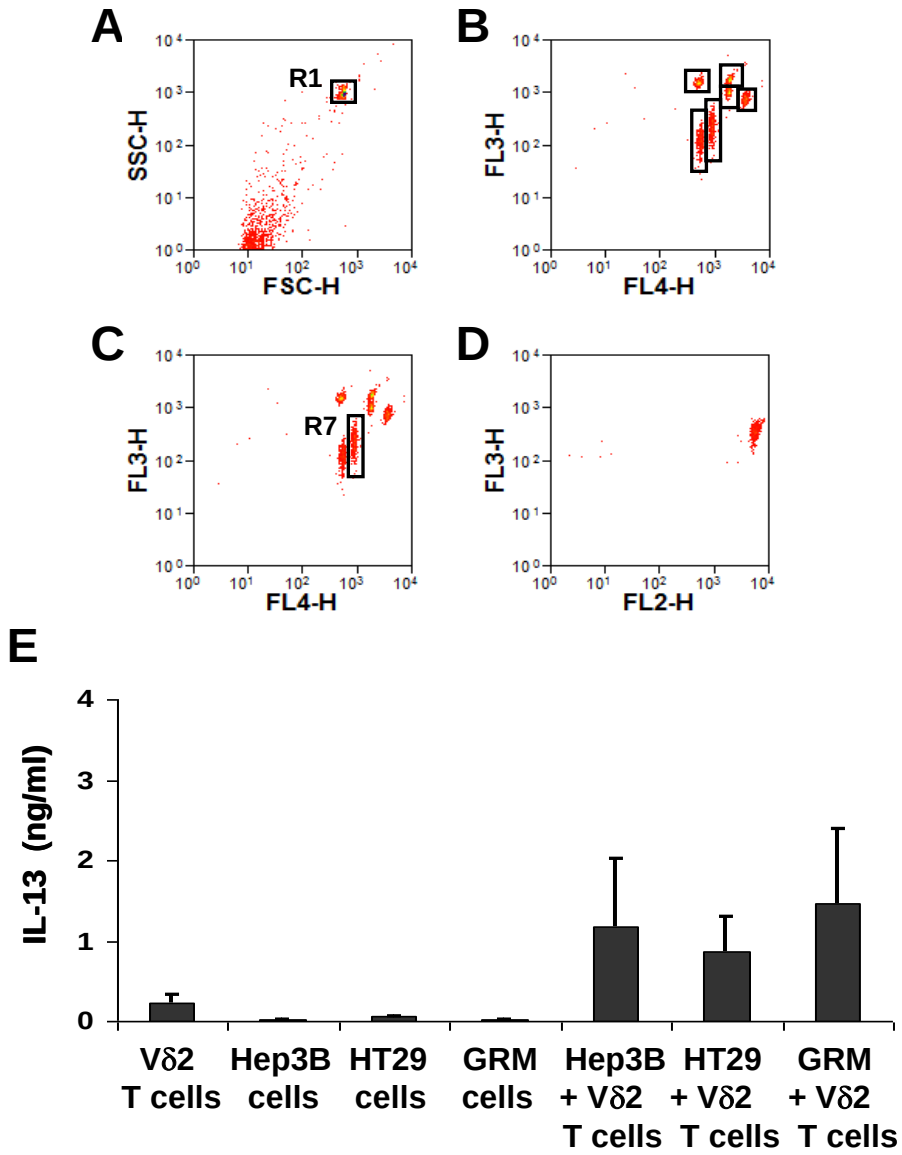

Figure 6.11: No significant difference in IL-13 expression following co-culture of epithelial cells with HMBPP-expanded Vδ2 T cells. A, representative dot plot of antibody coated beads with electronic gate R1 surrounding the antibody coated beads and excluding the debris. **B, C,** representative dot plots of all populations of cytokine beads, previously gated in R1 and now, divided by fluorescence intensity in the FL3 and FL4 channels. IL-13 conjugated beads are gated in R7 **(C). D,** dot plot showing IL-13 conjugated beads only from a single sample, because the plot has been gated on R7. The MFI of this population in FL2 indicates the level of IL-13 expression in the sample. **E,** barchart showing the concentration of IL-13 protein (ng/ml) in supernatants of HMBPP-expanded Vδ2 T cell cultures from 3-5 healthy donors, supernatants of Hep3B, HT29 or GRM cells and supernatants of co-cultures containing both HMBPP-expanded Vδ2 T cells and Hep3B, HT29 or GRM cells.

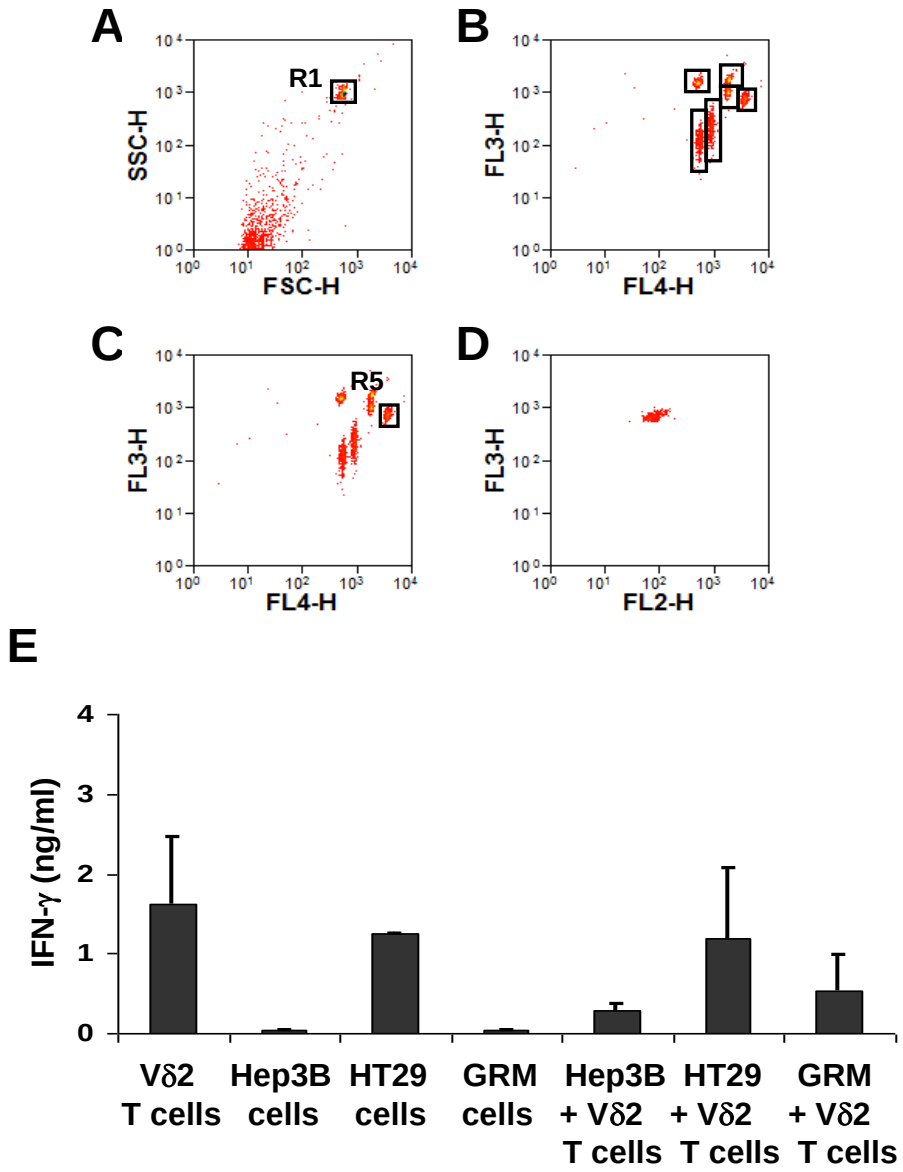

Figure 6.12: No significant difference in IFN-γ expression following co-culture of epithelial cells with HMBPP-expanded Vδ2 T cells. A, representative dot plot of antibody coated beads with electronic gate R1 surrounding the antibody coated beads and excluding the debris. **B, C,** representative dot plots of all populations of cytokine beads, previously gated in R1 and now, divided by fluorescence intensity in the FL3 and FL4 channels. IFN-γ conjugated beads are gated in R5 **(C). D,** dot plot showing IFN-γ conjugated beads from a single sample. The plot has been gated on R5. The MFI of this population in FL2 indicates the level of IFN-γ expression in the sample. **E,** barchart showing the concentration of IFN-γ protein (ng/ml) in supernatants from HMBPP-expanded Vδ2 T cell cultures from 3-5 healthy donors, supernatants from Hep3B, HT29 or GRM cells and supernatants from co-cultures containing both HMBPP-expanded Vδ2 T cells and Hep3B, HT29 or GRM cells.

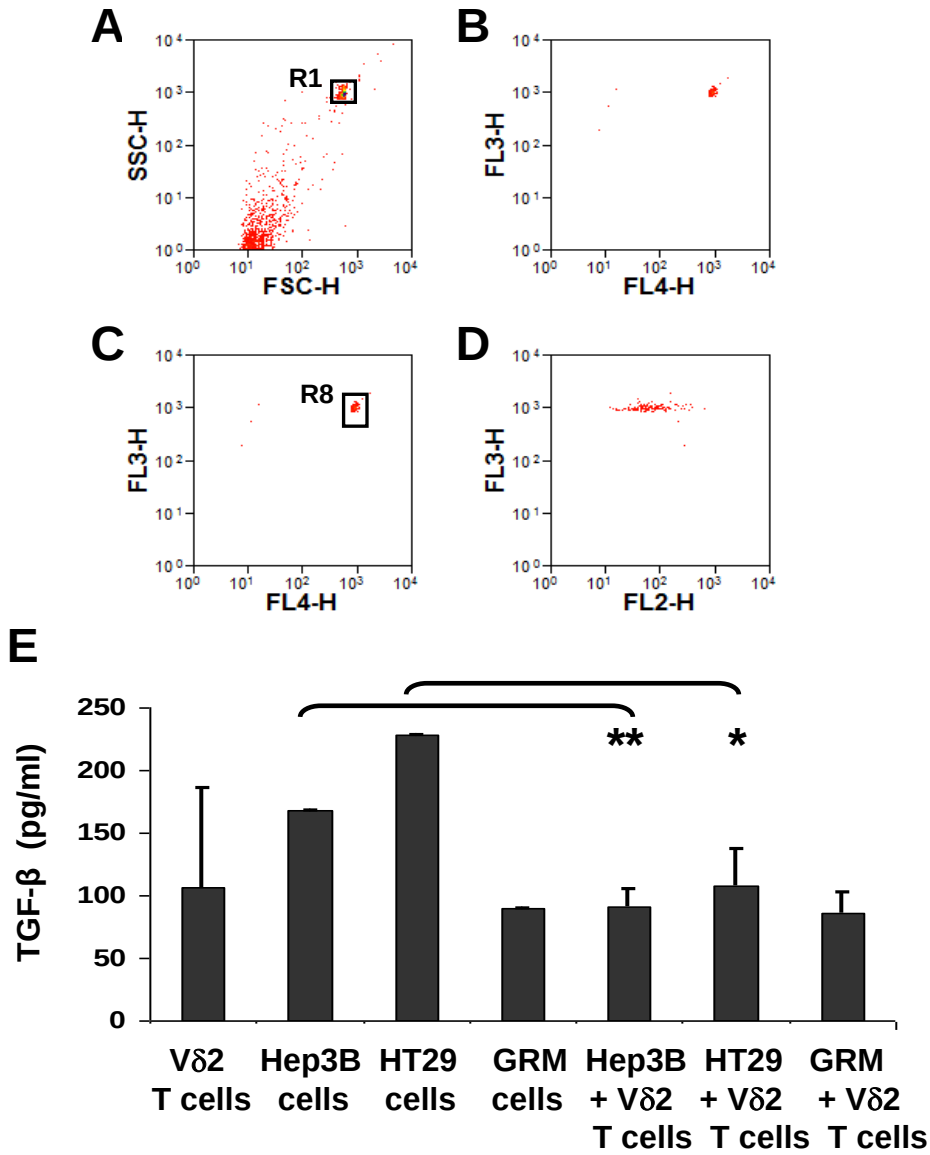

Figure 6.13: Lower TGF-β1 expression following co-culture of epithelial cells with HMBPP-expanded Vδ2 T cells, compared to that of epithelial cells cultured alone. A, representative dot plot of antibody coated beads with electronic gate R1 surrounding the antibody coated beads and excluding the debris. **B, C,** representative dot plots of single population of TGF-β1-conjugated beads in single-plex assay tube. TGF-β1 conjugated beads are gated in R8 **(C). D,** dot plot showing TGF-β1 conjugated beads from a single sample, because the plot has been gated on R8. The MFI of this population in FL2 indicates the level of TGF-β1 expression in the sample. **E,** barchart showing the concentration of TGF-β1 protein (pg/ml) in supernatants taken from HMBPP-expanded Vδ2 T cell cultures from 3-5 healthy donors, supernatants taken from Hep3B, HT29 or GRM cells and supernatants taken from co-cultures containing both HMBPP-expanded Vδ2 T cells and Hep3B, HT29 or GRM cells (*p=0.02, **p=0.005).

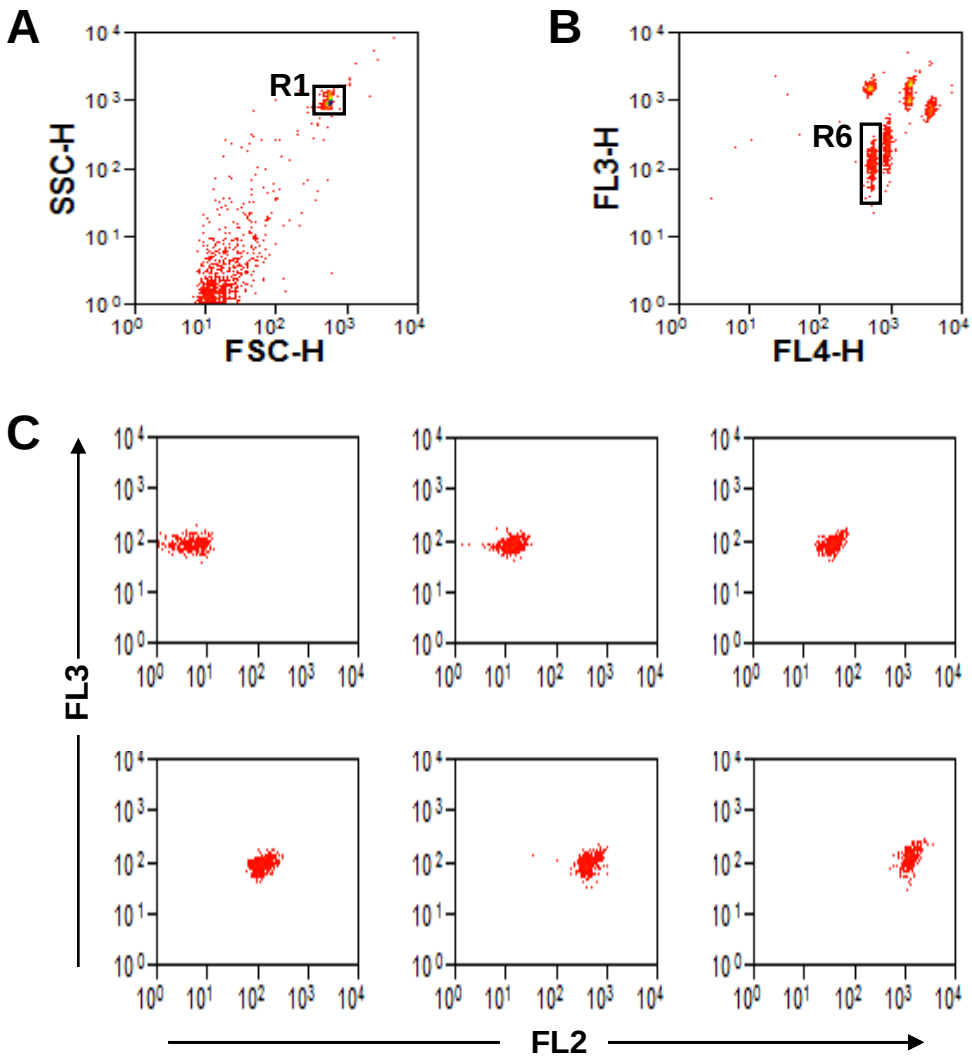

Figure 6.14: Undetectable levels of IL-12 in sample supernatants A, representative dot plot of antibody coated beads with electronic gate R1 surrounding the antibody coated beads and excluding the debris. **B,** representative dot plot of all populations of cytokine beads, previously gated in R1 to exclude debris and now, divided by their fluorescence intensity in the FL3 and FL4 channels. IL-12 conjugated beads are gated in R6. **C,** representative dot plots showing IL-12 conjugated beads only for 6 standard tubes. Dot plot in upper left represents the tube containing 0 pg/ml IL-12 and the dot plot in the lower right represents the tube containing 2500 pg/ml IL-12. Most dot plots from sample tubes were similar to that of the standard blank tube and therefore, IL-12 could not be detected in the majority of samples.